To the Graduate Council:

I am submitting herewith a dissertation written by Xiaoyu Luo entitled "Chemical Characterization of PAN based Carbon Fibers Produced by Microwave Assisted Plasma (MAP) Technology and Effect of Plasma Treatment on Carbon Fiber Surface and Interphase with Polymer Matrix." I have examined the final paper copy of this dissertation for form and content and recommend that it be accepted in partial fulfillment of the requirements for the degree of Doctor of Philosophy, with a major in Polymer Engineering.

Roberto S. Benson, Major Professor

We have read this dissertation
and recommend its acceptance:

Felix L. Paulauskas

Joseph E. Spruiell

Madhu S. Madhukar

Accepted for the Council:

Vice Chancellor and Dean of
Graduate Studies

CHEMICAL CHARACTERIZATION OF PAN BASED CARBON FIBERS PRODUCED BY MICROWAVE ASSISTED PLASMA (MAP) TECHNOLOGY AND EFFECT OF PLASMA TREATMENT ON CARBON FIBER SURFACE AND INTERPHASE WITH POLYMER MATRIX

A Dissertation

Presented for the

Doctor of Philosophy Degree

The University of Tennessee, Knoxville

Xiaoyu Luo

May 2006

DEDICATION

This dissertation is dedicated to my parents, Mr. Xuezhong Luo and Ms. Guiying Tian, for their unconditional love and support.

ACKNOWLEDGEMENTS

First and foremost, I would like to express my deepest appreciation to my advisor, Dr. Roberto S. Benson, for his guidance and encouragement during my study, and for his help in bringing this dissertation to fruition. I feel indebted to Dr. Felix Paulauskas for his guidance and support. I would like to thank Dr. Joseph E. Spruiell and Dr. Madhu S Madhukar for taking the time to serve on my committee and the helpful suggestions they made during this work.

I would like to give special thanks to Mr. Johnny C. Jones for his great assistances on running the X-ray photoelectron spectroscopy. I am very thankful to Dr. Harry M. Mayer for his assistance in operation of Auger electron spectroscopy. I wish to thank Dr. Wayne Jalenak from Varian for his assistance with FTIR imaging and interpretation of images. The financial supports from University of Tennessee Materials Science and Engineering department and Oak Ridge National Laboratory are most greatly appreciated.

My gratitude also goes to Materials Science and Engineering faculty members, staff and fellow students for the assistance and support during these years.

Finally, I would like to thank my colleges, family and friends for their love, support and understanding.

ABSTRACT

The first objective of this research was to chemically characterize the surface of conventional carbon fiber and carbon fiber produced by microwave assisted plasma (MAP) manufacturing process. The chemical composition and functional groups on the surface of the fibers were determined by X-ray photoelectron spectroscopy (XPS). The untreated unsized MAP carbon fibers were compared to untreated unsized conventional carbon fibers and showed a significant amount of oxygen. Comparison between treated unsized MAP carbon fiber and treated unsized conventional carbon fiber reveal a 100% enhancement of oxygen elemental concentration.

Two plasma systems, remote applicator and atmospheric plasma were used to treat untreated unsized conventional carbon fiber. XPS results indicated that both systems have changed the chemical composition of carbon fiber surface. Oxygen-containing functional groups were found on carbon fiber surface after plasma treatment.

Auger electron spectroscopy combining with chemical deritivazation was used to investigate the effect of morphological structure of carbon fiber surface on the placement of carboxyl groups. It was found that carboxyl groups were located preferentially in the valleys. A model of surface morphological structure of carbon fibers treated with plasma was proposed.

Chemical bonding formed in the interphase between plasma treated carbon fiber and urethane was investigated using FTIR imaging. Directed evidence of formation of hydrogen bonding between carbon fiber and urethane was observed.

TABLE OF CONTENT

LIST OF TABLE

LIST OF FIGURES

CHAPTER 1

INTRODUCTION

Carbon fibers are commonly used as reinforcement materials in advanced structural composites for aerospace applications due to its high specific strength and stiffness. In recent years, the use of carbon fiber composites is expanding into recreational, industrial and transportation markets. The major barrier to the application of advanced carbon fiber composites in other commercial industries is the current high cost of carbon fiber. Microwave-assisted plasma (MAP) technology is currently being developed at Oak Ridge National Laboratory (ORNL), utilizing high energy density oxygen-free plasma initiated pyrolysis process to replace the expensive carbonization and graphitization steps in conventional carbon fiber manufacturing process. The MAP technique has several advantages over conventional processing method: 1) processing is much faster than conventional furnace heating method; 2) economic studies indicate that MAP technology has the potential to reduce carbon fiber price by 20%; 3) the technique reduces emission of the hazardous gases associated with carbonization and graphitization steps in the conventional process.

The chemical and physical interactions between carbon fiber and polymer matrix are the important factors, which influence the properties, such as strength and stiffness, of the obtained composite materials. In order for carbon fibers to be used effectively in polymer matrix composites, the carbon fibers must have a surface treatment that

optimizes the interaction and adhesion between the fiber surface and polymer matrix to achieve good stress transfer from the matrix material into the filling fibers. Therefore, an understanding of the surface structure, chemistry and topography of carbon fibers is required for the optimization of desirable composite properties. One objective of this research is to conduct the chemical and morphological characterization of polyacrylonitrile (PAN) based carbon fibers produced using microwave assisted plasma (MAP) technology. The chemical characterization will identify the elemental composition, type, density and distribution of the chemical functional groups on the surface. Special interest will be placed on the topographic location of groups, and distribution as a function of surface treatment processing variables. The morphological characterization will identify topographical features of the fibers and for the first time, their effect on the placement of chemical groups during surface treatment of the fibers. The second objective was to study the effect of surface treatments by using plasma obtained from a range of gas compositions on the fiber surface. A correlation between plasma process parameters, including plasma density, microwave power and plasma chamber pressure and type, concentration and distribution of chemical groups placed on the fiber surface will be studied. The results from this study will contribute to increase understanding of the structure-property-processing relationship associated with manufacture and surface treatment of carbon fibers.

CHAPTER 2

LITERATURE REVIEW

2.1. Manufacture of Carbon Fibers

Carbon fibers are produced through the controlled pyrolysis of fibrous organic carbon precursors. Nowadays, carbon fibers available commercially are manufactured from three main precursors: polyacrylonitrile (PAN), pitch (petroleum or coal tar) or rayon. While the manufacture processes for various precursors are different in details, they all follow a basic sequence of spinning, stabilization, carbonization, graphitization, surface treatment, and a sizing to facilitate handling [1]. PAN-based carbon fibers will be used in this study, so only manufacturing methods associated with PAN carbon fiber process will be discussed in this section.

2.1.1 Conventional Technology

PAN-based carbon fiber is considered the most important and promising precursor for manufacturing of carbon fibers due to several advantages it possesses: a high degree of molecular orientation, high melting point, and a high yield of the carbon fibers [2].

The overall process for the conversion of PAN to carbon fiber involves the following steps: precursor preparation, stabilization (oxidation), carbonization, graphitization and surface treatment.

1. Precursor preparation

CH_2=CH-C≡N

Figure 2-1. Chemical formula of acrylonitrile

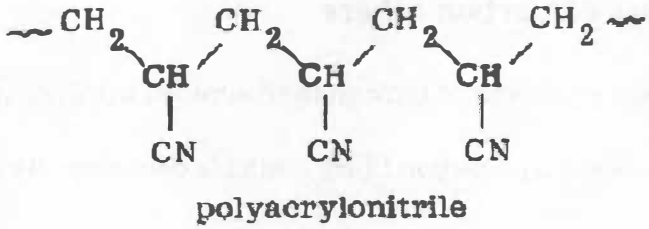

Figure 2-2. Chemical structure of polyacrylonitrile

The acrylonitrile molecule has a highly polar nitrile group, shown in Figure 2-1. Due to this high polarity, polymerization can take place in the presence of free radicals or negative initiators, leading to the production of the thermoplastic polyacrylonitrile, shown in Figure 2-2.

The next step in the conventional carbon fiber production process is spinning polyacrylonitrile into a fiber form. During this process, the PAN precursors become highly oriented. PAN precursor can be formed by different spinning processes including wet, dry, dry-jet/wet and semimelt. The principal commercial processes are wet and dry-jet wet spinning [3].

2. Stabilization

The stabilization step converts the precursor to a thermally stable structure, which is capable of withstanding high temperature processing at high rates with good yield [3].

In this process, PAN precursor is treated in an oxidizing atmosphere in a temperature range of 200-300° C. This treatment is carried out under tension in order to prevent shrinkage, and help in aligning the molecular chains along the fiber axis.

During this process, the chemical structure of PAN precursor undergoes a change from a thermoplastic PAN to a thermosetting cyclic or ladder compound capable of withstanding the higher temperatures necessary for the next processing steps. Along with cyclization, dehydrogenation and oxidation also take place during the stabilization process. Dehydrogenation reactions precede cyclization and continue during and after cyclization [4]. It is believed these reactions lead to the change of fiber color from white to yellow, brown, and ultimately black. The sequence of reactions during stabilization process is shown in Figure 2-3.

3. Carbonization

After stabilization, PAN fibers are subjected to a rapid thermal pyrolysis in an inert atmosphere, usually high purity nitrogen, at 1200-2000°C under low or very little tension. Almost all other noncarbon elements are removed as volatiles; only low nitrogen concentrations remain. These volatiles include substantial amounts of HCN, NH_3, N_2 and H_2O with fewer amounts of low molecular-weight nitriles, CO_2, CO, H_2 and CH_4. During carbonization a graphite like structure is formed by crosslinking of the cyclized compound with evolution of H_2O, HCN, H_2 and N_2, shown in Figure 2-4. The yield is about 50 percent of the mass of original PAN.

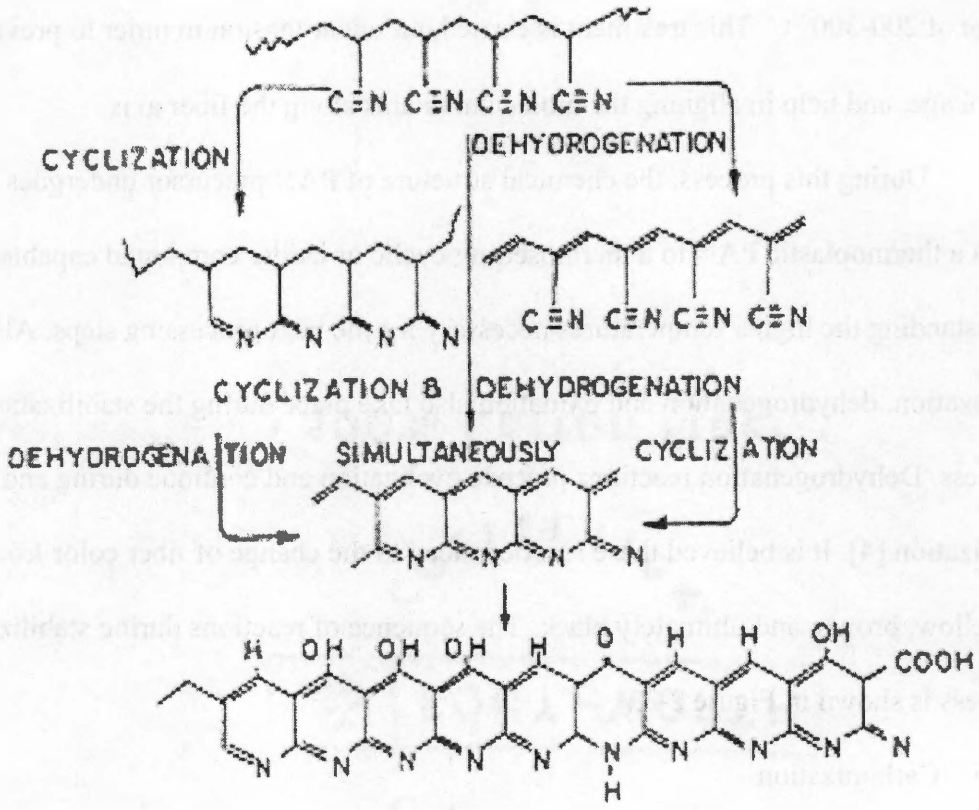

Figure 2-3. Sequence of reaction during thermooxidative stabilization of PAN precursor [4]

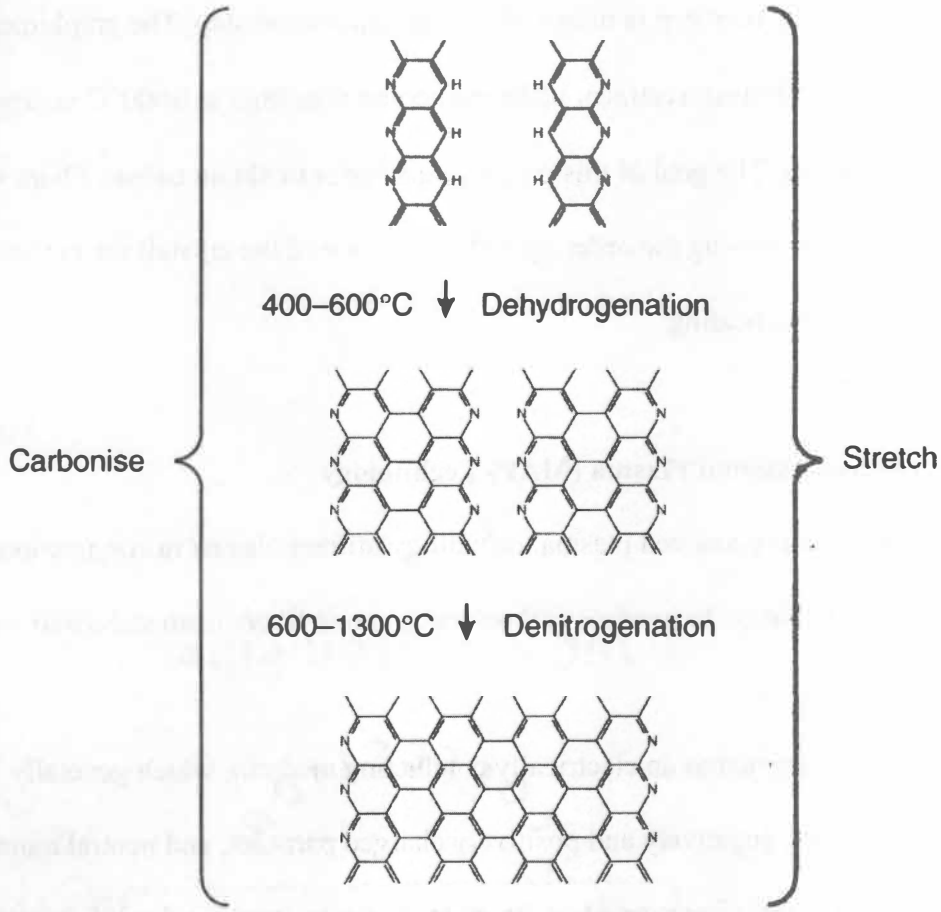

Figure 2-4. PAN-based carbon fiber chemistry: carbonization [3]

4. Graphitization

The carbonization step is followed by a graphitization step. The graphitization stage involves further heat treatment up to temperatures as high as 3000°C in argon or nitrogen atmosphere. The goal of this processing stage is to obtain carbon fibers with high modulus by improving the ordering and orientation of the crystallites in the direction of the fiber axis upon heating.

2.1.2 Microwave-Assisted Plasma (MAP) Technology

The microwave-assisted plasma technology utilizes plasma in conjunction with electromagnetic radiation to produce carbon and graphite fibers from stabilized carbon fiber precursors [5].

Plasma is defined as an electrically conducting medium, which generally is a mixture of electrons, negatively and positively charged particles, and neutral atoms and molecules. Since plasma has properties different from gas, liquid and solid, it is referred as the fourth state of matter.

Based on the gas temperature of various plasmas, they are divided into [6]:

1. high-temperature plasma: gas temperature is higher than 10^6K, representing the majority in the universe including all stellar, nuclear blast and controlled fusion reactions, etc.
2. low-temperature plasma: gas temperature is lower than 10^6K.

Low-temperature plasma can be further divided into: 1) hot plasma in which gas temperature is higher than 1000K, normally in the order of 10^4K,

which includes lightning, electrical arc and other high-power discharges. 2) cold plasma that has gas temperature lower than 1000K, normally in the order of 10^2K, including various glow discharges at low pressures.

Cold plasma is used for surface treatment of fibers due to its characteristic high electron temperature and relatively low gas temperature. The former refers to the electronic energy given in Kelvin and latter to the mean translational energy of molecules given in Kelvin. High electronic temperature affords a sputtering effect on the fiber surface and possibility of chemical modification. The low gas temperature is as low as room temperature in most cases, so it enables fibers to experience such plasma modification without loss of their mechanical properties [7].

In conventional carbon fiber manufacturing process, the thermal carbonization and graphitization steps are lengthy and expensive, which are performed in large furnaces and require several hours to complete. This is a major cost factor in conventional carbon fiber manufacturing. The microwave-assisted plasma (MAP) technology is being developed at Oak Ridge National Laboratory to utilize plasma technology in conjunction with microwave technology to produce carbon fibers from stabilized carbon fiber precursor. The MAP technology is developed to replace the expensive carbonization and graphitization steps of the conventional process with an oxygen free plasma to initiate the pyrolysis process with previously stabilized fibers. The illustration of conventional and microwave-assisted plasma processes is shown in Figure 2-5.

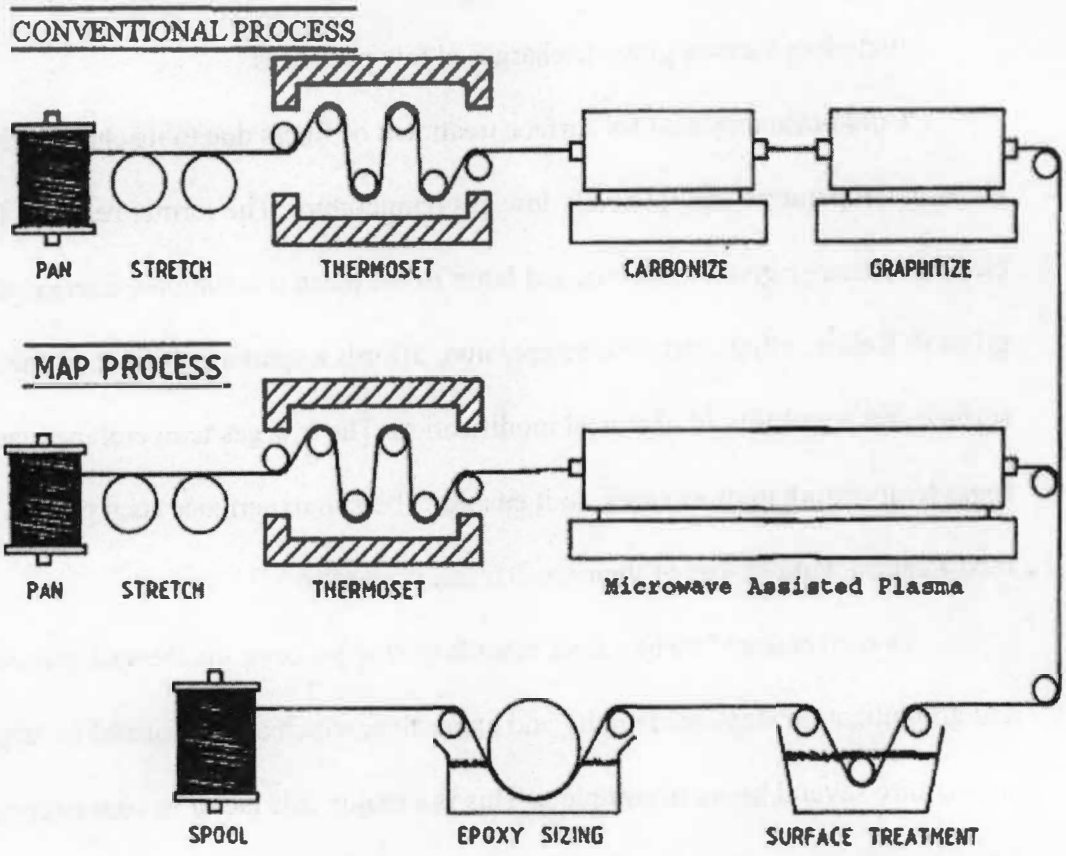

Figure 2-5. Comparison of conventional and microwave-assisted plasma processes

In MAP carbon fiber manufacturing process, the stabilized carbon fiber precursors are placed in an oxygen-free atmosphere and subjected to both plasma energy and microwave radiation which is increased as the fibers progress towards a final carbon or graphite product [5]. The plasma energy is initiated and sustained by microwave radiation as most of the microwave energy couples directly to the plasma, which comprise electrons, positive or negative ions, gaseous atoms and molecules in the ground state or excited state, neutral free radicals and photons. The combined flux of all of these species will impinge on the surface of the tow filaments and cause an enhanced carbonization because their energies are higher than those of the ordinary thermal fluxes used in conventional processing. This plasma is considered low-pressure "cold" plasma, which provides an ambient gas temperature along with electrons, which have sufficient kinetic energy to cause the cleavage of chemical bonds, thus enhancing the release of gases. The electronic temperatures of such plasmas remain relatively constant of the order of 10^4–10^5 K, about 1-10 eV [6]. The strengths of most common chemical bonds fall into this range as indicated in Table 2-1[8].

The microwave energy drives the plasma, and also deposits energy directly into the fiber. Carbon is an ideal microwave absorber. The microwave energy that did not couple with the plasma is absorbed directly by the carbon fiber, thus heating it directly. The plasma initiated by microwave radiation, in turn increases the fiber's dielectric loss tangent and consequently raises the fiber's coupling efficiency to the microwave energy [5]. The microwave is absorbed throughout the fiber's cross-section. Through the

Table 2-1. Strengths of some polyatomic chemical bonds [8] (in kJ mol^{-1})

Bond	Strength	Bond	Strength	Bond	Strength
H-C	305-450	C-C	250-500	N-N	40-275
H-Si	268-418	C=C	319-720	O-O	150-244
H-N	207-450	C≡C	962	C-F	450-530
H-O	327-498	C-N	120-300	C-Cl	260-420
H-S	172-381	C-O	92-290	O-N	96-208
Si-O	536	C=O	532	B-B	146
Si-Si	310-368	C-S	250-430	F-N	88

1eV=96.44 kJ mol^{-1}

coupling of plasma and microwave energy, a uniform and homogeneous volumetric heating is achieved, which promotes the mass exchange of oxygen and evolved gases across the entire fiber cross-section. The released gases can be used as an additional fuel for the plasma and to determine when carbonization is complete or whether an increase in the level of microwave energy is needed [5].

In an additional step, a small amount of oxygen can be carefully introduced in the plasma chamber once the carbonization and/or graphitization steps are complete. This oxygen is consumed by the plasma resulting in the treatment of the carbon or graphite fiber surface, which will improve the matrix-fiber adhesion. Microwave-assisted plasma

technology has several advantages over the conventional carbon fiber manufacturing process that makes it an attractive alternative technology for carbon fiber production:

1. Allow the production of surface treated carbonized or graphitized products in a single process step thus improve processing speeds and reduce energy demand.

2. Allow the production of carbon and graphite fibers having a wide range of final properties as a function of the processing parameters.

3. Allow the reduction of the amount of toxic off-gases present in this process since they are further consumed by plasma reaction.

To conclude, the Oak Ridge National Laboratory Micowave-Assisted Plasma (MAP) carbon fiber manufacturing process is a revolutionary technology for carbonizing and graphitizing carbon fibers at much higher speeds and reduced energy, which affords a significantly lower costs than those achieved by present conventional carbon fiber manufacturing process.

2.2 Surface Treatment of Carbon Fibers

2.2.1 Summary of Surface Treatment Methods

A good adhesion between fiber and matrix is a precondition for the stress transfer in fiber-reinforced polymer composites. The degree of adhesion between carbon fibers and matrix material depends considerably on the quality and the state of the carbon fiber surface. It is believed that adhesion is controlled by chemical bonding between fiber and matrix functional groups and by mechanical interlocking due to surface morphology.

Surface treatments of carbon fibers are essential for improving the bonding between the fibers and the polymer matrix. On a graphite crystal, there are potential active sites located on the incompletely bonded edges and faults in the structure, while those crystal basal surfaces of completely bonded carbon atoms are chemically inert. Reactions associated with carbon fiber surface treatment will take place at those potential active sites [9].

An effective surface treatment modifies the chemical, physical and topographical features of the surface of carbon fibers. Various approaches have been developed to change the fiber surface chemistry and surface topography simultaneously. They are classified into oxidation treatments, which can be subdivided into dry gaseous oxidation, wet oxidation and electrolytic oxidation; plasma treatment which will be discussed in a separate section; and non-oxidative treatments that includes depositing more active forms of carbon, such as the highly effective whiskerization, electropolymerization, or the grafting of polymers on the carbon fiber surface and sizing [10].

- **Oxidation Treatment**

This kind of treatment consists of controlled oxidation of the carbon fiber and is applied from the gaseous or liquid phase over a wide range of conditions. The objective of these treatments is to etch the surface by removing the weakly bonded carbon debris and other impurities. The polar hydrophilic oxygen-containing groups will be introduced on the surface, which increase its wettability and bonding ability to the polymer matrix. These treatments also permit some control over the extent of specific surface area and the rugosity change [11].

The oxidation treatments can double the surface concentration of oxygen functional groups. Functional groups on the fiber surface and at 50nm below the surface are listed below [12]:

At the surface: -CO, -C-OH, -COOH, -C=O

At 50nm depth: -CO, -C=O, -COOH

Whatever type of oxidation treatment is used, the number of chemical bonds to the fiber will be limited by the number of reactive sites available. This is governed in turn, by the physical structure of the fiber and micro-topography. As more pits and steps are produced by the oxidation of the carbon, the number of reactive sites increases and the number of attached chemical groups increases.

1. Dry gaseous oxidation

The gas-phase oxidative treatments are carried out with air, oxygen, or oxygen-containing gases such as ozone and CO_2. Oxidative treatment in air is not very effective in improving the composite shear properties. Herrick *et al.* [13] reported that almost no improvement in the composite shear properties of rayon based carbon fibers after the treatment in air for 16 hours at 500° C. In order to obtain better results, the treatment must be performed at higher temperatures. Degradation and large weight loss are associated with the elevated temperature process.

The use of oxygen for an efficient oxidative treatment of carbon fibers needs to be carried out at temperature above 400°C [10]. Oxygen containing groups such as carbonyl, carboxyl, and hydroxyl are introduced during the oxygen treatment. Surface area and pore diameter of carbon fibers tend to increase after the oxidative treatment.

Gas flow rates and temperature are the important parameters in this process. High oxidation rates will result in nonuniform etching of the carbon fibers and a loss of fiber tensile strength.

2. Liquid-Phase Oxidative Treatment

It has found that solution-phase oxidation of carbon fibers is quite effective in improving the shear properties of carbon fiber-polymer composites. Several types of oxidizing agents, such as nitric acid, acidic potassium permanganate, acidic potassium dichromate, hydrogen peroxide, and potassium persulfate have been used [10]. These liquid phase oxidative treatments are milder than the gaseous phase oxidative treatments and generally do not cause excessive pitting and degradation of the carbon fiber. This treatment permits chemisorption of oxygen with formation of functional groups such as –COOH and –OH. The oxygen content of the fiber surface increases with increase in time and temperature of treatment. Liquid phase oxidation by nitric acid and sodium hypochlorite results in an increase in interfacial area and formation of oxygenated surface groups due to fiber etching [14-17]. Wetting of the carbon fibers by the polymer is enhanced by these changes. Studies indicate that the less crystallized regions are more reactive toward nitric acid and the surface of untreated fibers are pitted and fragmented by the acidic solution [18]. The tensile strength of carbon fiber is strongly related with the flow patterns on the fiber surface [19]. The surface morphology changes considerable after acid treatment, hence, the distribution of fiber strength becomes broader [20].

3. Electrochemical Oxidation Method

Electrochemical oxidation (anodic oxidation) is fast, uniform and suited to mass production processes. It uses dilute nitric acid or dilute sodium hydroxide solutions and results in no significant decrease in tensile strength of the carbon fibers. The fiber weight loss is less than 2% and no great change in surface area or fiber roughness occurs [21]. The major change is an increase in the acidic surface groups, such as –COOH, -C-OH, and –C=O, and also esters and keto-enol groups on carbon fiber surface. They form at the edges of basal planes and at defects and subsequently form chemical bonds with matrix. The electrochemical oxidative treatment offers more control over surface chemistry and has become the preferred industrial process [10]. This treatment is preferred because it can allow continuous processing of the carbon fiber. The nature of the electrolyte used has a great influence on the surface properties of carbon fibers. Studies indicate that a basic electrolyte resulted in an improvement of composite transverse flexural strength and interlaminar shear strength (ILSS) due to an increase in the number of surface functional groups. An acid eletctrolyte treatment can result in the ILSS increasing while the transverse flexural strength decreased for composites because the carbon fibers have a high surface content [22].

- **Nonoxidative Surface Treatments**

1. Whiskerization

Whiskerization involves a nucleation process and growth of very thin and high-strength single crystals of other chemical compounds, such as silicon carbide (SiC), titanium dioxide (TiO_2) and silicon nitride (Si_3N_4) on the fiber surface perpendicular to the fiber axis [23]. The whiskers grow from individual fibers and

their growth on the fiber surface generally starts at points of defects such as structural irregularities, compositional heterogeneities, and imperfections. The whiskerization of a carbon fiber has been found to increase the interlaminar shear strength of the resulting carbon fiber composite significantly. The improvement in mechanical properties on whiskerization is attributed to a strong bonding of the whiskers to the graphite substrate and to an increase in the interfacial area rather than to any increase in bonding between the fiber and the resin matrix.

2. Electropolymerizatio

Organic polymeric materials such as polyvinyl benzene, polyamide, polyimide and organosilanes can be coated on the fiber surface to enhance the fiber-resin interfacial bonding [24]. The requirement for a polymer to be used as a coating is that it should be capable of being fixed on the carbon fiber surface by covalent or ionic bonds, and be compatible with the resin to produce a strong composite. To achieve better bonding between the resin and the polymer coating, it is better if the polymer coating has functional groups capable of reacting with the matrix. In this process, carbon fibers pass continuously through an electrolytic cell where polymers containing reactive function groups are coated on the fiber surface. After the electrodeposition, carbon fibers are washed until the weight of the deposit is reduced to a constant value, leading to the residual polymer coating with a structure more tightly held and more uniform. The composites made of polymers treated carbon fibers show a significant improvement in both interlaminar shear and impact strength. This approach modifies the carbon fiber surface without causing weight loss and reduction of fiber strength.

3. Sizing of Carbon Fibers

A sizing by definition is a protective coating for the fiber. In the manufacturing process, carbon fibers are usually coated with a very thin layer of epoxy resin or so-called "matrix-compatible sizings' after the proprietary surface treatment. These sizings are applied to carbon fibers for the protection of possible damage during transportation or handling. Carbon fibers are brittle materials that are susceptible to strength degradation due to the presence of surface flaws. It is believed that the fiber sizing is beneficial because it prevents fiber-to-fiber contact and hence the introduction of surface flaws. Other advantages of sizing are improvement of fiber wettability by the matrix, as well as prevention of surface reactivity by blocking the surface functional groups. A fiber sizing is designed to serve as a medium to insure adhesion between the matrix and fiber. Sizing is expected to have proper interaction with fiber and partial or total solubility with the matrix.

The choice of sizing material depends on the polymer matrix. In particular, thermoplastic-matrix composites require sizings that can withstand higher temperatures than thermoset-matrix composites, because of the higher processing temperature of the composite. Sizing materials include prepolymers/polymers, carbon, Silicon carbide (SiC), and metals. Due to the relative ease of application, polymers are the most common sizing materials. Sizing thicknesses typically range from 0.1 to 1 μm [4].

2.2.2 Plasma Treatment

Plasma is a gaseous mixture consisting of electrons, equally charged ions, molecules, and neutral atoms. In cold plasma, the electron temperature is 10 to100 times ambient temperature, but the electrons possess enough energy (1-10 eV) to break chemical bonds of the molecules [25]. A collision of plasma particles with substrate molecules transfers kinetic energy and activates the molecules so that they react with other species in bulk plasma [26]. The electrons among the particles are the principal sources for transferring electrical energy to the gas. Elastic electron-molecule collisions result in an increased kinetic energy of the particles and inelastic collisions generally result in the excitation, fragmentation or ionization of the molecules.

The basic reactions in plasma caused by inelastic collision can be summarized as follows:

Deexcitation	$A + e \rightleftharpoons A^* + e$	Excitation	(2.1)
Recombination	$A + e \rightleftharpoons A^+ + 2e$	Ionization	(2.2)
Photoemission	$A + h\nu \rightleftharpoons A^*$	Photo Excitation	(2.3)
Recombination	$A + h\nu \rightleftharpoons A^+ + e$	Photo Ionization	(2.4)
Photo Detachment	$A + e \rightleftharpoons A^- + h\nu$	Radiative Attachment	(2.5)
Recombination	$A^* + B \rightleftharpoons A + B^+ + e$	Penning Ionization	(2.6)
Charge Exchange	$A + B^+ \rightleftharpoons A^+ + B$	Charge Exchange	(2.7)

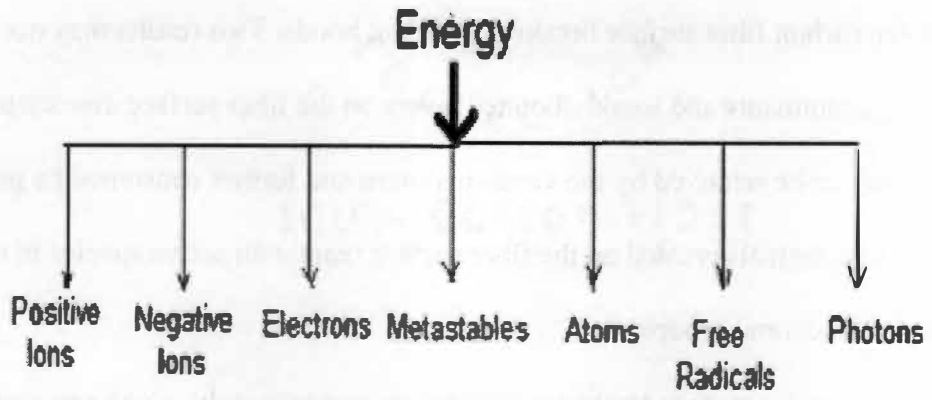

Figure 2-6. Components of cold plasma

The possible components generated in cold plasma are illustrated in Figure 2-6 [25].

As mentioned before, cold plasma is characterized by the high electron temperature and low gas temperature. This enables fibers to experience chemical and physical reactions in the surface only to a limited depth, while leaving the bulk material properties intact. This feature is particularly important for fibers because they are very susceptible to degradation by conventional processing in aggressive environment due to their small cross section area. This is one of the advantages plasma treatment has compared to chemical surface treatment. Over the past years, the concern about environmental pollution has made plasma treatment a popular choice, and it has become an important branch of plasma technologies.

A gas plasma is created by the introduction of the desired process gas into a vacuum chamber and using different energy source to dissociate the gas into electrons, ions, free radicals, and metastable excited species. The formed free radicals and electrons

collide with the carbon fiber surface breaking covalent bonds. Two results may occur at this point: 1) contaminants and weakly bonded layers on the fiber surface dissociate into volatile gas that can be removed by the vacuum system and further consumed by plasma process; or 2) free radicals created on the fiber surface react with active species in the plasma to form functional groups.

Plasma system for surface treatment requires an energy supply, a vacuum system for maintaining a plasma state, and a reaction chamber. Plasma reactors have been built in a wide range of frequencies, from direct current (DC), radio frequency (RF) to microwave frequency (MW). The efficiency of producing energetic electrons and excited species is greater at MW than at RF [25]. The effect of plasma treatment on carbon fiber surface is a result of processing variables including: type of gas, pressure, gas flow rate, power level, processing time and location of fiber with respect to generated plasma.

The plasma surface treatments at low temperature can be divided into plasma polymerization and plasma ablation based on the plasma gas used. If the plasma gas has high proportions of carbon and hydrogen atoms in its composition, such as methane, ethylene and ethanol, the plasma polymerization will occur. Otherwise, if the plasma gas has a strong electron affinity, such as oxidizing gas, air, CF_4 or SF_6, the plasma will have a strong ablation tendency [27].

Plasma surface modification of fibers and their application in fiber reinforced composites is widely used from the 1980s. The relations among chemical composition, structure, surface morphology, and mechanical properties of interphases as a function of parameters of plasma treatment has been studied by different research groups. Plasma

surface treatment of carbon fibers has been studied using air, O_2, CO_2 and NH_3 plasmas, and plasma polymers have been deposited using dioxane and xylene; acrylonitrile and styrene; aniline, pyridine, and benzene monomer [6]. Sun *et al.* [28] continuously treated PAN-based carbon fibers by means of a cold plasma. It was reported that the interlaminar shear strength of carbon fiber reinforced epoxy composites was increased, while debonding and fiber pull-out from the matrix did not occur. J.P. Boudou *et al* [29] treated pitch-based carbon fibers using microwave oxygen plasma under different microwave power and exposure time. It was found that very gentle plasma exposures were generally sufficient to provide the fiber surface with a large amount of oxygen functional groups and surface roughness exhibited moderate increase at nanometer scale. Farrow *et al.* [30] reported that a continuous treatment of a tow of carbon fibers by low-power air plasma is capable of increasing fiber-resin adhesion to levels comparable to those obtained by commercial electrochemical treatments. Lefebvre *et al* [31] found that carbon fibers subjected to surface treatments by plasma polymerization of nitrogenated compounds did not show improvement in the adhesion with epoxy, indicating a probable degradation of the fiber during plasma treatments. Heisey *et al* [32] concluded that carbon fibers become more wettable after oxygen plasma treatment. The oxygen plasma results in the generation of atomic oxygen, which attacks the surface of the carbon fiber. Since pitting is not observed after treatment, the mechanisms of oxidation in oxygen plasma are the simultaneous attack of edge and basal plane carbon atoms, a peeling off of one complete outer basal plane layer after another [8]. Oxygen plasma causes carbon atoms in the hydrocarbon to change into C-OH, C-OOH, C-OC and C=O groups, the concentration of

these groups increases with time but finally reaches a constant level. Gogoeva *et al* treated high modulus (HM) carbon fibers with pulse-voltage excited air, oxygen, nitrogen and acrylonitrile plasmas. They reported that oxygen- and nitrogen-containing species are generated on the surface under plasma treatment without significant changes in the fiber morphology. Comparable interfacial shear strengths are found, with a highest value of 61.4 MPa for air-plasma-treated fibers. The surface chemistry of the fibers was found to influence the degree of epoxy consumption at the earlier stages of the cure process.

To conclude, plasma treatment has been proven to be an efficient environmental friendly method for carbon fiber surface treatment. Since plasma treatment is a process of surface modification, the bulk properties of the fiber are maintained. Plasma surface treatment has the following functions that are important to improve adhesion between fiber and polymer matrix: 1) The removal of surface contamination. 2) The creation of polar groups on the surface that provide a high surface energy resulting in a better wettability. 3) The creation of reactive groups on the surface of the fiber, allowing covalent bonding between the fiber and the resin.

2.3 Characterization of Carbon Fibers

The degree of adhesion between the fiber and polymer matrix depends considerably on the quality and state of carbon fiber surface. A complete characterization and knowledge of surface chemistry as well as morphology and surface structure on the

micrometer and nanometer scale are essential for improving the adhesion between carbon fiber and matrix.

2.3.1 Chemical Characterization

- **Elemental composition and functional groups by X-ray photoelectron spectroscopy (XPS)**

Extensive research work has been undertaken to study the surface chemistry of carbon fibers prepared by different manufacturing methods and surface treatments. X-ray photoelectron spectroscopy (XPS) is one of the commonly used techniques to investigate the surface chemistry of carbon fiber. XPS measures the kinetic energy of electrons emitted from atoms under the influence of irradiation with x-rays. The kinetic energy of the electrons emitted is related to the binding energy of core electrons excited by the X-rays. This, in turn, depends on the chemical environment of the atoms that emit the electrons. Thus by measuring the kinetic energy of the emitted electrons, the magnitude of the binding energy of an electron can be obtained directly. The variation in binding energy of the electron with the environment of the atom gives rise to different peaks in the XPS spectrum, with varying intensity for the same atom depending on the nature of the atoms to which the emitting electron is attached. The small sampling escape depth of electrons from a solid material limits the analysis to the very surface (less that 10 nm) of the analyte.

For carbon fiber, the XPS spectra show distinct carbon and oxygen peaks, representing the major constituents of the carbon fibers. Relatively weak peaks of other

major elements such as nitrogen will also be observed. After surface treatment, oxygen-containing groups are introduced; the shape of C1s and O1s peak will become broad and asymmetrical, and a chemical shift occurs, indicating the presence of more than one type of oxygen on the carbon fiber surface. The broad carbon peak can be attributed to several carbon-based surface functional groups, which have different binding energies. The peak can be deconvoluted using a peak analysis procedure, which fits the measured peak to several Gaussian peaks. Figure 2-7 shows an example deconvolution of the C 1s peak area into surface functional groups for a surface treated carbon fiber [33].

Sherwood *et. al.* [34-43] reported many studies of the effect of electrochemical oxidation of carbon fiber surfaces using XPS. In each case it was found that this type of treatment leads to a greater degree of surface functionality. The type and concentration of functional groups were determined. In the case of plasma treatment, similar increases in oxygen content were obtained by Farrow *et al.* [30] using low-power air plasma, by Dilsiz *et al.* [40]using dioxane and xylene plasma polymerization, and by Okhusen et al. using CO_2 and NH_3 plasmas [45].

Most XPS studies on the surface chemistry of carbon fibers show one main graphitic peak at 284.7 eV [46] as shown in Figure 2-7 and four "oxide" peaks. Oxide 1 at ~286.3 eV is assigned to the carbon atom in alcohol or ether groups. The C1s signal from C=N groups also falls in this range. Oxide 2 at ~287.7 eV is assigned to the carbon atom in carbonyl groups, carboxyl or ester groups are assigned to peak 3 at 289.4 eV. Oxide 4 at ~290.6 eV can be a combination of ionized carboxyl and the π-π shake-up satellite. Xie Y *et al.* [47] investigated the effect of microwave plasma treatment on

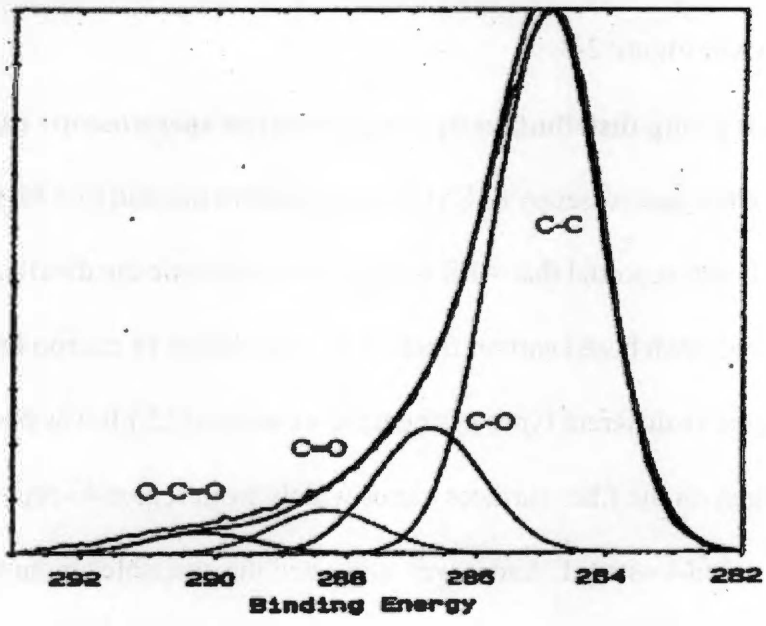

Figure 2-7. Deconvolution of the C 1s peak area into surface functional groups [33]

Pitch-based carbon fiber surfaces. It was found that microwave air-plasma treatment increases various functional groups on carbon fiber surfaces. The greatest increase is found in –COH and /or -C-O-C- functionality, with substantial –C=O functionality as well. Some –C-N functionality also results. Sherwood [47-50] found that the valence band XPS spectra of carbon fibers are a useful probe of surface chemical changes since the valence band region is more sensitive to chemical changes than the core regions Based on experimental results obtained by XPS, Nakayama *et al.* suggested that oxidative treatment may completely destroy the graphite-like structure of carbon fiber and convert it into an aliphatic structure. The carbon fibers were treated by an electrochemical

treatment [51]. The schematic illustration of the graphite-like and aliphatic model structures is shown in Figure 2-8.

- **Functional group distribution by Auger electron spectroscopy (AES)**

Auger electron spectroscopy (AES) is an alternative method to XPS for chemical surface analysis. It was reported that AES was used to determine the distribution of oxygen on PAN and pitch based carbon fibers with a resolution in micron level, which were surface treated by different types of chemical oxidation [52.] It was observed that formation of oxygen on the fiber surfaces varies widely from region-to-region, segment-to-segment, and strand-to-strand. And it was suggested the available amounts of surface oxygen are dependent on the fiber structure, as well as the precursors. However, the spatial distribution of different types of functional groups on a nanometer scale, which is related to fiber surface morphology, has not been studied.

The common microstructural features on carbon fiber surface are periodic ridges and valleys. It has been suggested that the characteristics of the ridges of the carbon fibers may be related to the capability of implanting chemical groups during surface treatment of the fibers. The dimensions of ridges on the carbon fiber surface fall into a range from 100nm to a few hundred nm in width, while the height of these ridges is less than two hundred nanometers. The technique, which can provide information regarding the placement of functional groups, has to satisfy three requirements: 1) surface technique whose depth of analysis is in a range of a few nanometers, i.e. the top atomic layers. 2) surface technique that can provide elemental composition and identify chemical

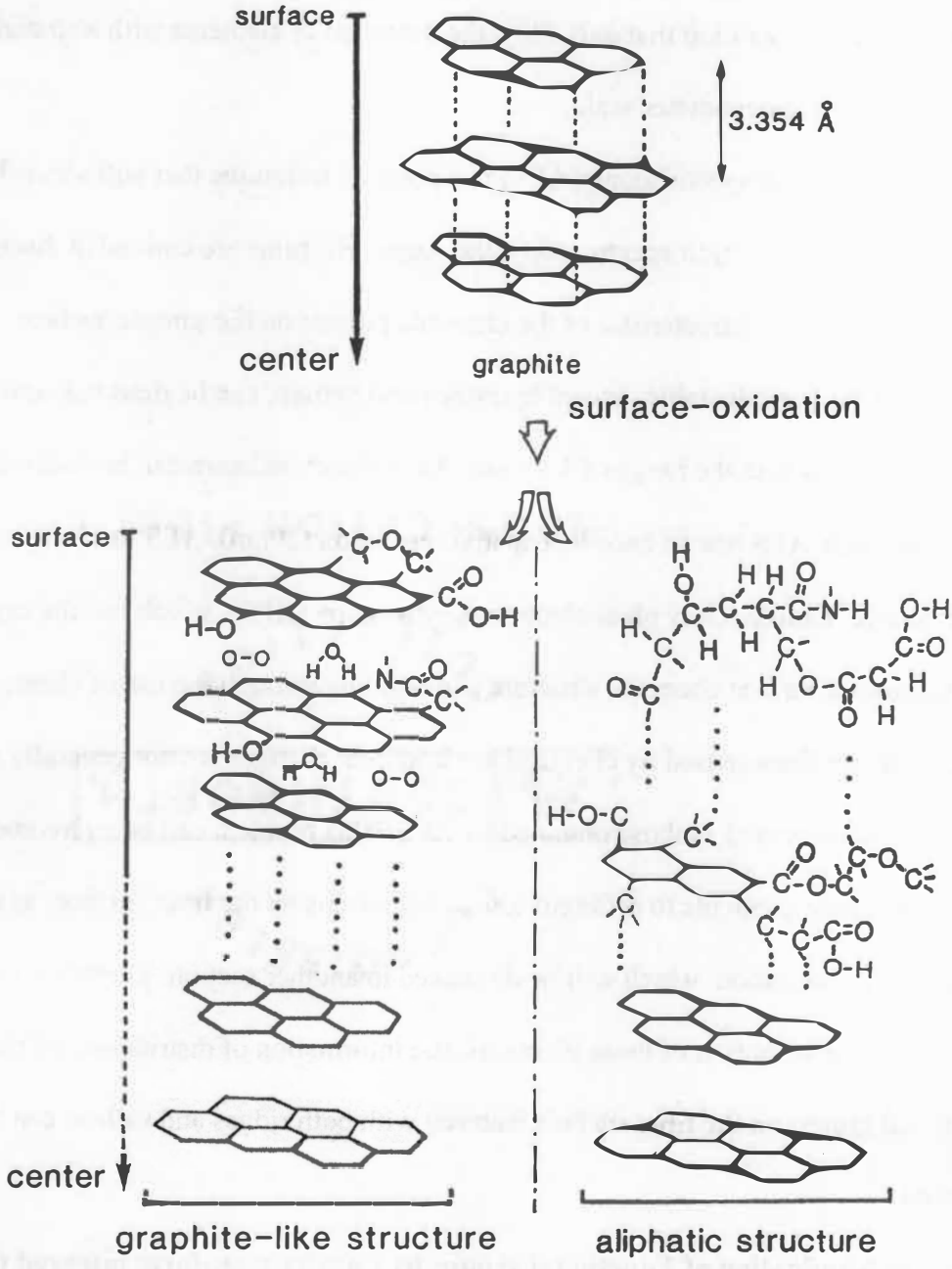

Figure 2-8. Schematic illustration of the graphite-like model and the aliphatic model for surface structure of the treated CF [51]

states of the elements present on the sample surface. 3) technique should possess excellent spatial resolution that will allow the detection of elements with a spatial resolution down to nanometer scale.

Auger electron spectroscopy (AES) is a possible technique that will serve this purpose. In Auger electron spectroscopy, the Auger electrons are emitted at discrete energies, which are characteristic of the elements present on the sample surface. All elements in the periodic table, except hydrogen and helium, can be detected, and the depth of analysis is in the range of 3 - 5 nm. As the electron beam can be focused to a very small size, AES has an excellent spatial resolution (20nm). AES has its own disadvantage. Unlike X-ray photoelectron spectroscopy (XPS), which has the capability of determining surface chemical structure and bonding through the use of chemical shifts, shifts in Auger lines caused by chemical environment changes are not generally as large or as well-documented as those obtained by XPS. This problem can be overcome by attaching certain elements to different functional groups on the fiber surface, so called chemical derivatization, which will be discussed in another section. Therefore by detecting the distribution of those elements, the information of distribution of chemical functional groups on the fiber surface featured with both ridges and valleys can be obtained.

- **Determination of Functional groups by Fourier transform infrared (FTIR) spectroscopy**

Fourier transform infrared (FTIR) spectroscopy has also been used to study the carbon fiber surfaces after surface treatment. Unlike XPS, which does not offer detailed

molecular information since only the nearest-neighbor information is detected, FTIR spectroscopy provides direct information regarding the type of functional groups placed on the surfaces as a result of surface treatment. But the black carbon fibers strongly absorb and scatter infrared radiation, so that surface characterization using FTIR is very difficult. Ohwaki *et al* [53] reported using FT-IR internal reflection spectroscopy to investigate carbonyl groups located on commercially surface-treated unsized PAN-based carbon fiber. They found maximum peak area occurred when polarized light was used at an angle of incidence of 34°. Takahagi and Ishitani [54] used FTIR reflection-absorption spectroscopy (FTIR-RAS) to try to confirm the functional groups on the carbon fiber surface observed by the XPS measurement. The difference spectrum between the treated fiber and the control fiber is shown in Figure 2-9. The peak was assigned to the carbonyl stretching vibration of carboxyl groups directly combined to an aromatic ring. The FTIR micro-ATR technique was used to analyze the functional groups on pitch-based activated carbon fibers by Shin *et al.* [55] IR spectra, shown in Figure 2-10, indicated different types of functional groups summarized in Table 2-2.

2.3.2 Chemical Derivatization

XPS studies provide some information about functional groups on treated carbon fiber surface. However, it is difficult to distinguish between two functional groups with a small chemical-shift difference, e.g., between carboxylic and ester groups, or hydroxyl

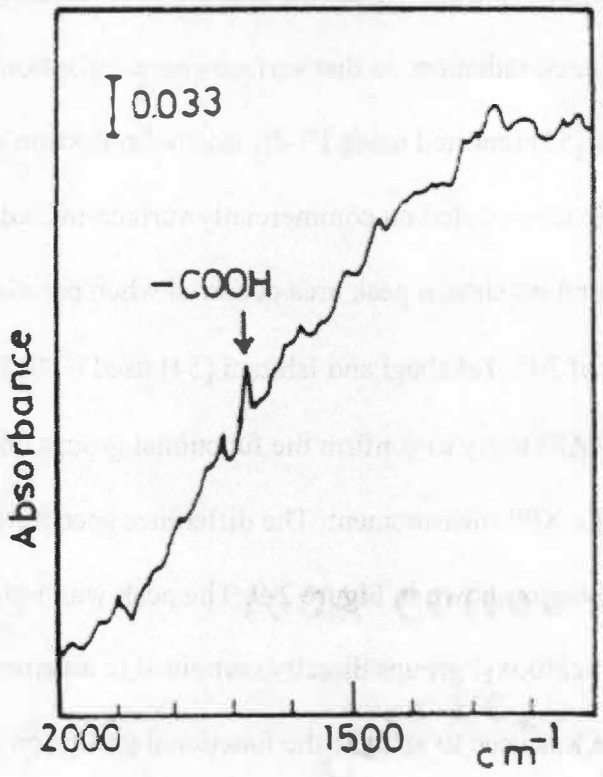

Figure 2-9. FTIR-RAS digital difference spectrum for CF before and after treatment [54]

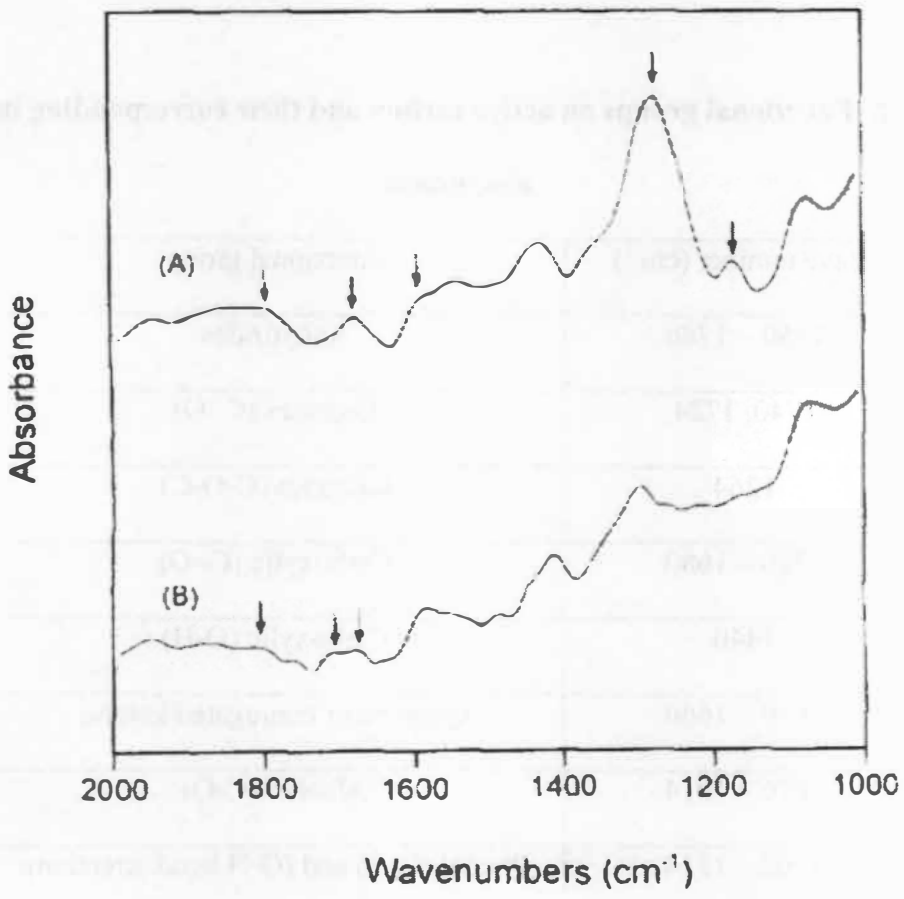

Figure 2-10. Micro-ATR spectra of the pitch based active carbon fiber [55]: (A) high treatment level; (B) low treatment level

Table 2-2. Functional groups on active carbon and their corresponding infrared assignment

Wave number (cm^{-1})	Functional group
1850 – 1786	Anhydrides
1740, 1724	Lactones (C=O)
1264	Lactones (C-O-C)
1710 – 1680	Carboxylic (C=O)
1440	Carboxylic (O-H)
1670 – 1660	Quinone or conjugated ketone
1076 – 1014	Alcohol (C-O)
1162 – 1114	Phenol (C-O) and (O-H bend/stretching
1250 - 1235	Ether bridges between rings

and ether groups, although we know carboxylic and hydroxyl groups are far more important for adhesion than esters and ethers because the former groups can react with the matrix to form chemical bonds. Chemical derivatization is a possible solution to this problem. The concept of chemical derivatization is to label a functional group of interest selectively with an element, which is not present in the original material and has a large cross section for XPS or AES detection. D.S.Everhart *et al.* [59] used trifluoroacetic anhydride (TFAA), tetrafluorophenylhydrazine (TFPH) and trifluoroethanol (TFE) to label carbonyl, carboxyl and hydroxyl groups. The three kinds of chemical modification reactions are shown in Figure 2-11. TFAA reacts with both the carboxyl and hydroxyl groups. TFPH and TFE selectively react with carbonyl and carboxyl groups, respectively. T.Takahagi and A.Ishitani [60] used this technique for examining surface functional groups of carbon fiber.

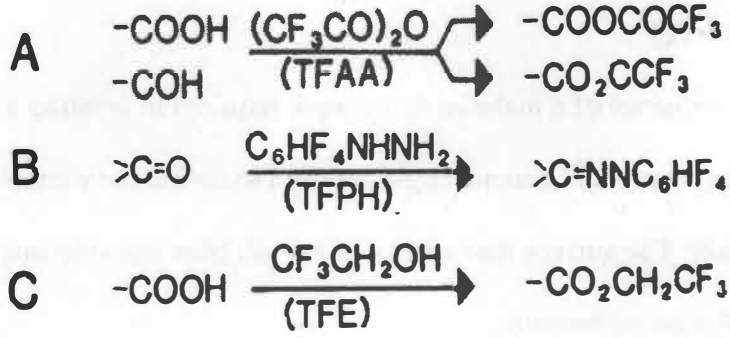

Figure 2-11. Chemical modification reactions used for examining surface functional groups of carbon fibers [60]

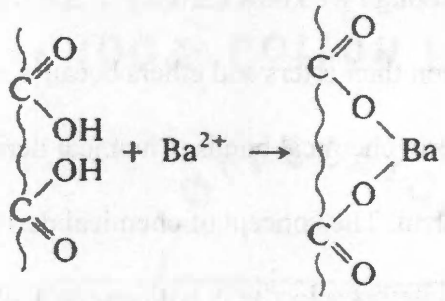

Figure 2-12. Barium labeling of carboxylic acid group [61]

Denison *et al.* [61] developed barium labeling procedure to quantitative analysis of carbon fibers. The fibers were labeled with barium ions to determine the surface carboxylic acid concentration, through the reaction illustrated in Figure 2-12.

In the labeling reaction, dibasic Ba^{2+} will bind to two adjacent COOH groups to form a relatively stable system, which permits the removal of excess reagent by washing in water without resulting in a loss of metal atoms, which are bound to these groups.

2.3.3 Surface Energy

Surface free energy of a material is the work required in creating a new surface. Both surface free energy and contact angle are used to define the wettability of one material to another. The surface free energy of carbon fiber can split into two components, polar and dispersive:

$$\gamma = \gamma^p + \gamma^d \qquad (2.8)$$

The introduction of oxygen-containing functional groups on carbon surface provides a higher surface energy and thus, allows an easy wetting of the fiber by the polymer matrix.

Bismarck *et al.* [62] investigated the influence of oxygen plasma treatment of PAN-based carbon fibers on their surface free energy. They reported that the surface free energy increases continuously with increasing treatment time up to 20 min. However, γ^d was drastically diminished to a constant value for the treated fibers compared to the untreated fibers; the polar part γ^p of the surface energy increased much more strongly. These results are shown in Table 2-3. It is believed that γ^d reflects the essential surface characteristics of carbon fibers or the graphitic structure of the fiber surface [63]. They concluded that the graphitic surface structure was disrupted by the bombarding species of the plasma.

Table 2-3. Surface energy of treated carbon fibers [63]

Plasma-treated carbon fibers (min)	γ (mN/m)	γ^p (mN/m)	γ^d (mN/m)
0	37.5 ± 2.3	10.0 ± 1.7	27.5 ± 1.7
1	47.4 ± 2.9	27.7 ± 0.2	19.7 ± 0.2
5	49.4 ± 1.2	30.8 ± 0.6	18.6 ± 0.6
10	53.4 ± 2.6	34.2 ± 0.8	19.2 ± 0.8
20	57.9 ± 3.3	39.4 ± 0.5	18.5 ± 0.5

2.3.4 Morphological Characterization

Surface morphology of carbon fibers varies with the precursor and manufacturing process; and influenced by surface treatment. Surface morphology and topographical features are contributing factors to fiber-matrix adhesion. Studies on correlations between carbon fiber morphology and fiber-matrix adhesion will help separate the various factors that contribute to adhesion in a carbon fiber composite system.

Different structure models for carbon fiber have been proposed. According to Johnson [2] carbon fiber has a three dimensional model shown in Figure 2-13. It shows a difference in ordering and density of the carbon ribbons or micro-crystallites between the peripheral zone, nearing the surface, and the case of the fiber. PAN-based carbon fiber has a circular or kidney-shape appearance. Many obvious striations and some small pits can be seen on the fiber surface [64]. Roughness and surface area of treated carbon fibers may be correlated with the mechanical properties of composites according to mechanical interlocking theory. In addition, the surface structure of carbon fiber affects its physicochemical properties because the reactivity of carbon atoms with unsatisfied valence at edge sites is greater than that of carbon atoms in the basal planes. In other words, these roughness and pits may become reactive sites during surface treatment of polymer addition.

Morphological information can be obtained on both micron and nanoscale using scanning electron microscope and scanning tunneling microscope, respectively. Morphology and surface structure on the micron scale have been extensively studied by

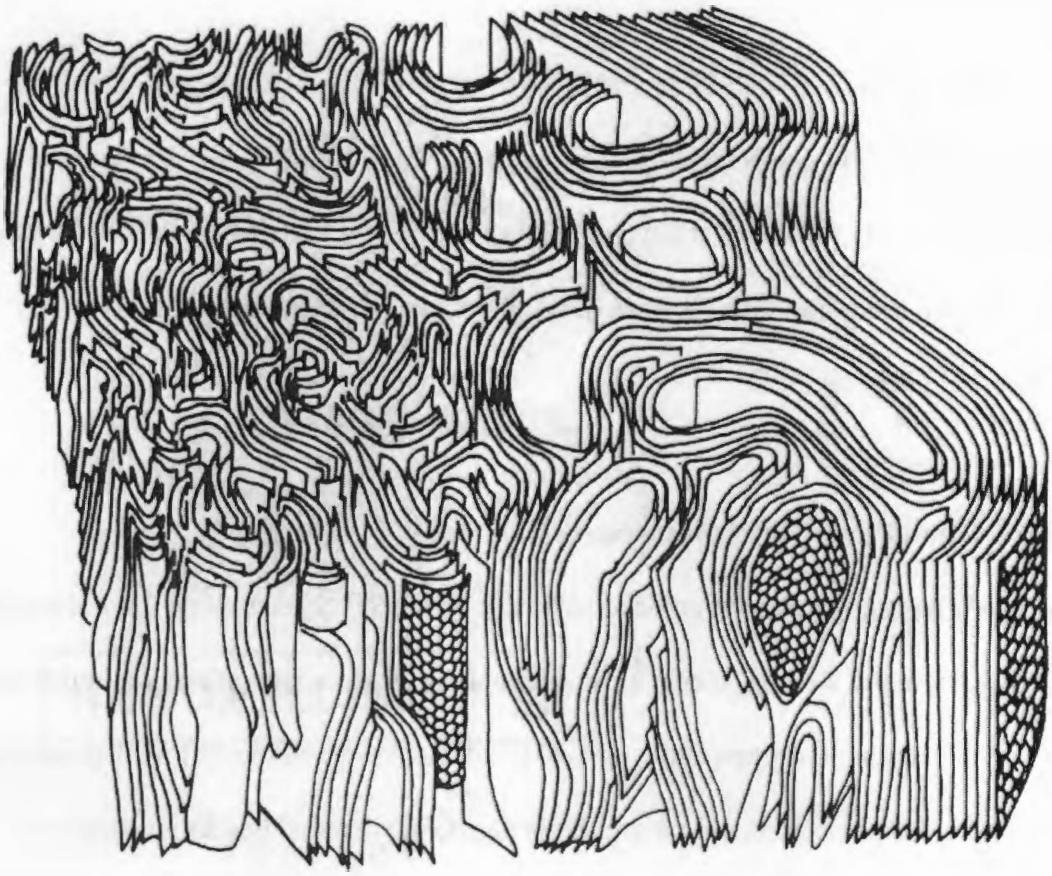

Figure 2-13. Carbon fiber three-dimensional model [2]

SEM [65-75]. Results on the surface structure on the nanoscale have also been published [76-79].

Zielke [79] used both SEM and STM to study the surface structure of various surface oxidized HT (high tenacity) carbon fibers. They observed, on the nanoscale, there are large graphitic regions that have not been observed on PAN fibers before. Drzal [80] used STM to investigate the changes of roughness and surface area with increasing surface treatment level.

2.3.5 Carbon Fiber-Matrix Interphase Chemistry

Adhesion in general can be attributed to mechanisms including, but not restricted to, adsorption and wetting, mechanical interlocking, electrostatic attraction, molecular entanglement, and hydrogen and chemical bonding. As one of the factors that contribute to adhesion between fiber and polymer, the nature of chemical bonding formed in interphase region i.e. the interphase chemistry has to be understood.

There are a number of investigative techniques available that provide useful information about the fiber/matrix interface. For example, mechanical tests (interlaminar shear strength (ILSS) give a measure of the strength of the interfacial adhesion; while the high resolution transmission electron microscopy (TEM) provides directly an image of the interface [81]. The information obtained by these techniques can be correlated with different manufacturing processes and surface treatments, thus combined with information from chemical characterization of fiber surface to determine main adhesion mechanisms at interphase region. However, this is not the best scenario since direct

information regarding the mechanism of chemical reaction, i.e., chemical bonding between fiber and matrix is not available. FTIR microscopy has been successfully used to investigate the interphase of epoxy-glass composite [82]. But in the case of carbon fiber, since the diameter of carbon fiber is much less than glass fiber and concentration of functional groups on the carbon fiber surface is much lower than the one on glass fiber, detailed spectroscopic information concerning the interphase chemistry cannot be obtained by conventional FTIR microscopy. A new technique to be chosen should be able to probe materials on scale level of a few microns or less. Moreover, this technique should be able to enable detailed analysis of the spatial distribution of chemical species at the fiber-matrix interphase and allows the *in situ* analysis of the interphase region. The coupling of micro-FTIR to a focal plane array detector (FPAD) has the potential to meet all these requirements. This technique allows the IR spectra to be taken from each pixel of the FPAD simultaneously. A plot of intensity at one frequency for all pixels will result in a chemical image of the sample area, i.e., a spatial distribution of that specific functional group. The best spatial resolution achieved under reflection/transmission mode is 5.5 micron, while under ATR mode is 1.4 micron, which means that individual spectra can be from as small as 5.5μm and 1.4μm square area, respectively. This level of spatial resolution would allow chemical imaging along regions of pure fiber, interphase region, pure polymer matrix. In addition, the use of micro-FTIR in conjunction with a focal plane array detector permits *in situ* imaging, i.e., an image of the spatial distribution of the functional groups prior, during and after the formation of the chemical bonds, which will

help understand the reaction kinetics. This technique was used in this research to provide information regarding the nature of interphase chemistry.

CHAPTER 3

THEORETICAL BACKGROUND

3.1 X-Ray Photoelectron Spectroscopy (XPS)

X-Ray Photoelectron Spectroscopy (XPS) is also known as Electron Spectroscopy for Chemical Analysis (ESCA). It utilizes photo-ionization and energy-dispersive analysis of the emitted photoelectrons to study the composition and electronic state of the surface region of a sample. This excitation with photons is shown in Figure 3-1

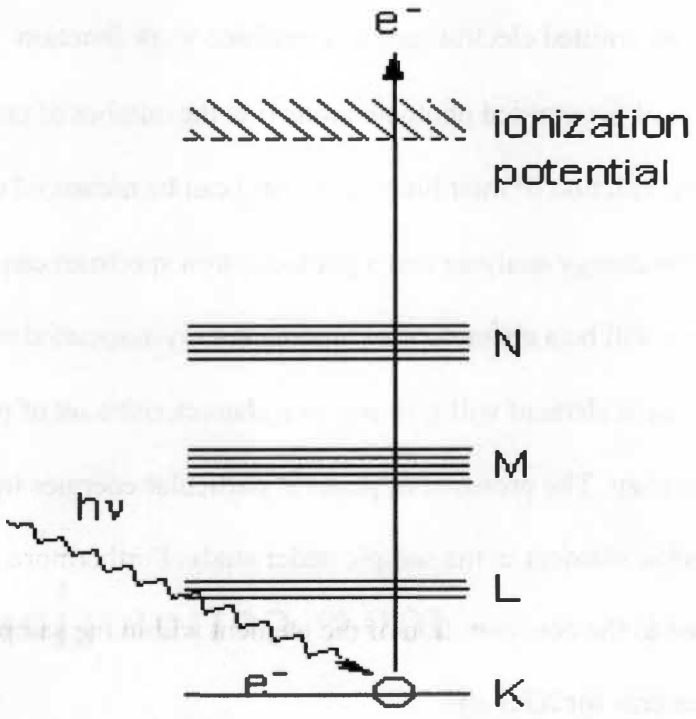

Figure 3-1. Scheme of excitation of photoelectrons in XPS [86]

Based on Einstein's Photoelectron effect, bombarding molecules or atoms with high energy x-rays caused the emission of core level electrons. The energy of these electrons is measured and their values provide information about the nature and environment of the atom from which they came. This photoelectron process is described by the following relationship:

$$BE = h\nu - KE - \phi \qquad 3.1$$

where BE is the binding energy, $h\nu$ is the energy of the x-ray photon, KE is the measured kinetic energy of the emitted electron and ϕ is machine work function. The binding energy distribution of the emitted photoelectrons (i.e. the number of emitted photoelectrons as a function of their binding energy) can be measured using any appropriate electron energy analyzer and a photoelectron spectrum can be recorded. For each element, there will be a characteristic binding energy associated with each core atomic orbital i.e. each element will give rise to a characteristic set of peaks in the photoelectron spectrum. The presence of peaks at particular energies indicates the presence of a specific element in the sample under study. Furthermore, the intensity of the peaks is related to the concentration of the element within the sampled region.
The basic requirements for XPS are:

1. a source of x-ray radiation with fixed energy

2. an electron energy analyzer (which can disperse the emitted electrons according to their kinetic energy, and measure the flux of emitted electrons of a particular energy)

3. a high vacuum environment (to enable the emitted photoelectrons to be analyzed without interference from gas phase collisions)

Such a system is illustrated schematically in Figure 3-2.

Although the x-rays penetrate much deeper, photoelectrons that are detected only escape from the top 10 nm. Photoelectrons from deeper within the sample usually have multiple collisions and do not make it out of the sample or show up as background in the spectrum. XPS is particularly useful because information related to chemical shifts can be extracted from the observed binding energies. The chemical binding of valence electrons cause a shift in the binding energy of the core electrons. Therefore, the measured binding energy gives information about the chemical environment of the atom. Positions of shifted peak positions for different elements are well documented and the functional group associated with a particular binding energy can be determined.

3.2 Auger Electron Spectroscopy

Auger electron spectroscopy (AES) identifies elemental compositions of surfaces by measuring the energies of Auger electrons. AES is based upon the measurement of the kinetic energies of the emitted electrons. Each element in a sample being studied will give rise to a characteristic spectrum of peaks at various kinetic energies. An Auger

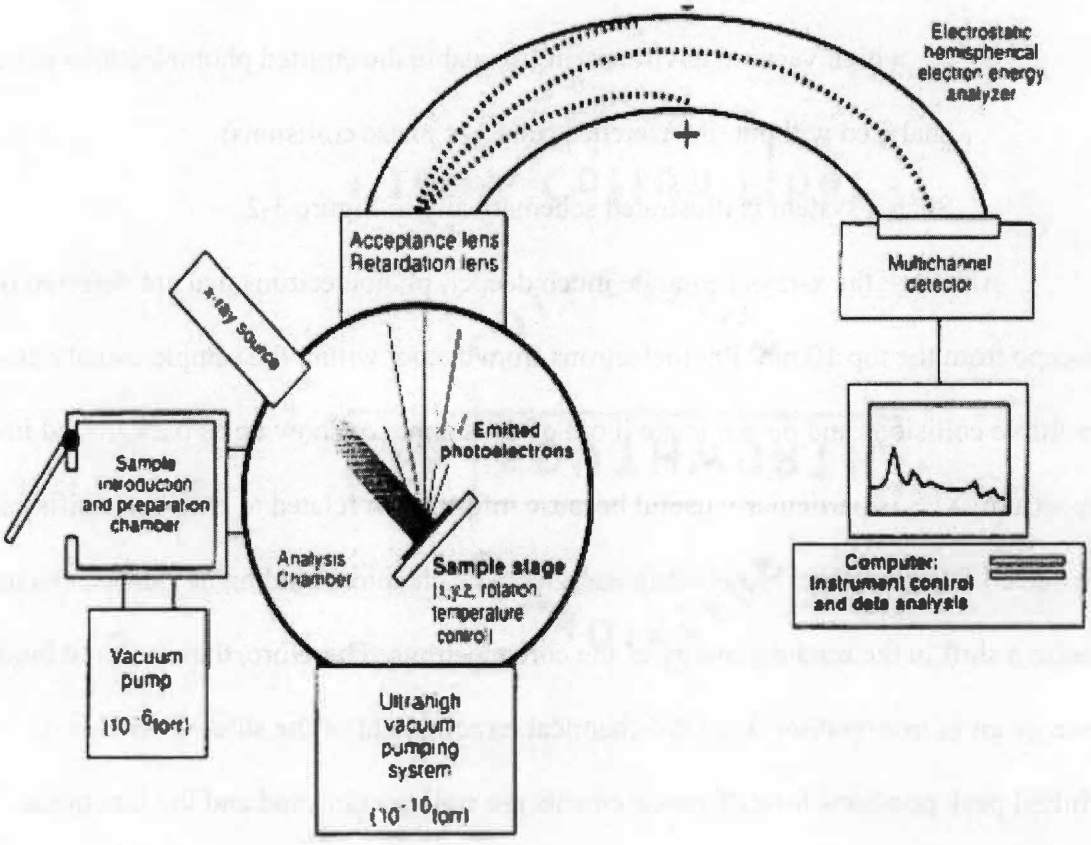

Figure 3-2. Schematic representation of a XPS set-up [87]

spectrum plots a function of electron signal intensity versus electron energy. Figure 3-3 shows Auger process.

The Auger process is initiated by creation of a core hole - this is typically carried out by exposing the sample to a beam of high energy electrons (typically having a primary energy in the range 2 - 10 keV). Such electrons have sufficient energy to ionize all levels of the lighter elements, and higher core levels of the heavier elements. The ionized atom that remains after the removal of the core hole electron is in a highly excited state and will rapidly relax back to a lower energy state by one of two routes [88]:

1. X-ray fluorescence
2. Auger emission

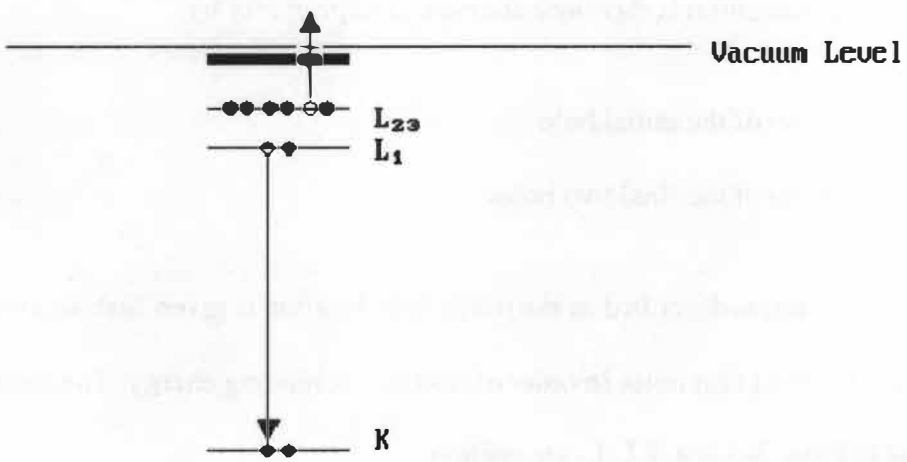

Figure 3-3. Scheme of excitation and relaxation processes of Auger effect [88]

We will only consider the latter mechanism. As shown in Figure 3.3, one electron falls from a higher level to fill an initial core hole in the K-shell and the energy liberated in this process is simultaneously transferred to a second electron; a fraction of this energy is required to overcome the binding energy of this second electron, the remainder is retained by this emitted Auger electron as kinetic energy. In the Auger process the final state is a doubly-ionized atom with core holes in the L_1 and $L_{2,3}$ shells.

The KE of the Auger electron can be estimated from the binding energies of the various levels involved. In this particular example,

$$KE = (E_K - E_{L1}) - E_{L23} \qquad 3.2$$

An Auger transition is therefore characterized primarily by:

1. the location of the initial hole
2. the location of the final two holes

The transition is described as the initial hole location is given first, followed by the locations of the final two holes in order of decreasing binding energy. The transition illustrated in Fiber 3-3 is a $KL_1L_{2,3}$ transition.

In general, since the initial ionization is non-selective and the initial hole may therefore be in various shells, there will be many possible Auger transitions for a given element - some weak, some strong in intensity. Auger electrons fail to emerge with their characteristic energies if they start from deeper than about 1 to 5 nm into the surface.

Thus, Auger analysis is surface specific. Auger electrons that escape from deeper in the sample contribute loss tails to the spectrum background.

Compared to XPS, the major advantage the AES possesses is the high spatial resolution since high energy electron beam instead of x-ray radiation is used as the probe. Therefore, AES can be used for determining the composition of a surface, mapping the spatial distribution of the surface constituents.

3.3 FTIR Imaging

The combination of a Focal Plane Array (FPA) detector with a step-scan spectrometer is the state of art in FTIR microspectroscopy instrumentation.

The concept of imaging using an FPA is illustrated with a typical example in the Figure 3-4. The beam of a step-scan spectrometer is diverted through standard microscope optics with the FPA at the end of the optical train. Each pixel on the FPA corresponds to a unique spatial region on the sample. The time required to collect a spectrum for a single pixel is the time required collecting the whole image.

Contrary to FTIR mapping in which image is built up point-by-point, FTIR imaging is used to describe the collection of a chemical profile of the sample area in a single experiment [89]. The major instrumental difference between a mapping and an imaging instrument is the incorporation of a Focal Plane Array detector at the end of the optical train in the microscope. Average chemical information (i.e. the infrared spectrum)

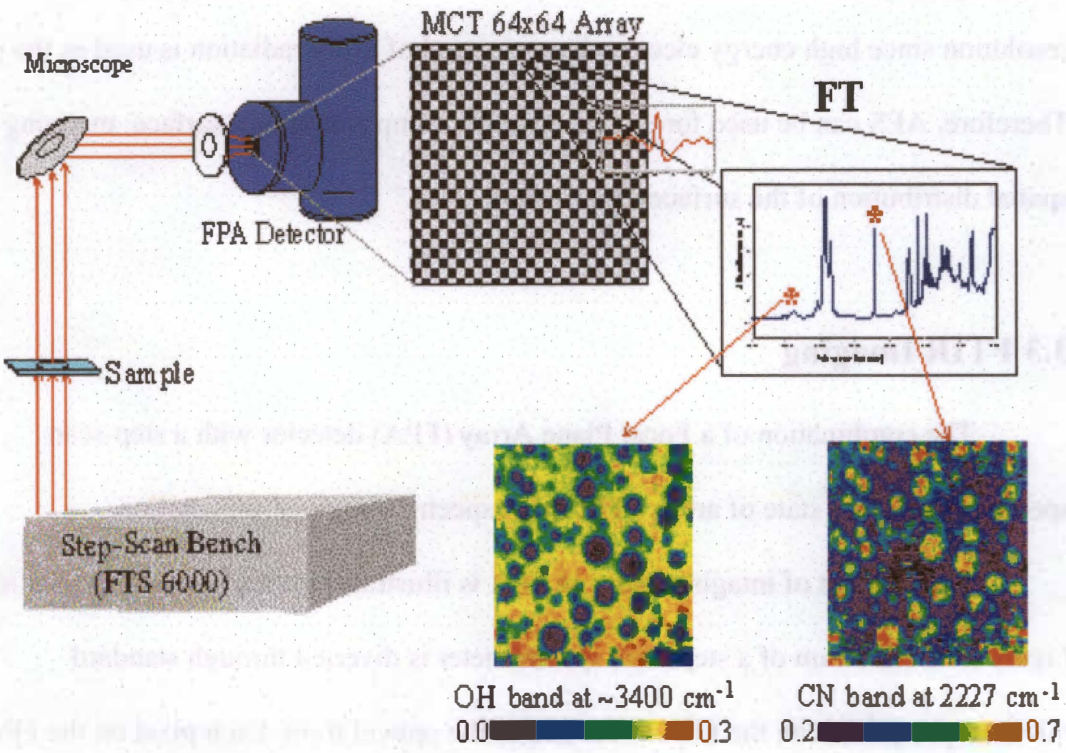

Figure 3-4. Scheme of principle of FTIR imaging system

of a specific spatial area on the sample can be uniquely correlated to the output of a pixel in the FPA [89]. Hence, no apertures are required to limit the sample area examined.

Moreover, the sample does not need to be moved as a given field of view is imaged in a single collection experiment. It may be immediately seen that the collection time is decreased by a factor of n^2, where n is the number of spatial resolution elements in one direction of a square sample area imaged (n is the number of steps in a mapping experiment considered equivalent to a pixel in the imaging experiment). Moreover, the practical spatial resolution limit in the mapping technique is close to 10 microns. For imaging, the resolution is essentially wavelength limited and governed by the following relationship:

$$R = 1.22 \lambda / 2 n \sin \theta \qquad 3.3$$

λ: Probe wavelength, $2 n \sin \theta$ = NA

n: Refractive index of medium

θ: half-cone angle of light captured by the objective

In Transmission mode

e.g. λ: 10 μm (=1000cm^{-1}), n: 1(air), θ: 30°

R = 1.22 x 10 / (2 x 1 x 0.5)= 12.2 μm

In ATR with a Ge IRE (Internal Reflection Element)

e.g. λ: 10 μm (=1000cm^{-1}), n: 4 (Ge), θ: 30°

R = 1.22 x 10 /(2 x 4 x 0.5) = 3.1 μm

Hence, the imaging technique has allowed for the collection of images in faster time with higher resolution.

CHAPTER 4

EXPERIMENTAL PROCEDURES

4.1 Materials

PAN based carbon fibers produced by conventional process (F3(c) by AKZO Fortafil) and MAP technique were provided by Oak Ridge National Laboratory. Conventional fibers treated with Remote Applicator plasma system (RA) and Atmospheric Plasma system (AP) under different processing conditions were also provided by ORNL for the investigation of effect of plasma activation on carbon fiber surface and interphase with polymer matrix. All fiber tows were stored in vacuum desiccators prior to testing. Processing conditions are summarized in Table 4-1.

4.2 Elemental and Chemical Composition by XPS

A PHI 5000LS spectrometer was used in this study to determine the surface elemental composition of the conventional and MAP processed fibers. This was done by acquiring a full spectrum for elemental analysis based on the binding energy required for the photoelectron to escape. For each sample, a bundle of fiber were cut from the fiber tow and mounted on the sample holder. The samples were 6 to 20 cm long and XPS survey was carried at different locations along the fiber length to investigate the distribution of elemental composition on fiber surface. At least 3 measurements were

Table 4-1. Summary of the initial conditions, as received, and designation of the conventional and MAP samples

Sample	Condition
ConUU	Untreated Unsized Conventional Fiber
ConTU	Treated (ozone) Unsized Conventional Fiber
MAPUU	Untreated Unsized MAP Fiber
MAPTU	Treated (ozone) Unsized MAP Fiber
Conventional Fiber treated by Remote Applicator	
RA-a	80/20 N_2/O_2, 500w, 3min
RA-b	80/20 N_2/O_2, 1kw, 3min
RA-c	80/20 N_2/O_2, 2kw, 3min
RA-d	80/20 N_2/O_2, 2kw, 70sec
RA-e	pure O_2, 1.1kw, 2.0 torr, 3min
RA-f	pure O_2, 2.6kw, 3.0 torr, 3min
RA-g	pure O_2, 1.1kw, 3.0 torr, 70sec
RA-h	50/50 N_2/O_2, 129w, 1.5 torr, 70sec
RA-j	5/95 N_2/O_2, 220w, 1.2 torr, 70sec
Conventional Fiber treated by Atmospheric Plasma	
AP-A	80/20 N_2/O_2 (dry air) for 70 sec

Table 4-1. Continued.

Sample	Condition
AP-B	80/20 N_2/O_2 (dry air) for 3min
AP-C	pure O_2 for 70 sec
AP-D	pure O_2 for 190 sec
AP-E	pure O_2 and water for 90 sec
AP-G	pure O_2 for 75 sec
AP-H	80/20 N_2/O_2 for 75 sec
AP-J	80/20 N_2/O_2 for 3.5 min on both sides
AP-K	80/20 N_2/O_2 and water 60/90 sec on both sides
AP-L	20/80 N_2/O_2 and water 60/90 sec on both sides
AP-O2-130 sec	Pure O_2 130 sec

taken for each sample. The elemental composition can be obtained by comparing the area under each element's peak divided by the sensitivity factors for the XPS instrument. Operating conditions and parameters used on this instrument are:

EV/Step: 0.5 eV

Time/Step: 50 mSec

Vacuum: 10^{-9} Torr

Source: Al

Pass Energy: 89.45 eV

Binding Energy Range: 0-1000 eV

Number of scans: 20

Aperture Size: 0.8mm in diameter

High-resolution scans was taken for C1s to determine functional groups present on the fiber surface. The curve fitting of the XPS spectrum was carried out using a nonlinear-least-squares curve-fitting program with a Gaussian/Lorentzian product function under condition of 0.1eV/Step and 300 scans.

4.3 Chemical Derivatization

Since the high cross section of the metal atoms makes detection and analysis by AES easier and more accurate, we choose to use cobalt acetate to form stable coordination compound with carboxylic group (COOH) present on fiber surface by coordinate covalent bonds. Since the size of ligands is small, cobalt acetate molecules

will have enough penetration ability into the structure of the micropores of fiber to react with those reactive sites located at edges of fiber planes. This approach should provide a more accurate account of the functionalization after exposure to the plasma. Figure 4-1 shows the chemical derivatization reaction used for examining carboxyl groups of carbon fibers. For each sample, approximately 5cm lengths were cut to form the 'labeled' specimens. Solutions containing 105mg cobalt acetate and 75ml distilled water and triethylamine were used for chemical derivatization reaction. Fibers were immersed in the solution and kept in water bath at 75 °C for 4 hours. The treated carbon fibers were washed well with distilled water to remove residual reagents from the surface and dried in vacuum oven at 70°C before the XPS and AES measurement. This process was repeated several times until the cobalt concentration reached a constant level.

4.4 Functional Groups Distribution by Auger Electron Spectroscopy

A PHI 680 Scanning Auger Microprobe was used to study functional group distribution on carbon fiber surface. Experiment was conducted at High Temperature Materials Laboratory (HTML) in Oak Ridge national Laboratory (ORNL).

For each sample, a bundle of fibers were cut into approximately 1 cm long and mounted to the sample holder. The electron beam energy was set to be 20keV to achieve a spatial resolution of 20 nm. After placing the desired fiber surface to the optimum electron imaging position, the surface image was taken to ensure that no substantial charging and background scattering occurred. Prior to AES imaging, a stationary Auger

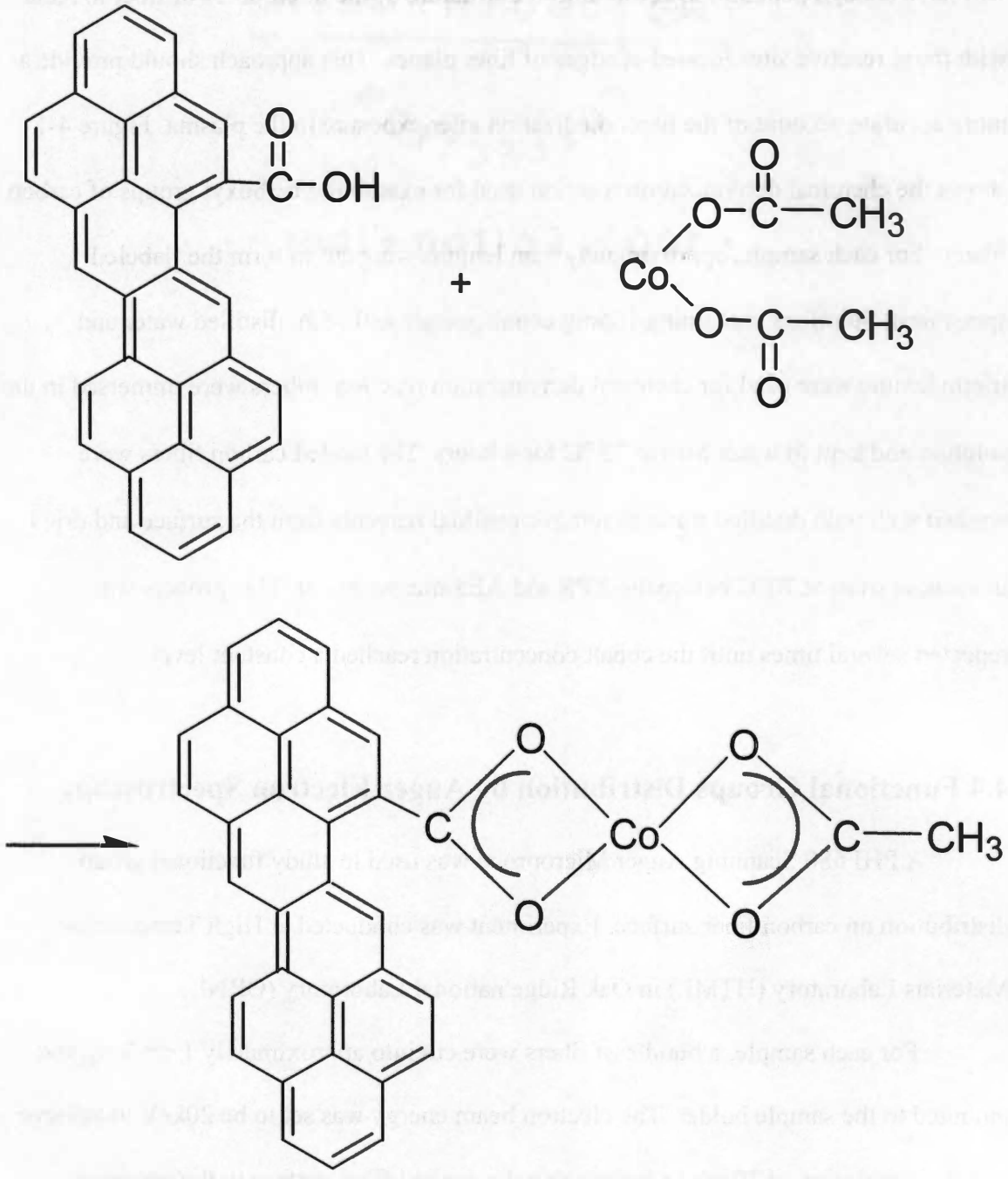

Figure 4-1. Chemical derivatization reaction for examining carboxyl groups of carbon fibers

spectrum of the fiber surface was recorded for the existence of the elements of interest. The peak intensity of carbon, oxygen and cobalt were used to plot two-dimensional display of the direct elemental image. The areas used for point analysis were selected to represent specific morphological features (ridges and valleys) marked in SEM micrograph, the elemental composition corresponding to these specific features were determined separately.

4.5 Interphase Chemistry Characterization by FTIR Imaging Technique

Micro-FTIR coupled with focal plane array detector was used to investigate interphase chemistry between carbon fibers and polyurethane matrix. Experiments were performed by the following instrumentation:

FTS 7000 FTIR Spectrometer

KBr beam splitter

Mid-IR source

UMA 600 Microscope

Lancer 64 x 64 MCT Focal Plane Array

For each sample, fibers with length of around 2 cm were carefully separated and aligned parallel to one direction with both ends fixed on a PTFE plate using double-sided tape. A small volume of a polyurethane solution was dropped on the fibers. Slowly tilt the plane to make sure the solution spread uniformly to form a thin polyurethane layer

with carbon fibers embedded in it. After the sample was dried, a small frame was stuck to the edges of the sample to prevent sample shrinkage. Finally the framed sample was carefully removed from the PTFE plate. The spectra were collected from different areas within the sample and the results provided images of the spatial distribution of the functional bonding.

CHAPTER 5

RESULTS

5.1 Chemical Composition by X-Ray Photoelectron Spectroscopy (XPS)

As stated previously, one of the objectives of this work is to compare the surface chemistry of carbon fibers produced or treated by plasma technology and carbon fibers produced by conventional manufacturing processes.

5.1.1 Chemical composition of conventional carbon fibers

The XPS spectra of untreated, unsized conventional (conventional UU) fibers and ozone treated, unsized conventional (conventional TU) fibers were obtained, which show distinct carbon and oxygen peaks, representing the major constituents of the carbon fibers investigated. Relatively weak peaks of other major elements such as nitrogen and silicon were also observed. No other major elements were detected from wide scan spectra on the surface of these two carbon fibers. XPS wide scan spectra of the two carbon fiber samples are shown in Figure 5-1.

In general, as seen in Figure 5-1, carbon is the dominating component on the surface of all samples, which accounts for over 90% of the untreated unsized carbon fibers, while in most cases over 85% of the treated unsized carbon fibers. Oxygen concentration varies from 2~5% among the untreated unsized samples that were taken off the production line at different dates. The oxygen concentration of treated unsized

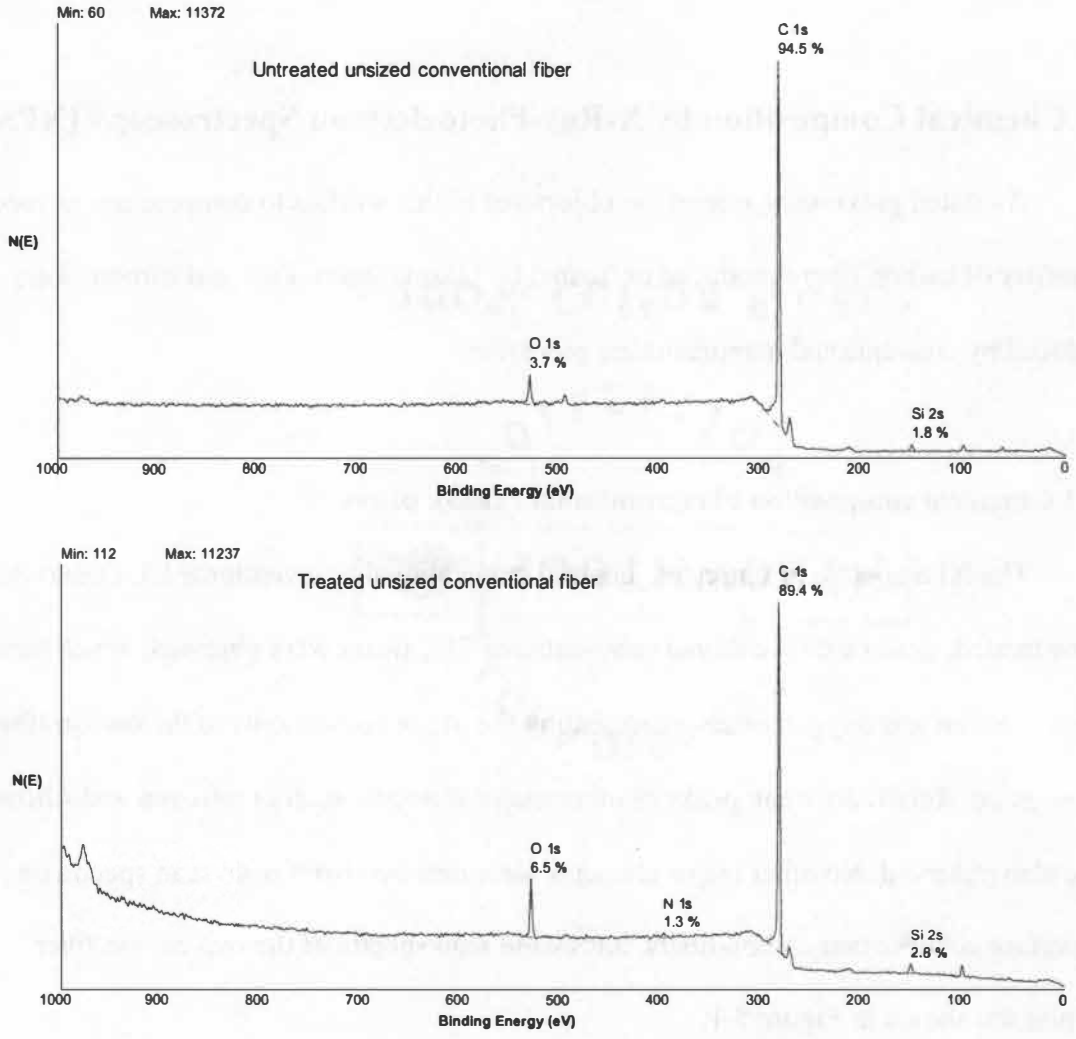

Figure 5-1. XPS spectra of conventional UU and conventional TU carbon fibers

samples shows higher level from 5% to 9%, which can be attributed to formation of oxygen containing groups on the carbon surface due to ozone treatment.

To investigate the elemental distribution along fiber direction on both untreated unsized and treated unsized carbon fibers produced by conventional process, a bundle of fibers with a length of 20 cm were cut from the fiber tow of each sample. An overall XPS spectrum was taken every 1cm. The selected results of both fibers are shown in Table 5-1, 5-2 and Figure 5-2, 5-3.

As seen from the results, the distribution of oxygen concentration along the fiber shows that elemental concentration along the fiber length is not uniform. It varies in a random pattern for both untreated and treated samples. Similar trends were observed in other samples. It is worth to mention that both treated and untreated conventional fibers were received from the supplier at the same time for the best comparison.

5.1.2 Chemical Composition of MAP fibers

XPS experiments were carried out for untreated unsized MAP (MAP UU) fibers and ozone treated unsized MAP (MAP TU) fibers. Same as conventional fibers, carbon, oxygen, nitrogen and silicon are the principal elements detected on the surface of both untreated and treated MAP fibers. The elemental composition varies randomly along the fiber axis. The results are summarized and shown in Table 5-3, 5-4 and Figure 5-4, 5-5.

The concentration of oxygen on MAP UU fibers is on the same level as conventional fibers with surface treatment.

Table 5-1. Distribution of elemental composition on the surface of conventional UU fibers

Elemental Composition of Conventional UU Fibers %				
Positions		O	N	Si
1	87.4	6.0	3.5	3.0
2	93.1	4.9	1.0	1.0
3	89.4	6.1	1.7	2.9
4	93.8	4.1	1.5	0.7
5	92.9	5.1	1.5	0.4
6	93.0	4.0	2.7	0.3
7	96.0	4.0	0	0
8	94.1	3.3	2.6	0
9	90.7	5.4	2.7	1.2
10	89.5	5.6	2.7	2.1
11	87.1	5.5	5.2	2.2
12	94.8	2.6	1.9	0.7
13	91.4	5.1	1.9	1.6
14	89.5	5.5	3.0	2.0
15	93.1	4.2	1.8	0.9
16	93.5	4.2	1.5	0.8
17	95.4	3.5	1.2	0
Average	92.0	4.7	2.1	1.2
STDEV	2.6	1.0	1.1	0.9

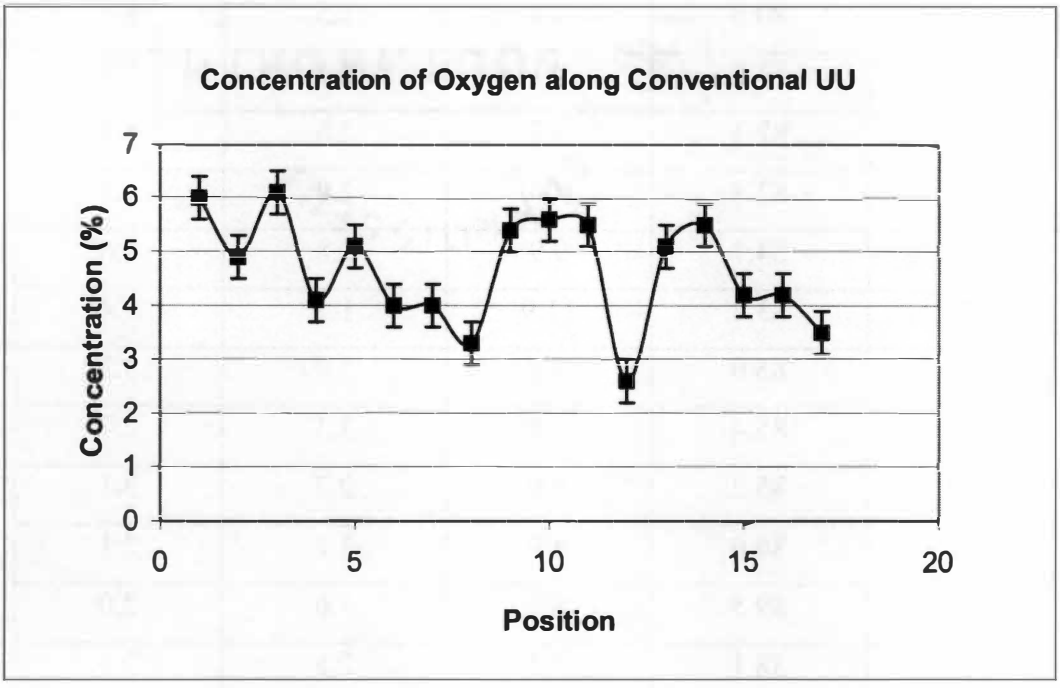

Figure 5-2. Concentration of oxygen along conventional UU fibers

Table 5-2. Distribution of elemental composition on the surface of conventional TU fibers

Elemental Composition of Conventional TU fibers %				
Position				
	C	O	N	Si
1	79.7	9.8	1.4	9.1
2	80.6	9.9	1.5	8.1
3	83.7	9.1	2.1	5.1
4	82.3	9.7	2.6	5.5
5	82.8	10.0	2.9	4.3
6	84.7	9.9	1.8	3.6
7	83.2	11.9	1.5	3.4
8	85.0	9.8	1.9	3.3
9	85.4	8.5	3.3	2.7
10	85.2	9.0	2.7	3.1
11	86.0	8.8	3.1	2.1
12	89.5	6.9	1.6	2.0
13	88.1	7.2	2.1	2.5
14	87.5	7.0	2.5	3.0
15	88.4	6.7	2.7	2.2
16	88.0	6.5	2.7	2.8
17	85.7	8.4	2.6	3.3
18	86.2	6.7	4.5	2.7
19	89.3	6.5	1.6	2.6
20	86.9	8.6	0	4.6
Average	85.4	8.6	2.23	3.8
STDEV	**2.7**	**1.5**	**0.9**	**1.9**

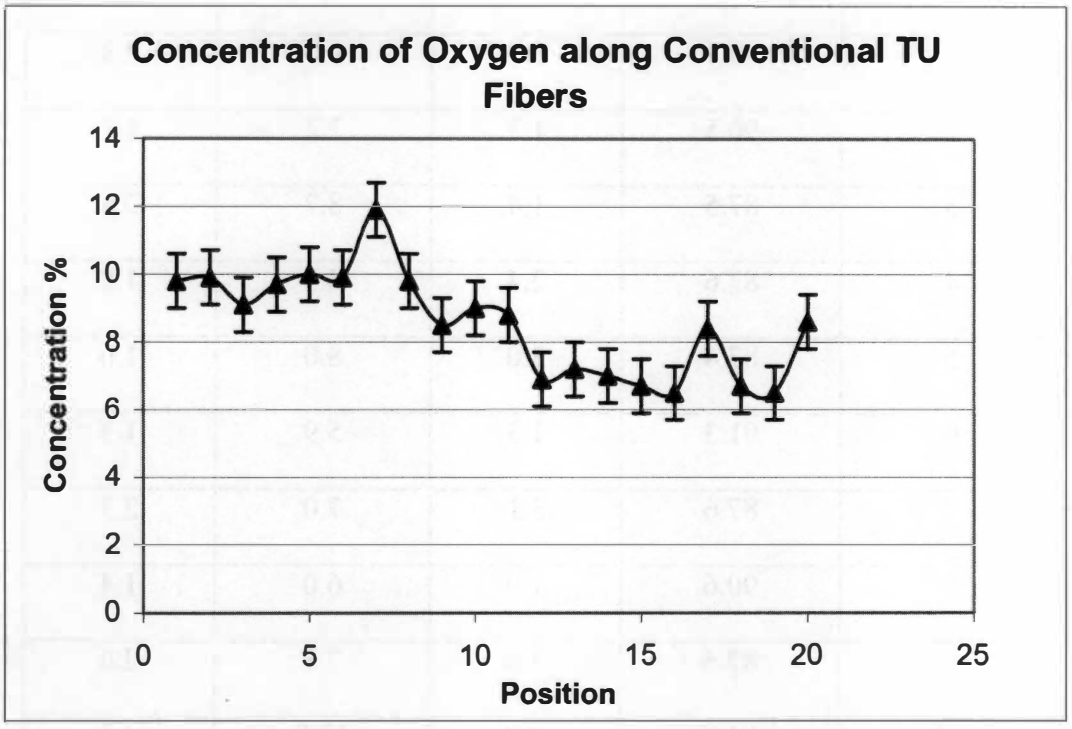

Figure 5-3. Variation of oxygen concentration along conventional TU fibers

Table 5-3. Distribution of elemental composition (%) on the surface of MAP UU fibers

Elemental Composition of MAP UU fibers %				
Position	C	N	O	Si
1	86.1	1.4	9.7	2.8
2	90.5	1.3	7.2	1.1
3	87.5	1.4	8.7	2.4
4	87.6	2.4	8.3	1.8
5	87.4	3.0	8.0	1.6
6	91.3	1.3	5.9	1.5
7	87.6	3.1	7.0	2.3
8	90.6	1.9	6.0	1.4
9	87.3	3.0	7.1	2.6
10	81.8	0.9	13.0	4.3
11	87.9	1.8	6.9	1.6
Average	87.8	2.0	8.0	2.1
STDEV	2.5	0.8	1.9	0.9

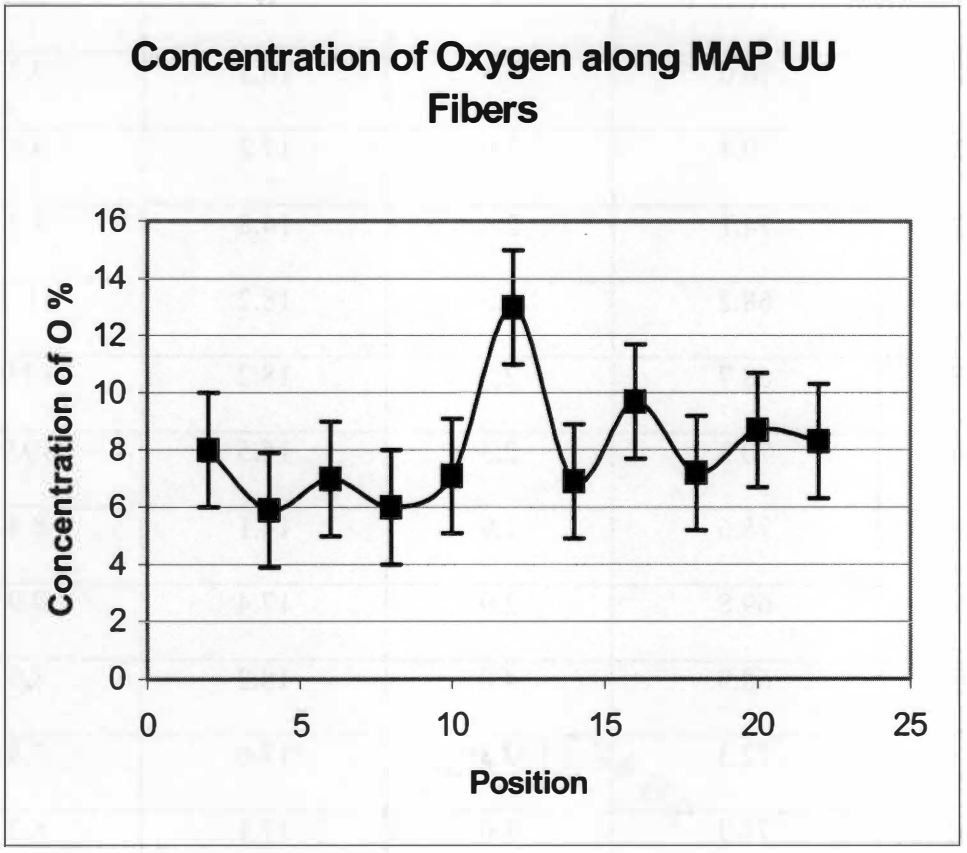

Figure 5-4. Concentration of oxygen along MAP UU fibers

Table 5-4. Distribution of elemental composition (%) on the surface of MAP TU fibers

Elemental Composition of MAP TU fibers %				
	C	N	O	Si
1	70.0	3.8	16.5	9.7
2	70.4	3.0	17.2	9.4
3	74.1	2.4	14.8	8.7
4	68.2	2.3	18.2	11.3
5	68.7	2.2	18.2	10.9
6	70.3	2.3	16.5	10.9
7	75.6	1.9	14.1	8.4
8	69.8	2.9	17.4	9.9
9	68.9	4.0	18.2	8.9
10	72.3	2.3	17.6	7.8
11	71.3	3.0	17.1	8.7
12	73.7	2.0	16.2	8.0
13	74.5	2.3	15.8	7.4
14	77.7	2.7	13.7	5.9
15	74.9	2.4	15.3	7.4

Table 5-4. Continued

	C	N	O	Si
16	78.8	1.3	13.3	6.6
17	77.0	2.1	14.4	6.5
18	76.3	3.3	14.6	5.7
19	77.1	2.2	14.4	6.3
20	79.1	2.3	12.8	5.9
21	73.8	2.8	15.3	8.0
22	79.6	2.6	12.3	5.5
23	75.4	2.0	15.6	7.0
24	69.6	1.7	21.2	7.6
25	73.0	2.1	16	8.9
26	77.5	2.4	13.1	7.1
27	76.4	1.3	14.3	8.0
28	74.2	2.4	14.5	8.9
29	73.6	2.4	15.4	8.6
30	76.8	2.9	13.2	7.0
31	73.3	1.8	16.1	8.8
32	76.4	4.3	12.5	6.8
Average	74.0	2.5	15.5	8.0
STDEV	3.2	0.7	2.0	1.5

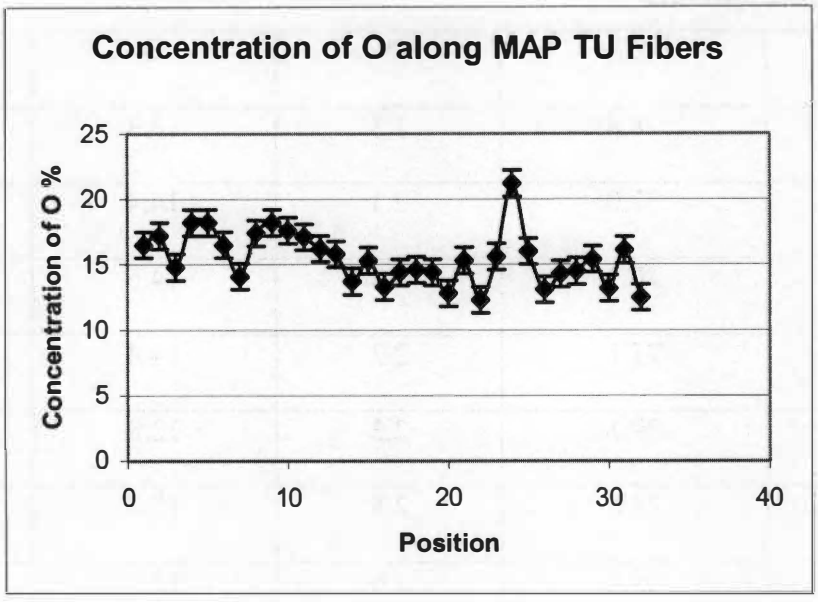

Figure 5-5. Concentration of oxygen along MAP TU fibers

Comparison of MAP UU and MAP TU shows that after surface treatment the concentration of oxygen has increased dramatically from an average of 8.0% to an average of 15.5%. Again, MAP TU samples show a random variation of the elemental concentration of oxygen along the fiber axial direction. But in this case, the results are relatively constant in MAP TU, most values for oxygen concentration fall between12%-17%, with a standard deviation of 2.0%. It is also noticed that MAP fibers have a very high concentration for silicon.

To investigate if the plasma is able to penetrate the interior of the fiber bundle in the process to ensure a uniform product rather than only affecting the exterior fibers, both

treated and untreated MAP fiber bundles were scraped to expose the interior fibers to the surface and same XPS experiments were conducted. The results are shown in Table 5-5.

Due to the cumbersome XPS experience, only 5 positions were tested for each sample with approximate 2.5 cm between two positions. The above results are very close to the data shown in Table 5-3 and 5-4. This indicates that in MAP processing, sufficient energy is generated through coupling of plasma and microwave radiation to provide a uniform and homogeneous heating across the fiber cross section and consequently results in the carbonization of stabilized PAN-precursors. Input power of microwave radiation, gas flow rate, processing time, pressure and geometry of plasma reactor are the main factors that control the extent of carbonization and graphitization.

Table 5-5. Elemental composition (%) of interior fibers in sample bundles of MAP UU and MAP TU

	C	N	O	Si
MAP UU				
Average	87.3	3	7.1	2.6
STDEV	2.6	0.8	2.1	1.0
MAP TU				
Average	76.5	3	14.4	6.1
STDEV	3.0	0.6	2.4	1.3

5.1.3 Functional Groups Distribution on Carbon Fiber Surface by X-Ray Photoelectron Spectroscopy (XPS)

The distribution of functional groups on the carbon fiber surface and subsequent changes in surface chemistry can be identified through examination of the C1s core region of the XPS spectra. However carbon fiber surfaces, even under severe surface treatment conditions, have substantial amounts of primary type carbon present and chemically shifted carbon must be distinguished from the primary carbon and then associated with specific surface functional groups. The interpretation of chemical shifts in XPS spectra of carbon fibers is not straightforward. First of all, the spectra must offer sufficient resolution to identify changes in functional groups. Second, the changes must be assigned. In this work, the C1s spectra of all samples were obtained using 0.1 eV/step with 300 scans. The C1s peak of each carbon fiber sample was deconvoluted using a peak fitting procedure that fits the measured peak to several Gaussian/Lorentzian peaks.

XPS spectra of the C1s peak region for samples Con UU, Con TU, MAP UU and MAP TU was deconvoluted into surface functional group contributions and shown in Figure 5-6. Ideally carbon chemical shift data should be obtained from standard surface functional groups for suitably prepared samples, but unfortunately such standard surface groups cannot easily be prepared. A comprehensive study of carbon shifts caused by surface treatment has been carried out by Sherwood and coworkers [46-52]. In this work, the C1s spectra show one main "graphitic" peak at 284.5 eV and three oxide peaks. The three types of oxygen functionalities called oxide 1, 2, and 3, shifted by 1.5, 3.1, and 4.7 from the graphitic peak, respectively. Oxide 1 is assigned to the carbon atom in alcohol

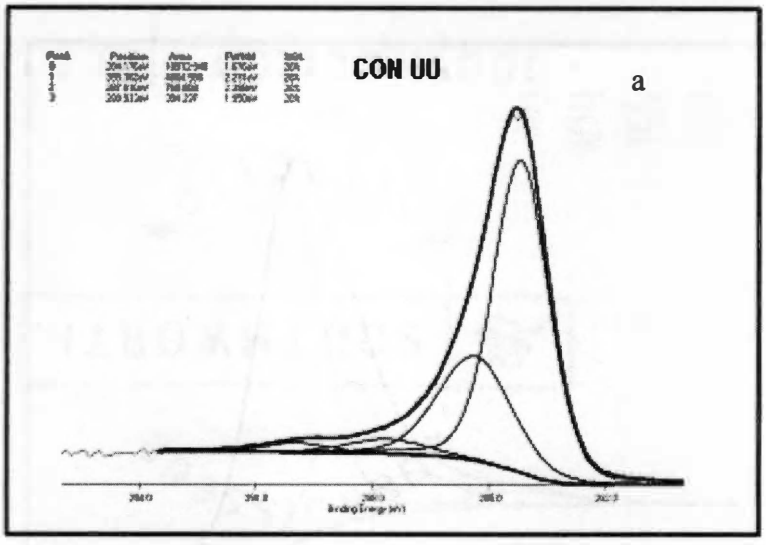

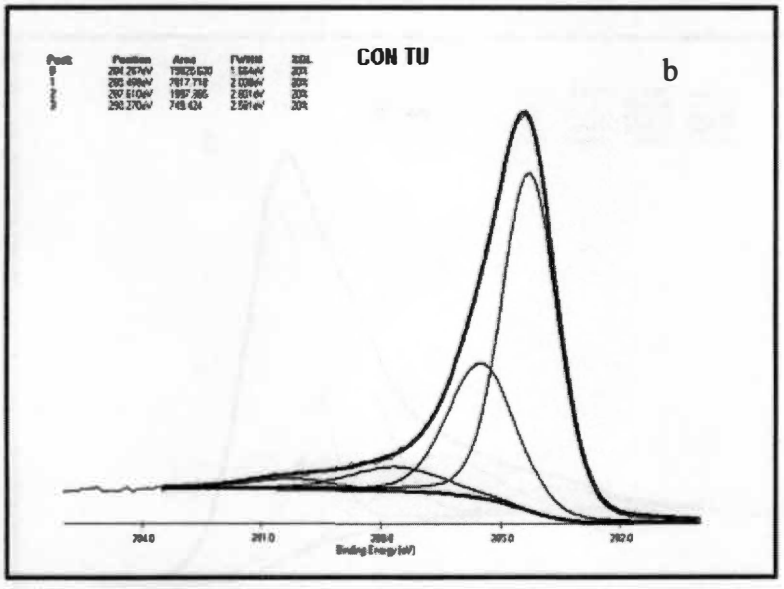

Figure 5-6. C1s spectra of carbon fiber samples

(a) CON UU; (b) CON TU;

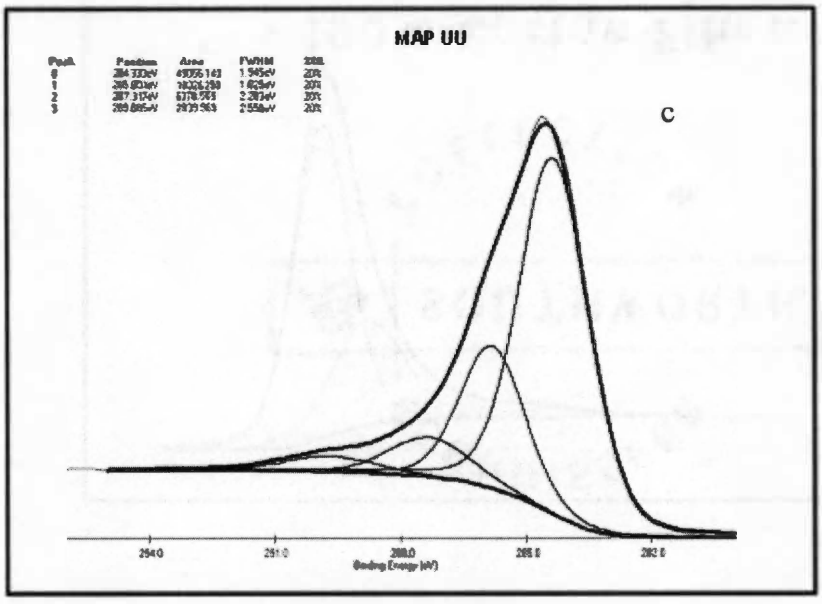

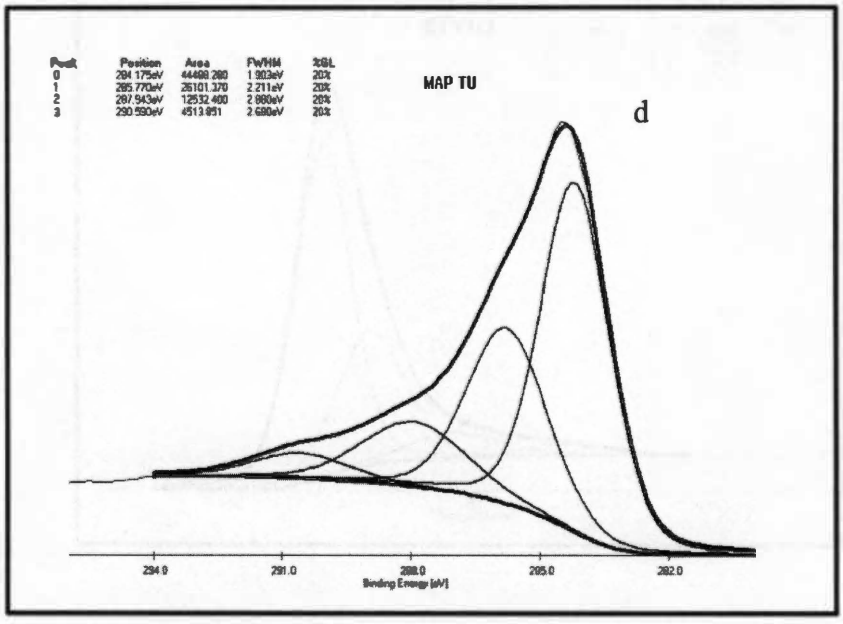

Figure 5-6. Continued

(c) MAP UU; (d) MAP TU

(C-OH) or ether (C-O-C) groups. The C1s signal from C=N type groups also falls into this range. Oxide 2 corresponds to the C atom in carbonyl (C=O) type groups. Oxide 3 is the C1s peak of carboxyl (COOH) or ester (COOR) groups.

The quantitative analysis of XPS spectra is tabulated in Table 5-6.

C_{ox}/C_{graph} is the percentage ratio of oxidized carbon atom verses graphitic carbon atoms. A significant increase in C_{ox}/C_{graph} ratio was found for MAP UU and MAP TU fibers compared to Con UU and Con TU. This is caused by increased amount of various functional groups, present on the surface. In the case of MAP TU, almost half of the carbon atoms on the fiber surface are oxidized.

Table 5-6. Contribution (%) of chemical functional groups to C 1s band and full width at half maximum (FWHM) of the graphitic band

	Graphitic Peak	Peak 1 (C-OH) or (C-O-C)	Peak 2 C=O	Peak 3 (COOH) or (COOR)	C_{ox}/C_{graph}	FWHM (eV)
Con UU	82.9	12.7	3.0	1.4	0.21	1.4
Con TU	75.7	17.6	5.1	1.6	0.32	1.7
MAP UU	62	28.6	6.6	2.8	0.67	2.0
MAP TU	52.3	27.4	14.8	5.5	0.91	2.3

5.2 Surface Treatment of Conventional Fibers by Plasma

Untreated unsized conventional fibers used to compare with MAP fibers were surface treated with two plasma systems. To further understand the process, the effects of time, gas system and power on chemical composition and functional groups on carbon fiber surface were examined by X-Ray Photoelectron Spectroscopy (XPS). For each sample, XPS survey scan was conducted in at least 5 positions. The average value and standard deviation were recorded.

5.2.1 XPS Results of Remote Applicator (RA) Samples

1. Chemical composition

General comparison of the surface composition of all RA samples is shown in Table 5-7 and Figure 5-7. The lower case letter in the sample nomenclature refers to the processing conditions presented in Table 4-1.

Overall XPS spectra are not shown for any of these samples since they are all essentially similar in showing a strong C 1s peak and O 1s peak. Weak signals of N 1s and Si 2p are also observed in all spectra. It is noticed that all samples have certain amount of sodium showing on the surface.

The overall comparison of samples treated by the remote applicator process (RA) shows that this treatment can produce considerable change of the surface chemistry of the carbon fiber. Each sample showed an increase in oxygen concentration. The variations of silicon and nitrogen are relatively small compared to oxygen. The appearance of sodium

Table 5-7. Comparison of all elements in RA samples

	Average Concentration %				
	C	N	O	Si	Na
RA-a	74.6	1.3	13.5	1.5	9.7
RA-b	86.5	1.8	8.2	1.9	1.7
RA-c	89.1	1.8	6.1	1.1	2.3
RA-d	85.5	2.3	9.2	1.3	1.9
RA-e	80.7	2.3	12.8	0.7	3.5
RA-e-2	85.5	1.7	7.9	1	4.3
RA-f	80.8	1	9.9	0.6	7.8
RA-f-2	70.8	3.3	14.1	1.4	12
RA-g	81	0.7	8.9	4.8	6.8
RA-h	86.4	1.5	9.2	0.7	2.2
RA-j	79.4	2.1	16.4	1.1	1.7

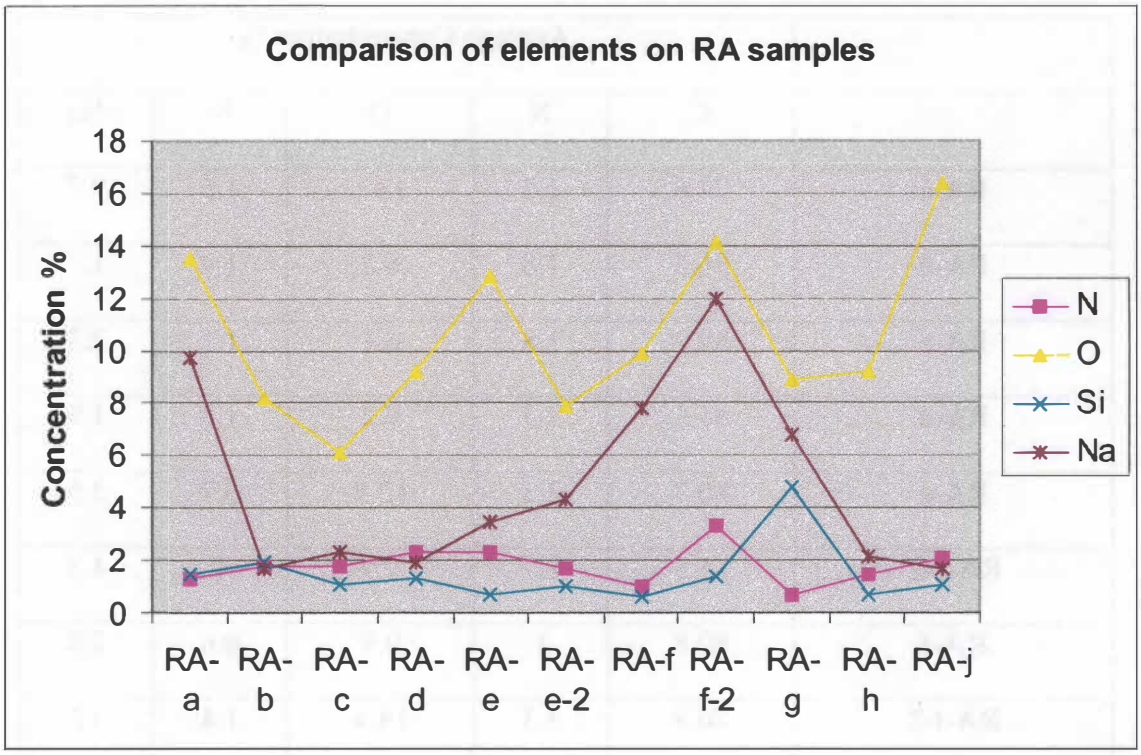

Figure 5-7. Comparison of elements on RA samples

in the XPS spectra was due to the erosion of quartz tube and deposition of sodium onto the fiber surface during the treatment.

The surface oxygen concentration on the RA samples was also calculated by including and excluding sodium and summarized in Table 5-8.

RA-a, RA-f-2 and RA-j showed an oxygen concentration of more than 15%. These increases represent approximately 300 and 200% when compared to the untreated unsized conventional fibers (Con UU) and conventional fibers treated with ozone (Con TU), respectively.

2. Functional groups

Carbonyl (-C=O), hydroxyl (-OH) or ether (-C-O-R) and ester (-COOR) or acid (-COOH) functionalities are created on the carbon fiber surface as a result of exposure to the oxygen-containing plasma. The XPS C 1s spectrum of each RA sample was obtained at one location where the maximum amount oxygen concentration appeared. Deconvolution was performed for each RA sample and shown in Figure 5-8. The analysis of the percentage of each functional group is summarized in Table 5-9.

All the RA samples have shown significant amount of oxygen-containing functional groups, while each differs in the contribution of the various functional groups. In most samples, carboxyl group accounts for the least amount of oxygen as hydroxyl or ether group accounts for the most. The presence of ester and ether groups may not be beneficial since the COOH and OH are largely responsible for enhancement of strength at the fiber interphase due to their chemical interaction with the matrix. But it is not feasible

Table 5-8. Surface oxygen Concentration (%) of RA samples

Oxygen concentration %				
	Without Na		With Na	
	Average	STDEV	Average	STDEV
RA-a	15.1	3.6	12.7	2.7
RA-b	8.3	2	8	2
RA-c	6.3	1.8	6	1.6
RA-d	9.4	0.5	8.9	0.5
*RA-e	13.2	5.4	12.4	5.3
*RA-e-2	8.3	1.9	7.6	3.8
*RA-f	10.7	1.9	9.5	1.5
*RA-f-2	16.3	6.4	12.8	1.5
RA-g	9.7	3.7	8.6	2.9
RA-h	9.4	1.1	9	0.9
RA-j	16.7	6.4	16	6.2
*RA-e-2 and *RA-f-2 are repeat sample for RA-e and RA-f				

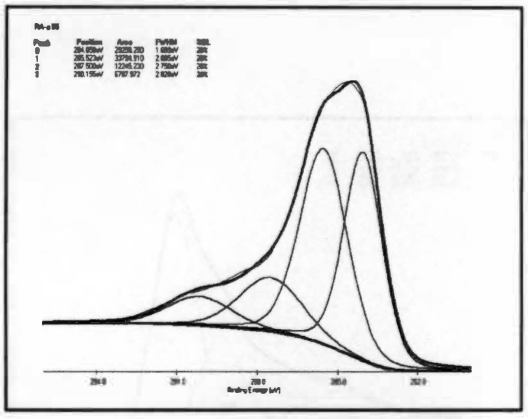

RA-a

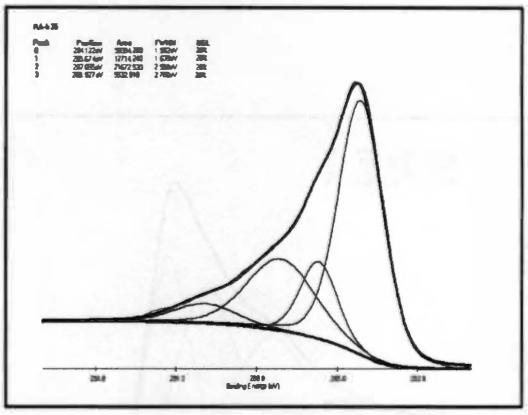

RA-b

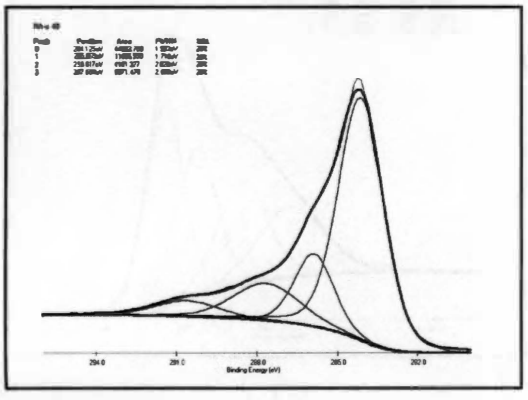

RA-c

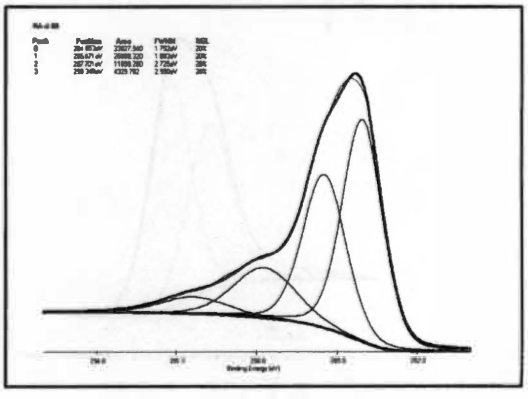

RA-d

Figure 5-8. C1s core-level spectra of RA fibers

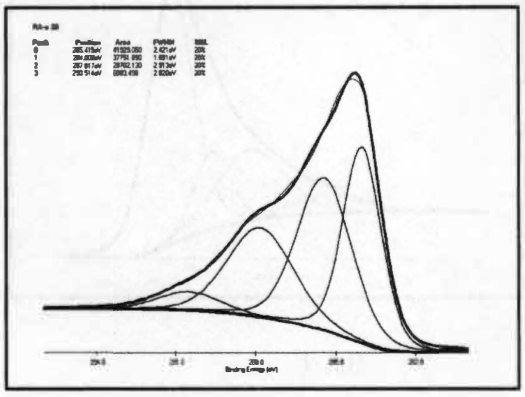

RA-e

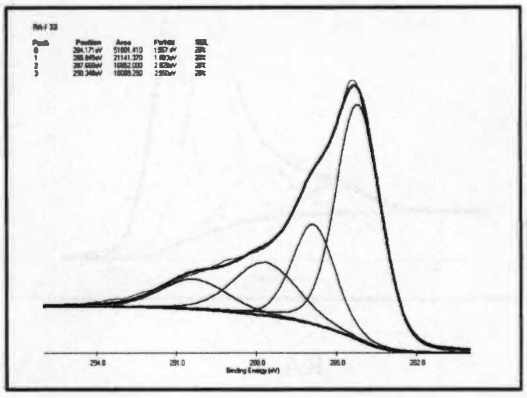

RA-f

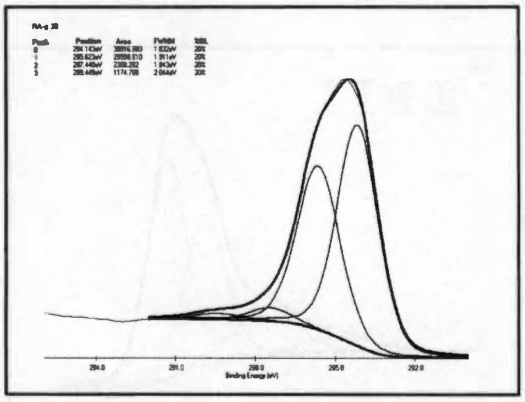

RA-g

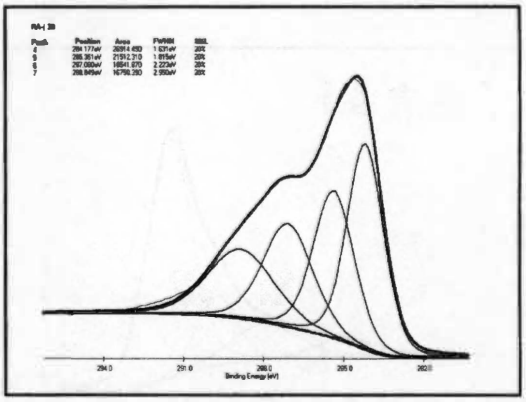

RA-j

Figure 5-8. Continued

Table 5-9. Peak area percentages for each peak in C1s spectra of RA samples

	Graphitic peak	-OH or -C-O-R	-C=O	-COOH or -COOR
RA-a	35.64	41.17	14.92	8.27
RA-b	55.78	14.08	24.01	6.13
RA-c	63.55	16.43	14.12	5.89
RA-d	45.02	33.39	15.83	5.76
RA-e	32.58	36.42	25.71	5.29
RA-f	51.90	21.18	16.89	10.03
RA-g	53.50	41.45	3.35	1.70
RA-h	75.30	4.68	14.26	5.75
RA-j	32.15	25.70	22.15	20.01

to differentiate hydroxyl group, carboxylic acid group from ether and ester using XPS data

5.2.2 XPS Results of Atmospheric Plasma (AP) Samples

1. Chemical composition

The elemental surface concentration for samples treated by Atmospheric Plasma (AP) process is summarized in Table 5-10 and Figure 5-9. The processing condition for individual sample was presented in Table 4-1.

General comparison on oxygen concentration of AP samples is shown in Table 5-11. The concentration of oxygen on the samples prepared by the atmospheric plasma process varies from 5.3 to 18.3% and exhibit a dependence on processing conditions. Sample AP-B, AP-D, AP-E and AP-O2-130-sec showed an oxygen concentration of more than 10%. Using same conditions for AP-C and AP-E, sample AP-C-2 and AP-E-2 were prepared and their surface oxygen concentration was determined by XPS. There is a noticeable difference in the oxygen concentration in every sample. The difference shown in Figure 5-10 indicates that due to the complicated nature of plasma chemistry, this plasma process has not achieved a good repeatability at this stage.

2. Functional groups

The XPS C 1s spectrum of each AP sample was obtained from the location where the maximum amount oxygen concentration appeared. Deconvolution was carried out for each AP sample and shown in Figure 5-11. The analysis of the percentage of each group is summarized in Table 5-12.

Table 5-10. Comparison of the elemental composition

	Average concentration %			
	C	N	O	Si
AP-A	87.7	1.7	7.7	3.0
AP-B	78.7	3.6	12.7	7.0
AP-C	91.7	2.1	5.3	1.8
AP-D	80.4	1.9	10.8	6.9
AP-E	73.9	2.6	18.3	5.2
AP-A-2	91.7	0.6	6.1	1.4
AP-B-2	89.9	1.0	8.3	0.8
AP-C-2	86.0	1.8	9.4	2.8
AP-D-2	88.1	1.3	9.2	1.4
AP-E-2	84.1	1.5	11.8	2.6
AP-G	91.0	1.0	6.8	1.6
AP-H	90.3	1.3	8.0	0.8
AP-O_2-130 sec	86.1	1.4	11.8	0.7
AP-J	91.9	1.8	5.5	1.3
AP-K	86.3	1.6	10.0	2.1
AP-L	90.0	2.4	6.4	1.2

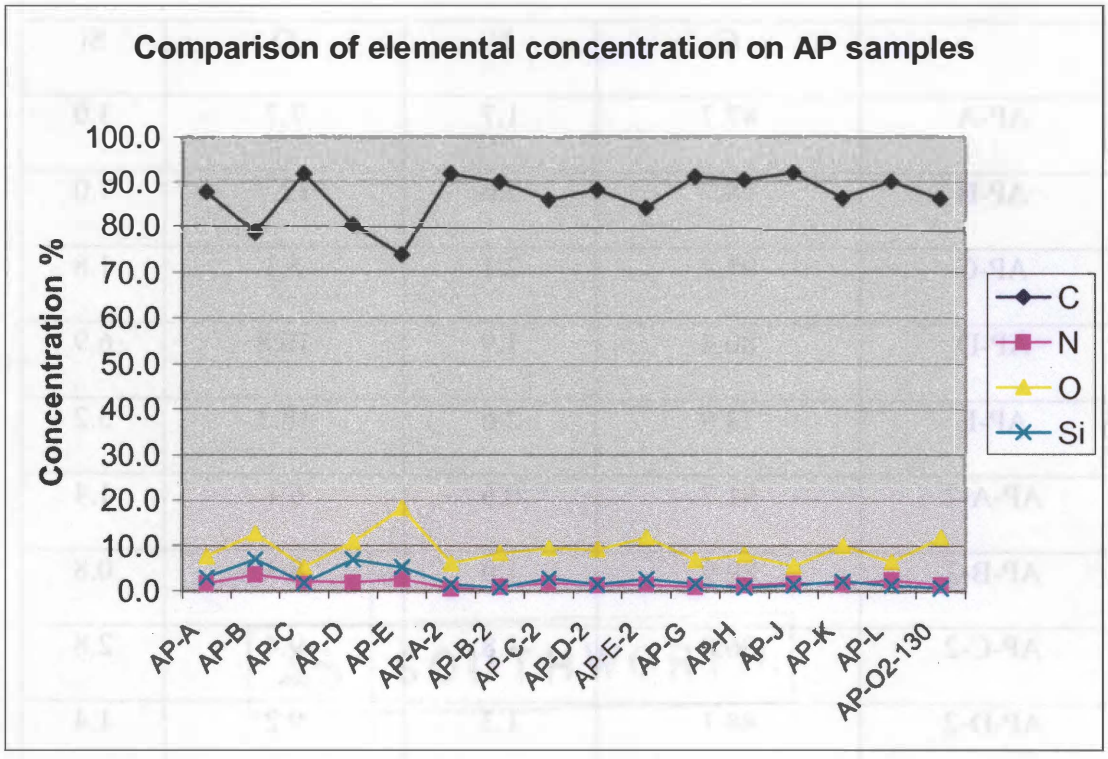

Figure 5-9. Comparison of all AP samples

Table 5-11. Oxygen concentration of AP samples

	O	STDEV
AP-A	7.7	0.9
AP-B	12.7	2.7
AP-C	5.3	0.9
AP-D	10.8	1.8
AP-E	18.3	2.3
AP-A-2	6.1	0.9
AP-B-2	8.3	1.6
AP-C-2	9.4	1.4
AP-D-2	9.2	0.6
AP-E-2	11.8	2.3
AP-G	6.8	1.2
AP-H	8.0	0.8
AP-J	5.5	1.3
AP-K	10.0	2.0
AP-L	6.4	0.5
AP-O2-130	11.8	2.2

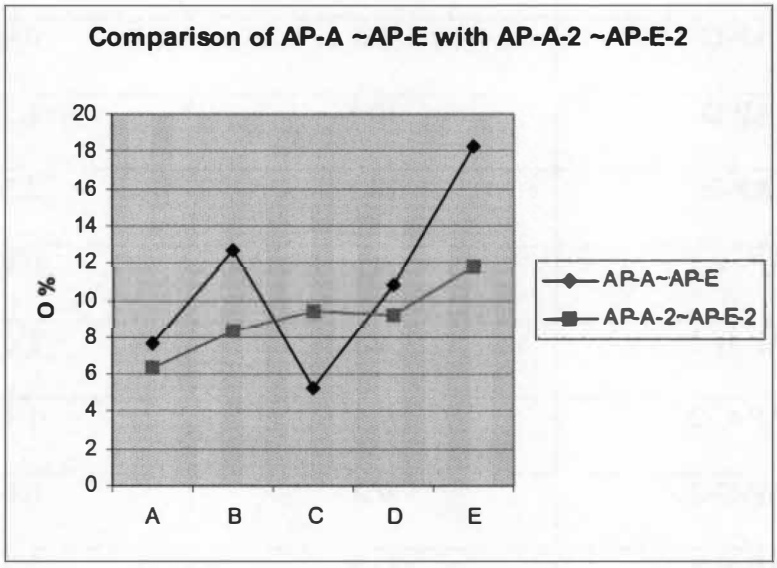

Figure 5-10. Comparison between samples AP-A~AP-E

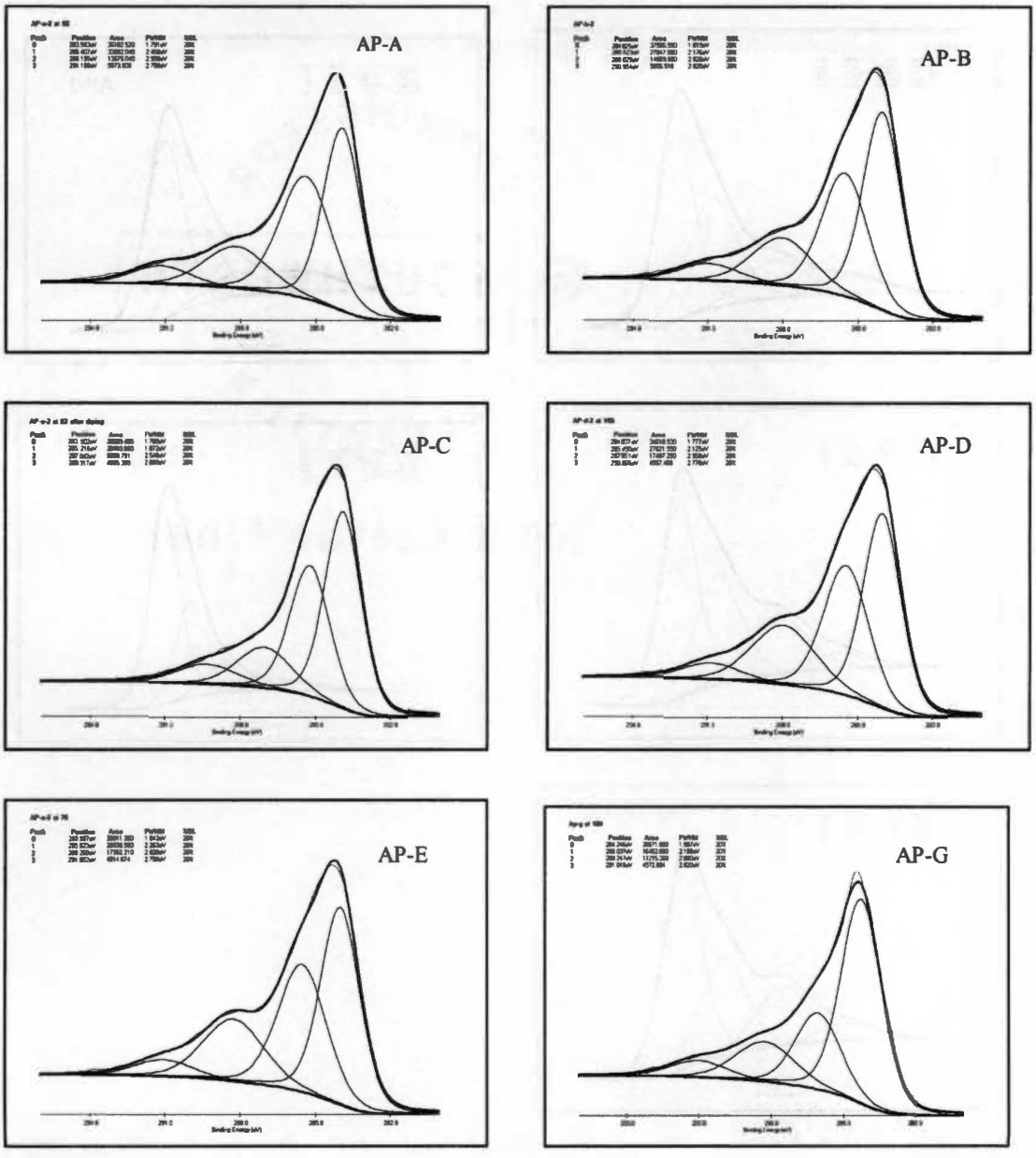

Figure 5-11. C1s core-level spectra of AP fibers

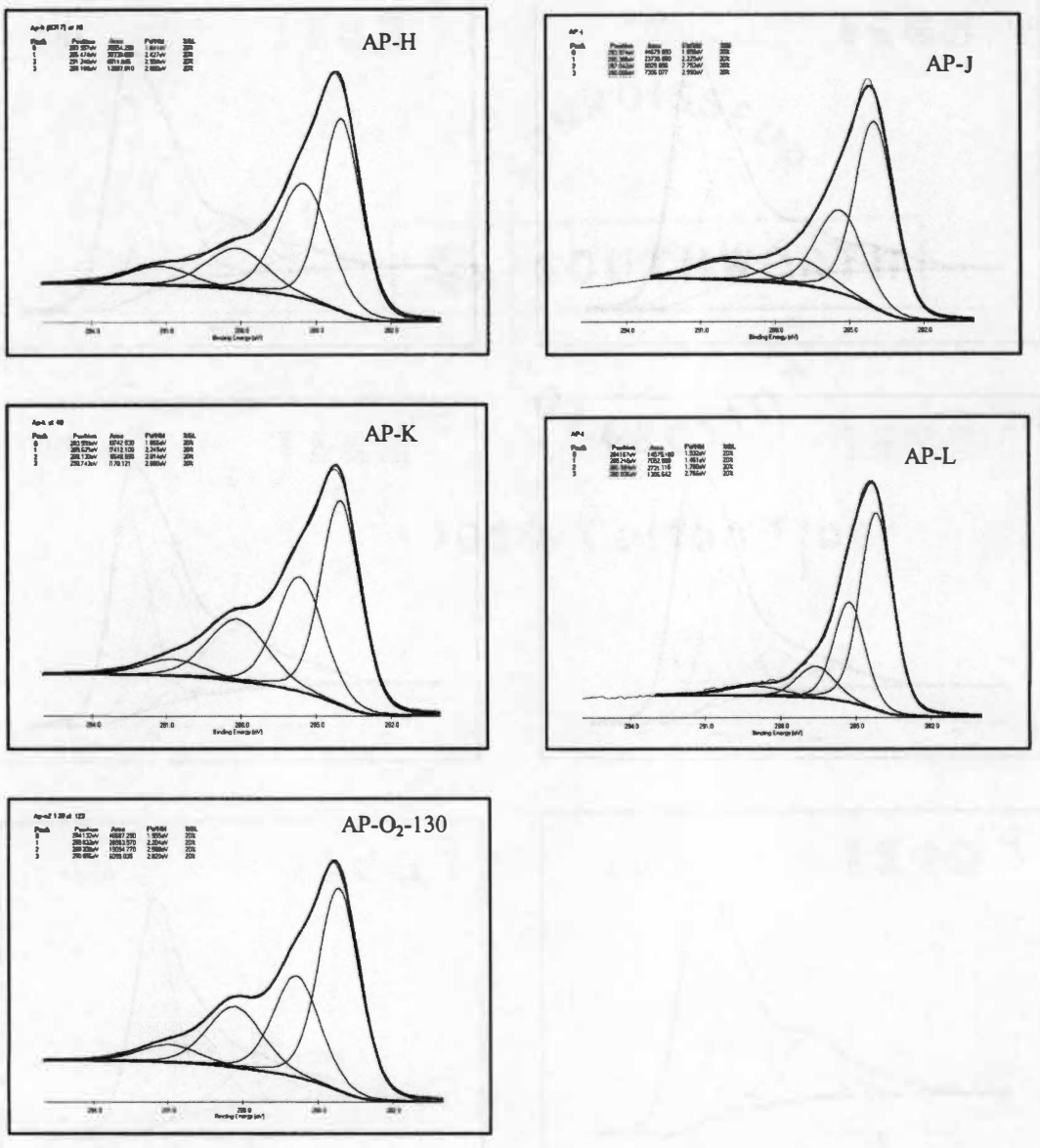

Figure 5-11. Continued

Table 5-12. Peak area percentages for each peak in C1s spectra of AP samples

	Graphitic peak	C-OH or –C-O-C	-C=O	-COOH or -COOR
AP-A	64.50	19.43	11.07	4.89
AP-B	58.78	21.08	16.01	5.13
AP-C	69.55	17.69	8.12	4.64
AP-D	45.02	27.83	23.39	4.76
AP-E	47.42	26.70	20.01	5.87
AP-G	70.82	14.56	11.23	4.39
AP-H	66.90	15.60	11.10	5.40
AP-J	74.30	11.68	7.27	6.75
AP-K	52.50	25.45	18.35	3.70
AP-L	77.31	14.28	6.21	2.20
AP-O_2-130	55.11	21.49	18.03	5.37

The results indicate the presence of all three types of oxygen-containing functional groups on fiber surface of samples treated by atmospherics plasma process. The concentration of carboxyl varies over a range of 2.2 to 6.75.

5.3 Functional Groups Distribution by Auger Electron Spectroscopy

The common microstructural features on carbon fiber surface are periodic ridges and valleys. It has been suggested that these morphological characteristics on the carbon fibers may be related to the ability to successfully undergo surface modification, e.g. placement of chemically active functional groups. The dimensions of ridges on the carbon fiber surface fall into a range from 100nm to a few hundred nanometers in width, while the height of these ridges is less than two hundred nanometers. The chemical derivatization technique was used to label the carboxyl groups implanted on the surface through plasma treatment, which is believed to contribute to chemical bonding between fiber and matrix. Fiber morphology will also have an influence on the surface treatment. It is important to investigate the correlation of placement of functional groups and fiber surface morphology in order to provide the information to see the possibility of using plasma treatment to tailor surface chemistry to enhance adhesion in fiber-matrix interphase to a specific polymer resin. Due to the limited availability of AES, only samples possessing higher carboxyl group concentration according to XPS data were chosen for this experiment.

To have a control sample for the later comparison, conventional UU fibers was used to conduct first Auger experiment. These results were compared with SEM micro graphs are shown in Figure 5-12.

Figure 5-12 (a), (b) gives the details of fiber surface under high magnification. As mentioned before, the valleys and ridges on the fiber are very clear. No evidence of defects is observed; the fibers exhibit a smooth surface on the micro scale. Figure 5.12(c) shows the Auger image of the same section of a single fiber as shown in Figure 5.12(b). The Auger scan of the entire region shows the elemental distribution of carbon and oxygen on the fiber surface. The peak intensity of carbon (red) and oxygen (blue) were used to plot a two-dimensional display of the direct elemental image. As can be seen in Figure 5.12(c) the absolute dominant element is carbon. This is expected since the conventional UU fiber has more than 90% of carbon given by XPS data. The areas used in point analysis were selected to represent specific morphological features (ridges and valleys). High spatial resolution of 20 nm was obtained for the marked regions in Figure 5.12(d) by setting the electron beam energy at 20 kV. It is necessary to mention that the small circles next the numbers do not represent the area that was under investigation, but rather indicate the position where the electron beam was focusing. Four positions from this single fiber surface, including valleys and ridges were scanned. The elemental concentrations are presented in the table included in Figure 5-12 (d). The results are very constant and show lower oxygen concentrations than the ones shown in Table 5-1. This is because those Con UU fibers used in Auger experiment was freshly taken from production line, thus, experienced less oxidation due to exposure to air.

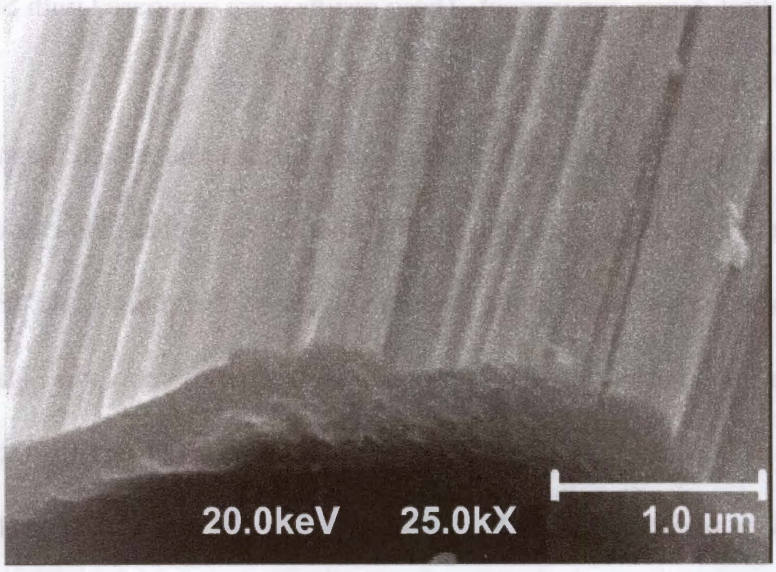

(a) SEM image of Con UU fiber

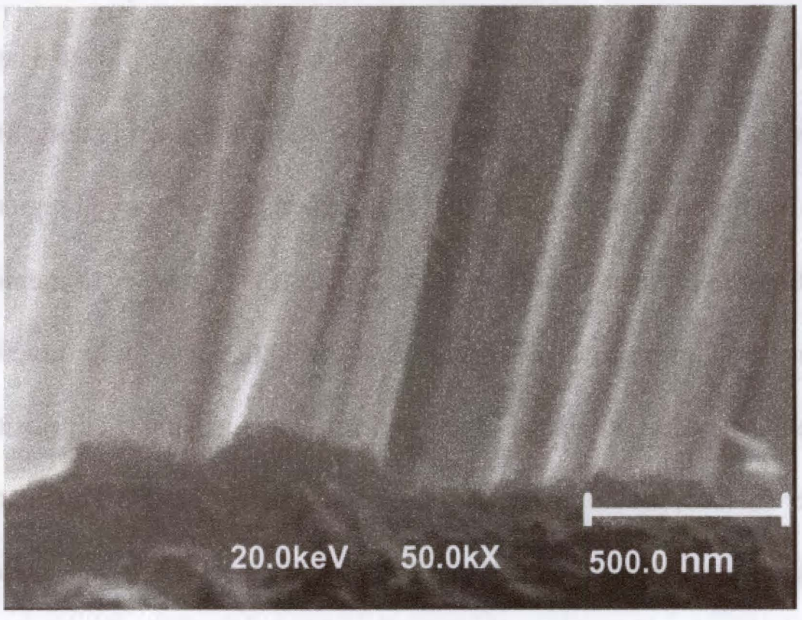

(b) SEM image of Con UU fiber

Figure 5-12. Morphology and elemental distribution of Con UU fibers by AES

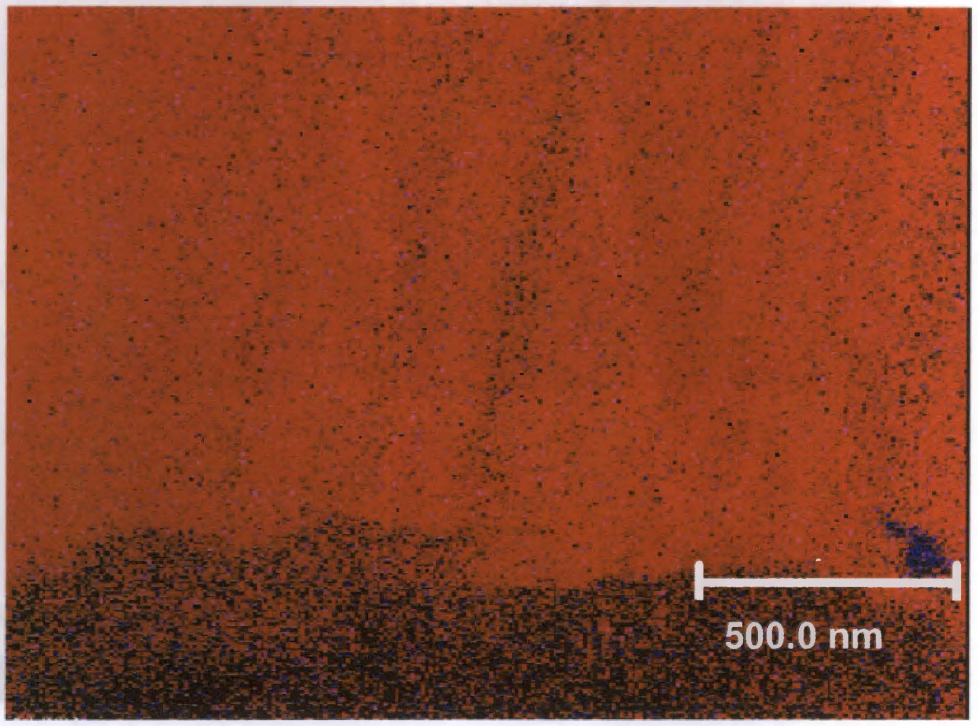

(c) Auger image of Con UU fiber

Figure 5-12. Continued

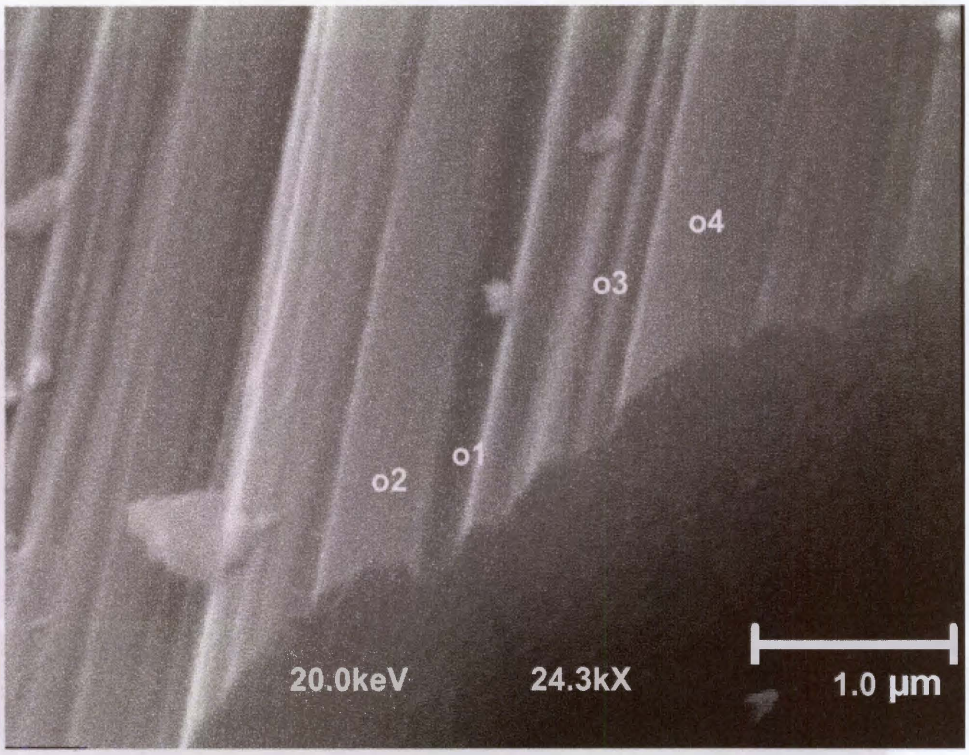

Atomic Concentration Table

Point	C	N	O
1	94.54	2.80	2.67
2	94.98	2.36	2.66
3	93.23	4.19	2.58
4	94.79	2.74	2.47

(d) SEM image of Con UU fiber and elemental point analysis by AES

Figure 5-12. Continued

Chemical derivatization experiment was first conducted on conventional UU fibers to compare with other samples, which supposedly have more carboxyl groups according to XPS results. The procedure described in experimental section was carefully followed for all samples. Before conducting Auger spectroscopic analysis, XPS was used to determine the presence of any coordinate cobalt compound on the fiber surface. The samples were dried in vacuum oven at 70°C until the cobalt concentration reached a constant level to ensure the exclusion of cobalt caused by absorption of cobalt acetate solution rather than chemical bonding. The elemental compositions are summarized in Table 5-13.

For each sample, three positions were scanned. Except for conventional UU samples, every sample shows a large deviation for oxygen and cobalt concentration. This is not surprising due to the fact that XPS only gives a spatial resolution on the millimeter scale and thus, hundreds of fiber filaments are contributing to the final composition. At each position, electron signals from an area with a diameter of 0.8 mm will finally reach the analyzer; the rest is blocked by the aperture. In each position, the average number of reactive sites that form the cobalt coordinate compound will show a considerable variation. Nonetheless, the results indicate clearly that all treated sample show higher cobalt concentration than conventional UU fiber, while each of them has an increase in oxygen concentration. This is because of the inclusion of oxygen from cobalt acetate.

The elemental composition as determined by AES for conventional UU fibers after derivatization is shown in Figure 5-13.

Table 5-13. Elemental composition by XPS of chemical derivatized fibers

		C %	O %	Si %	Co %
Con UU	Average	86.5	7.7	1.5	1.7
	STDEV	2.1	1.9	0.4	0.6
RA-a	Average	78.9	13.5	2.2	5.4
	STDEV	4.1	3.1	0.3	2.5
RA-f	Average	79.6	14.5	1.8	4.1
	STDEV	4.4	3.4	0.3	1.5
RA-j	Average	72.9	17.4	2.6	7.1
	STDEV	3.9	4.6	0.3	2.3
AP-B	Average	76.3	17.3	2.3	4.3
	STDEV	4.2	5.4	0.4	1.4
AP-E	Average	75.9	17.8	2.4	3.9
	STDEV	4.5	6.2	0.3	1.6

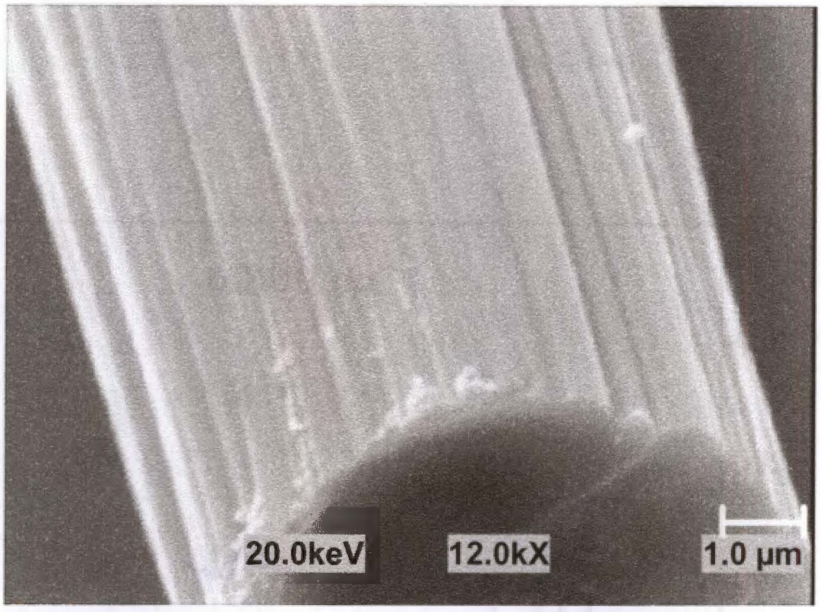

(a) SEM image of derivatized Con UU fiber

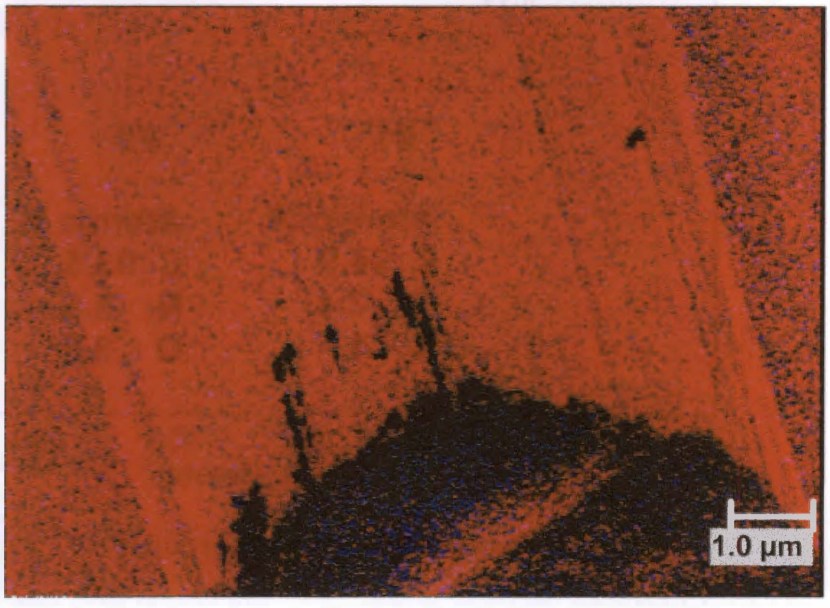

(b) Auger image of derivatized Con UU fiber

Figure 5-13. Morphology and elemental distribution of derivatized Con UU fibers by AES

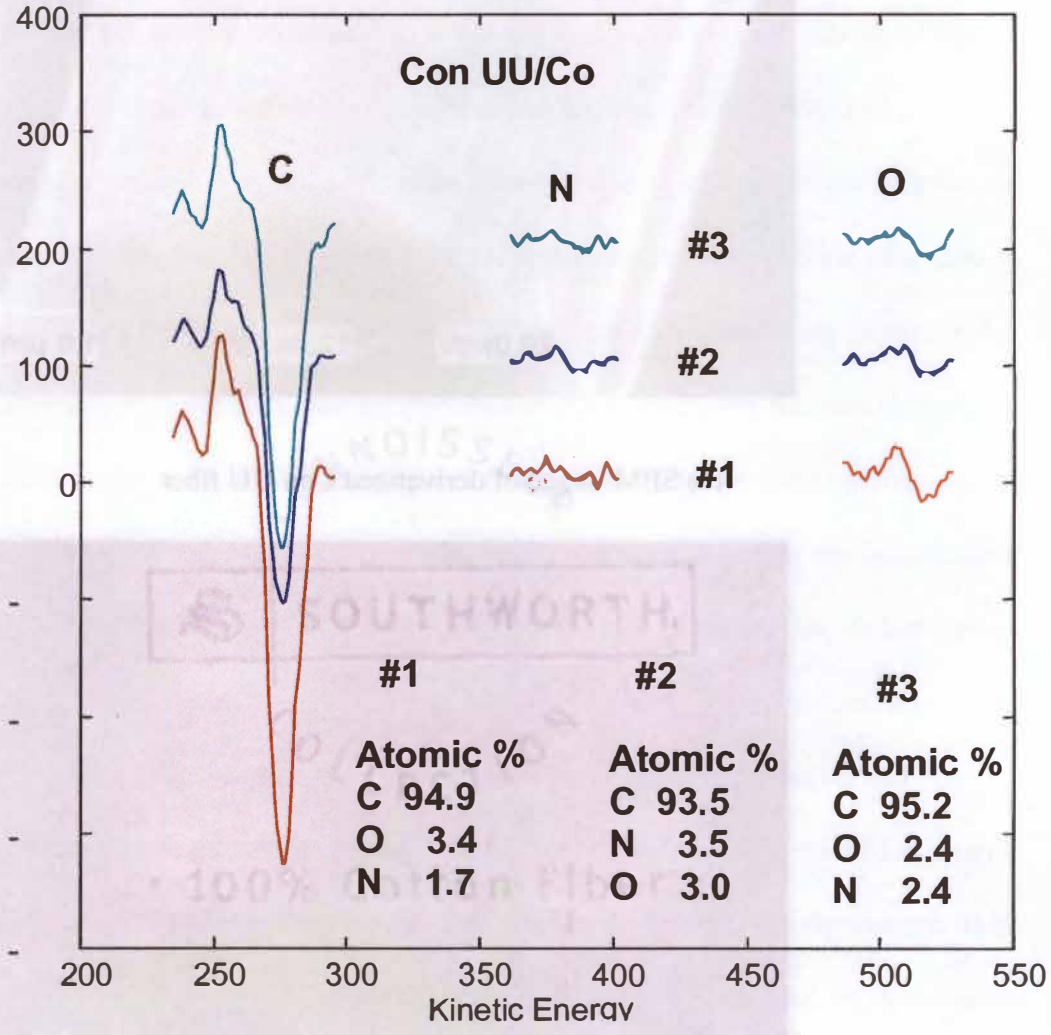

(c) Elemental concentration at points

Figure 5-13. Continued

From the SEM image, one can see that after derivatization, the overall appearance of fiber surface did not change. Splinters were found near the fractured surface. Similar to conventional UU fibers, the two-dimensional elemental imaging using carbon and cobalt intensities leads to an imaging with red carbon as the dominant element. The scattered blue dots on the fractured surface are caused by background noise. The black regions are corresponding to deposits seen from SEM image. The elemental analysis proves they are oxygen-rich regions. It seems they most likely are contaminants caused when cutting the fibers for Auger sample preparation. Point analysis for areas in valleys and ridges were also conducted in this sample. Unfortunately the exact locations of these areas were not recorded after scanning, the Auger peaks for each element detected and calculations are shown in Figure 5-13 (c). The results did not show any existence of cobalt and the oxygen level is close to conventional UU fibers (Table 5-1) without derivatization.

The Auger experimental results for RA-j fibers after derivatization are shown in Figure 5-14. The point analysis of RA-j fiber shows a high concentration of cobalt. The high concentration of cobalt agrees with the high percentage of carboxylic groups determined by XPS and presented in Table 5-9.

Same procedure was followed for RA-j; a single fiber was chosen to take high magnification image to check the surface morphology. The increased roughness and small particles are observed in Figure 5-14 (a). Elemental analysis was conducted on areas chosen from both valley and ridge. There are obvious differences of cobalt concentration between locations. To further investigate the distribution of cobalt element,

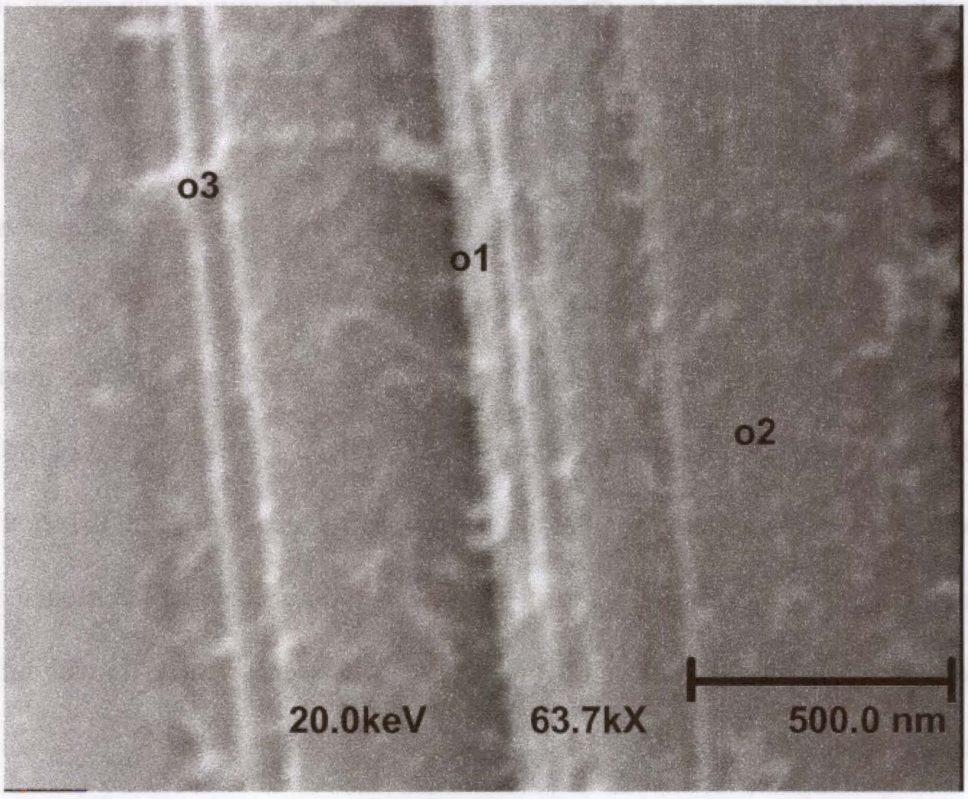

Atomic Concentration Table

Point	C	O	Co
1	74.59	17.10	8.32
2	91.98	5.28	2.75
3	72.21	16.68	11.10

(a) SEM micrograph of derivatized RA-j fiber and elemental point analysis by AES

Figure 5-14. Morphology and elemental distribution of derivatized RA-j fibers by AES

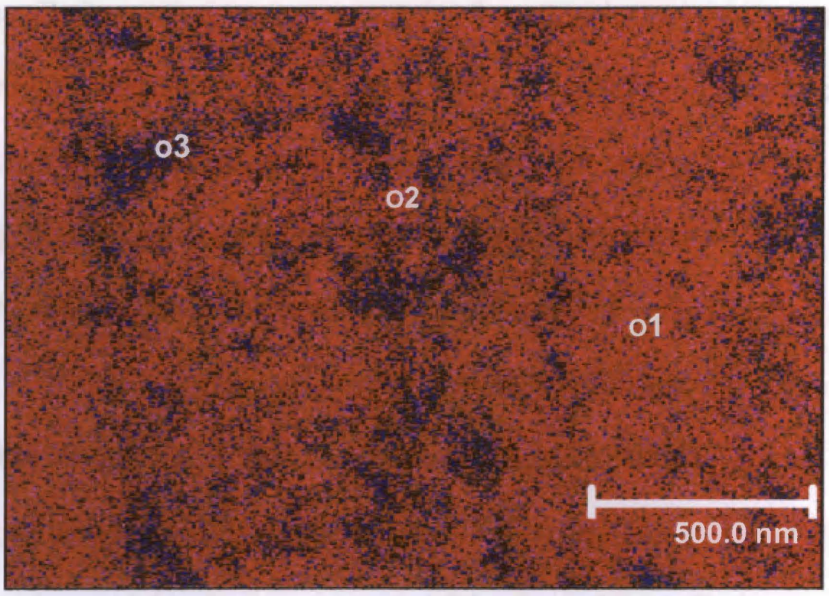

(b) Auger image of derivatized RA-j fiber

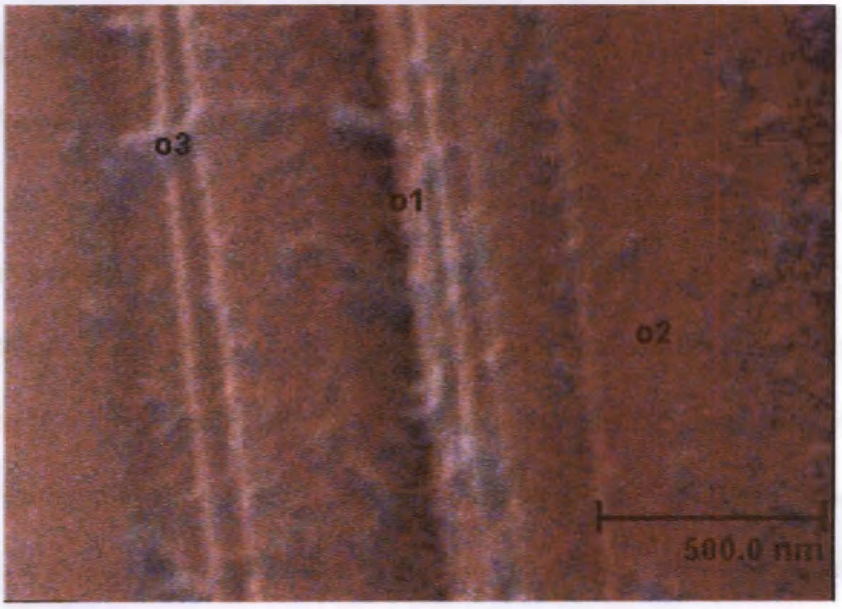

(c) Superimposed image

Figure 5-14. Continued

the Auger image was taken from the entire region and is shown in Figure 5-14 (b). Different from conventional UU fibers, which have carbon as the dominant element that covers the entire region, RA-j has a considerable amount of cobalt that has distribution preferring the valleys. These results provide information regarding the placement of carboxyl groups since the distribution of cobalt element with regard to fiber surface morphology indicates the distribution of carboxyl groups.

To have a better understanding of how cobalt is distributed on the scanned region, the SEM image and Auger image were superimposed and shown in Figure 5-14 (c). Another single fiber of derivatized RA-j was examined and the results are shown in Figure 5-15. Additional fibers with relative high concentration of acid groups as determined by XPS C 1s (Table 5-9, 5-12) deconvolution were investigated and the results are shown in Figure 5-16 ~ 5-19. The preferential placement of cobalt on valley regions was also observed in these fibers.

The superimposed images clearly show a correlation between microstructural features and distribution of acid groups implanted during plasma surface treatment. It is observed that most cobalt was distributed along the valley regions. It seems that compared to ridges, there are more active site groups located along the valley, at which carbon atoms with unpaired electrons were attacked by oxygen species generated in plasma, leading to the formation of oxygen-containing functional groups. The orientation of graphite planes with regard to the fiber surface in both ridges and valleys, and the graphitic organization in both areas, i.e. any distortion present will be discussed in the next section.

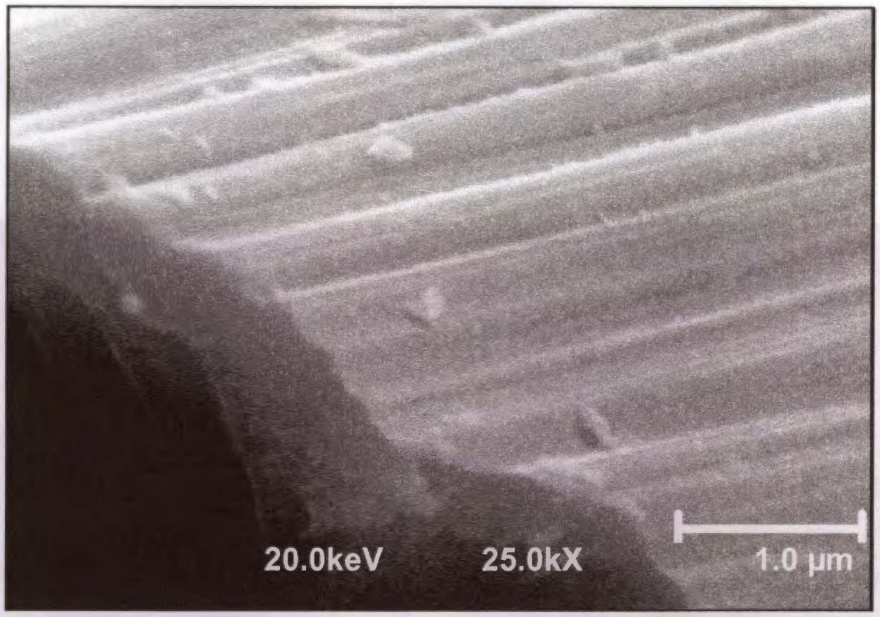

(a) SEM image of derivatized RA-j fiber

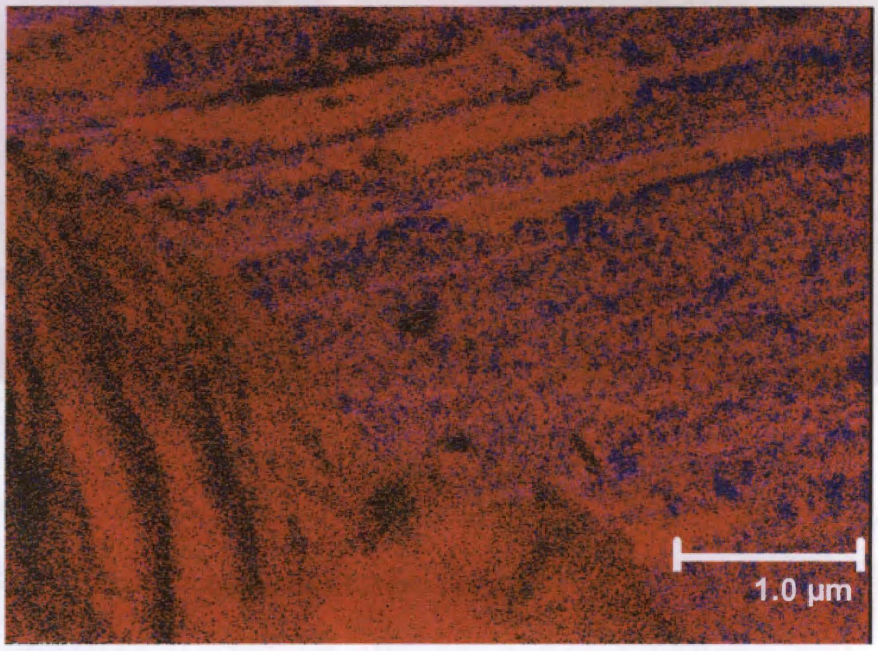

(b) Auger image of derivatized RA-j fiber

Figure 5-15. Morphology and elemental distribution of derivatized RA-j fiber by AES

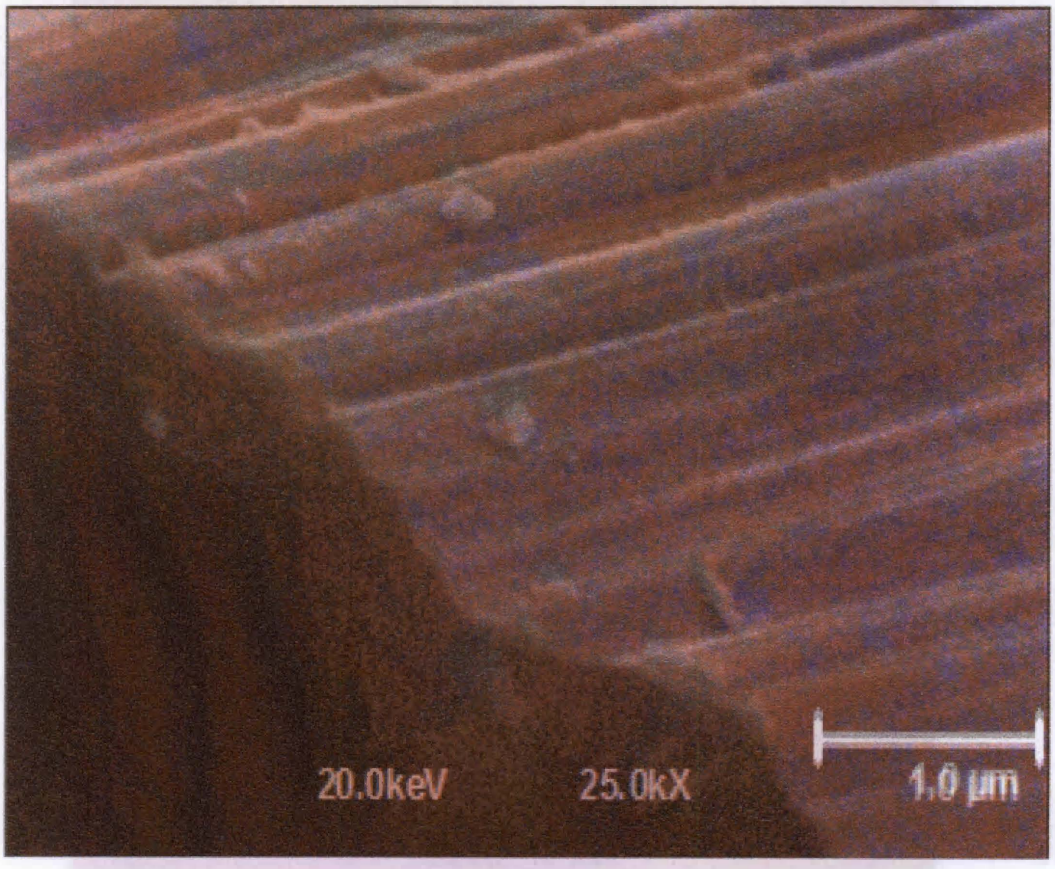

(c) Superimposed image

Figure 5-15. Continued

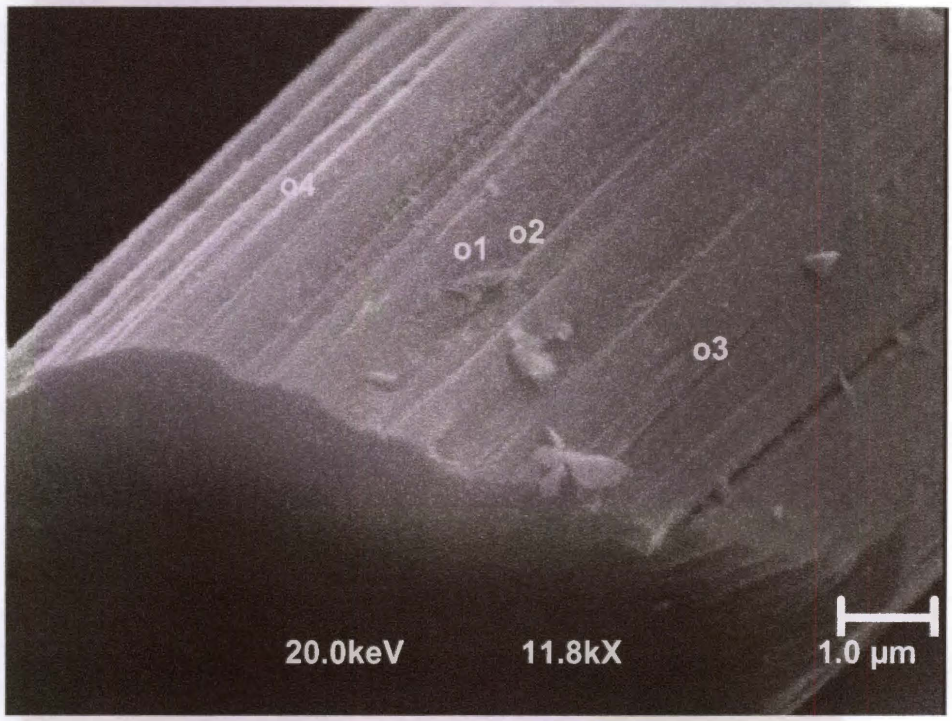

Atomic Concentration Table

Point	C	N	O	Si	Co
1	81.25	2.33	9.73	0.71	4.98
2	66.45	3.28	16.06	0.91	13.30
3	81.38	3.43	8.74	0.53	5.92
4	71.83	2.88	12.84	1.21	11.24

(a) SEM image of derivatized RA-f fiber and elemental point analysis by AES

Figure 5-16. Morphology and elemental distribution of derivatized RA-f fiber by AES

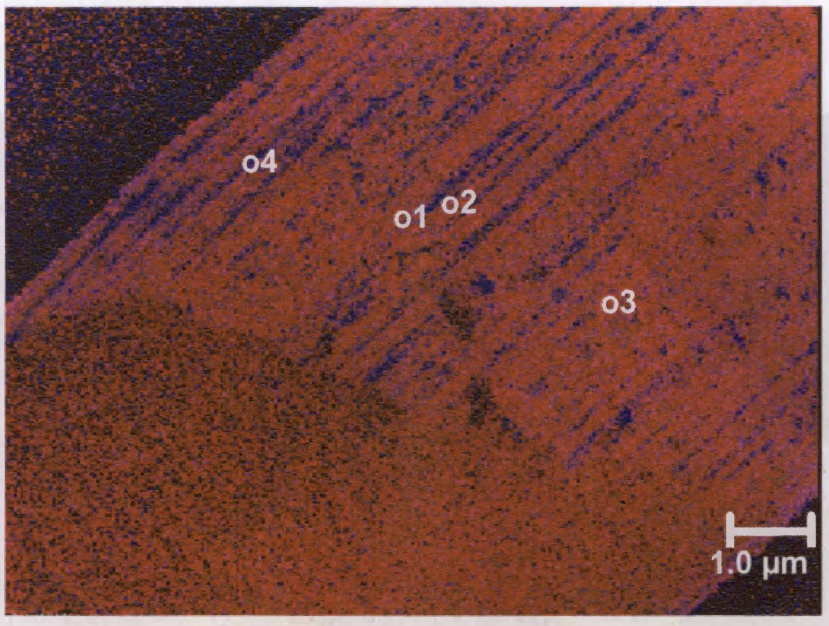

(b) Auger image of derivatized RA-f fiber

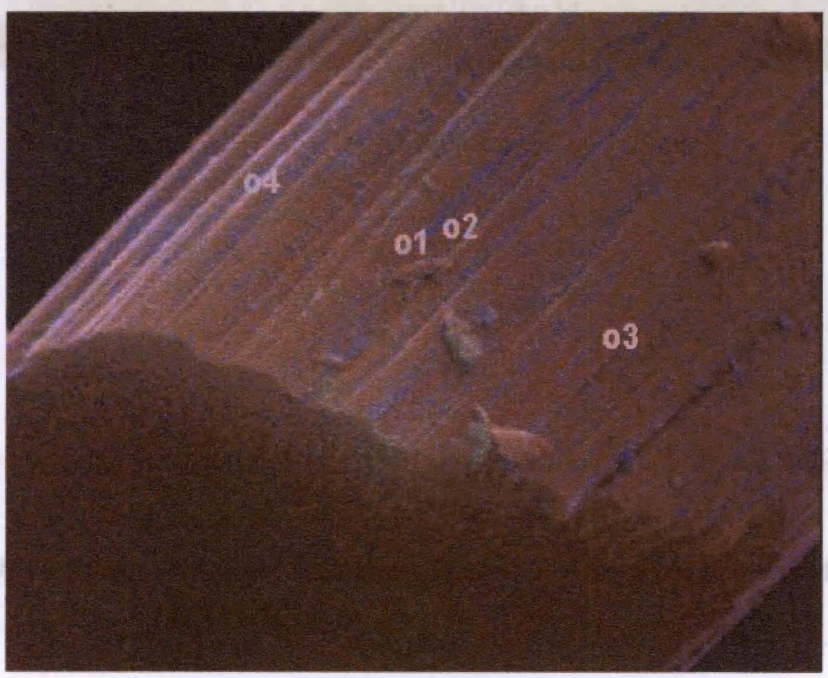

(c) Superimposed image

Figure 5-16. Continued

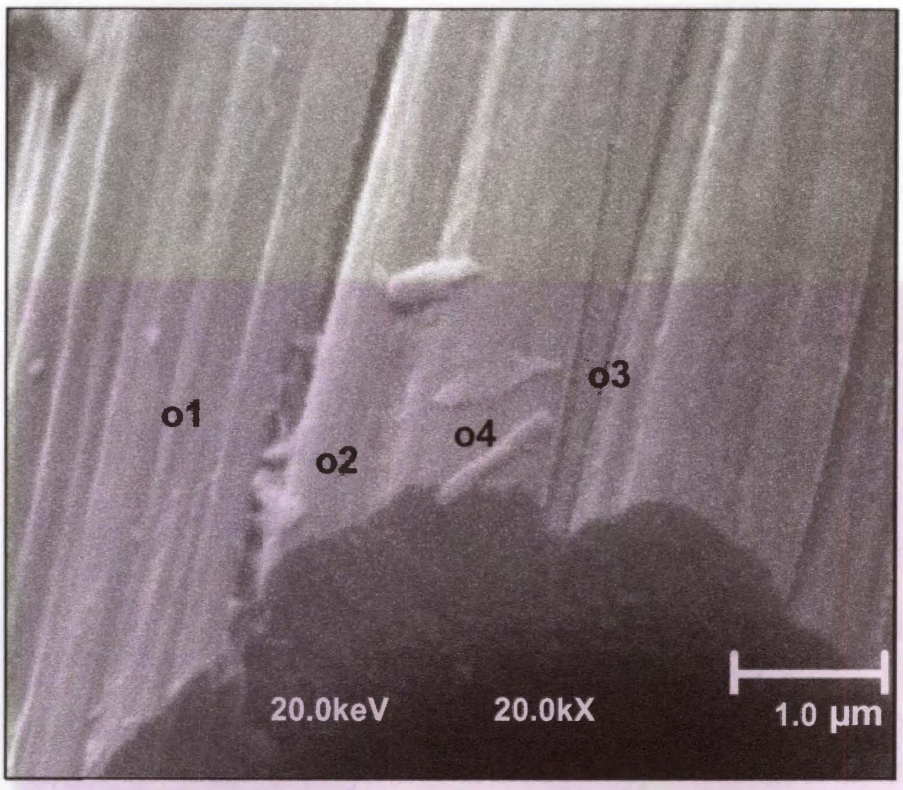

Atomic Concentration Table

Point	C	N	O	Cl	Co
1	71.31	1.23	14.71	0.24	10.51
2	83.99	3.03	8.63	0.28	4.07
3	72.92	1.80	13.60	0.16	11.52
4	81.13	3.69	9.49	0.12	5.58

(a) SEM image of derivatized RA-a fiber and elemental point analysis by AES

Figure 5-17. Morphology and elemental distribution of derivatized RA- a fibers by AES

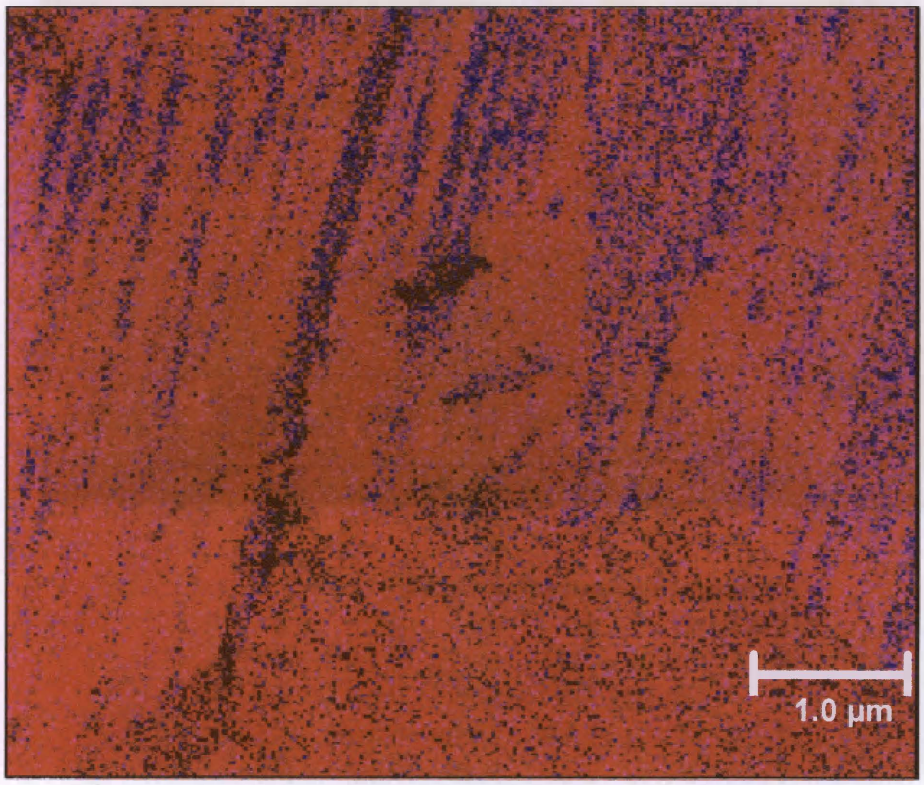

(b) Auger image of derivatized RA-a fiber

Figure 5-17. Continued.

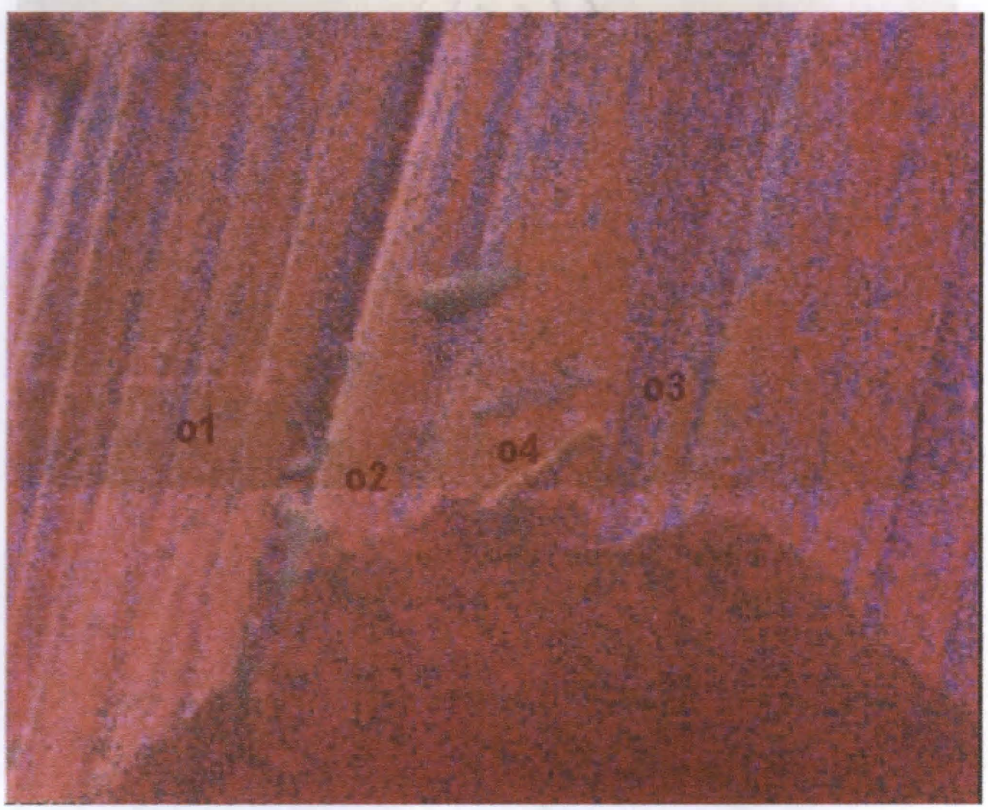

(c) Superimposed image

Figure 5-17. Continued.

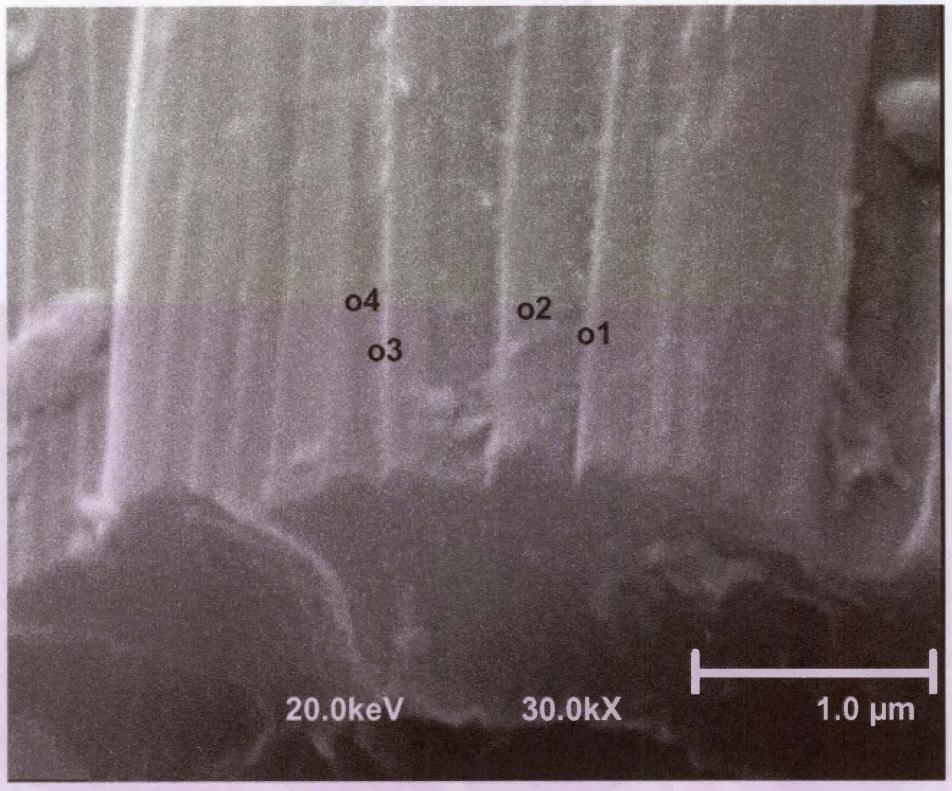

Atomic Concentration Table

Point	C	N	O	Cl	Co
1	72.05	2.01	14.52	0.23	11.19
2	81.40	1.69	8.32	0.33	7.26
3	65.44	2.17	18.51	0.21	13.67
4	86.89	3.46	5.85	0.25	3.56

(a) SEM image of derivatized AP-B fiber and elemental point analysis

Figure 5-18. Morphology and elemental distribution of derivatized AP-B fibers by AES

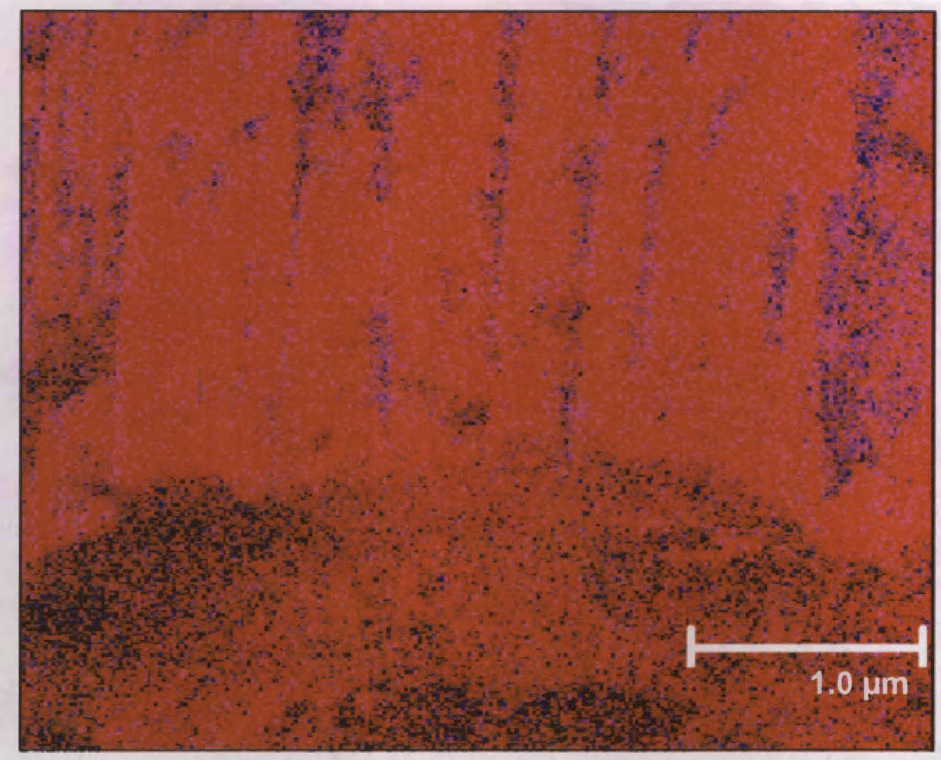

(b) Auger image of derivatized AP-B fiber

Figure 5-18. Continued.

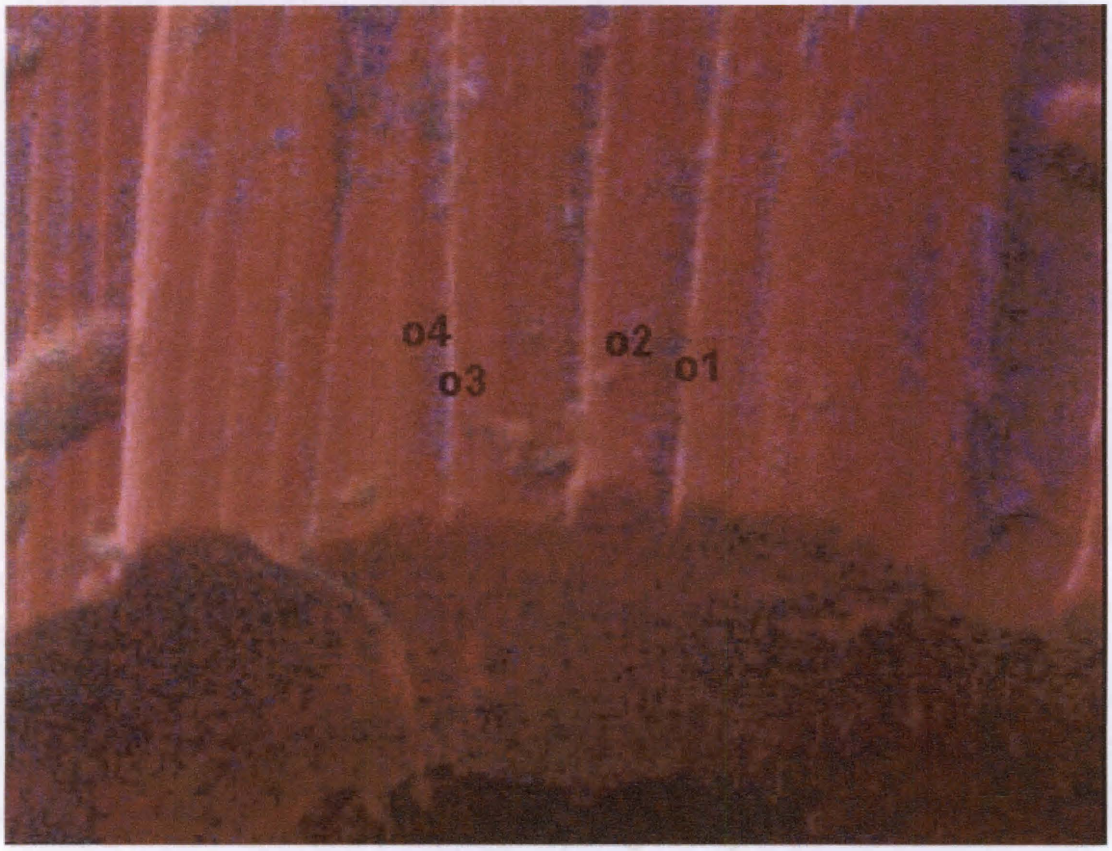

(c) Superimposed image

Figure 5-18. Continued.

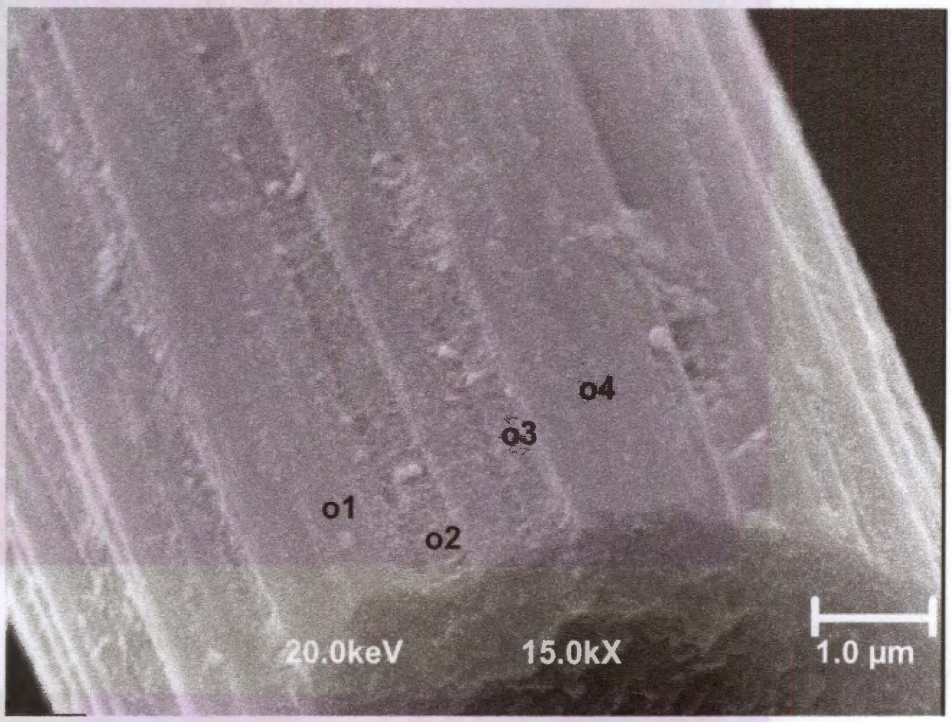

Atomic Concentration Table

Point	C	N	O	Si	Cl	Co
1	83.84	3.23	6.12	1.18	0.17	5.47
2	72.29	1.66	10.68	1.30	0.22	11.86
3	70.09	2.08	12.44	1.37	0.38	12.63
4	83.45	3.56	5.75	0.83	0.26	6.15

(a) SEM image of derivatized AP-E fiber

Figure 5-19. Morphology and elemental distribution of derivatized AP-E fibers by AES

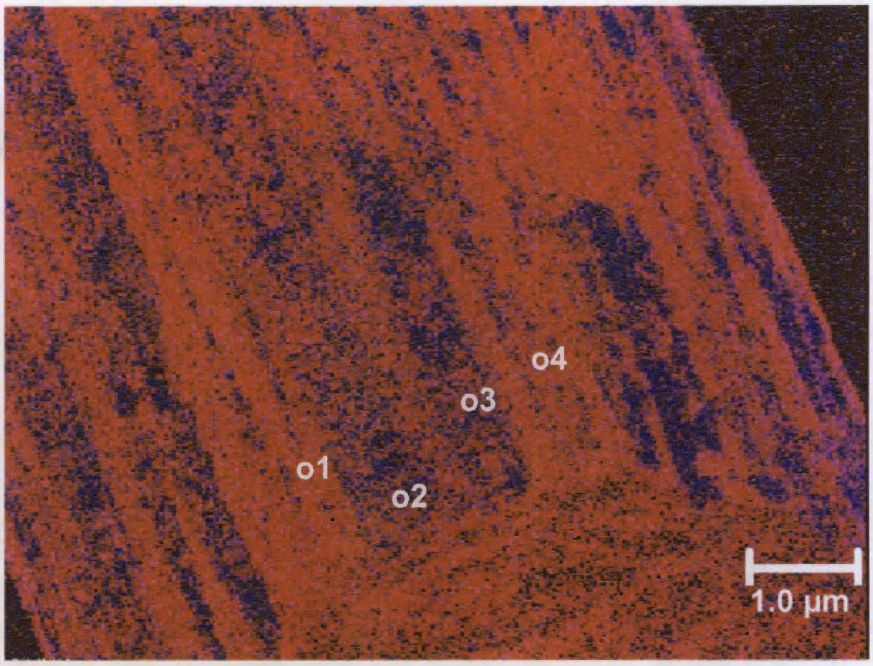

(b) Auger image of derivatized AP-E fiber

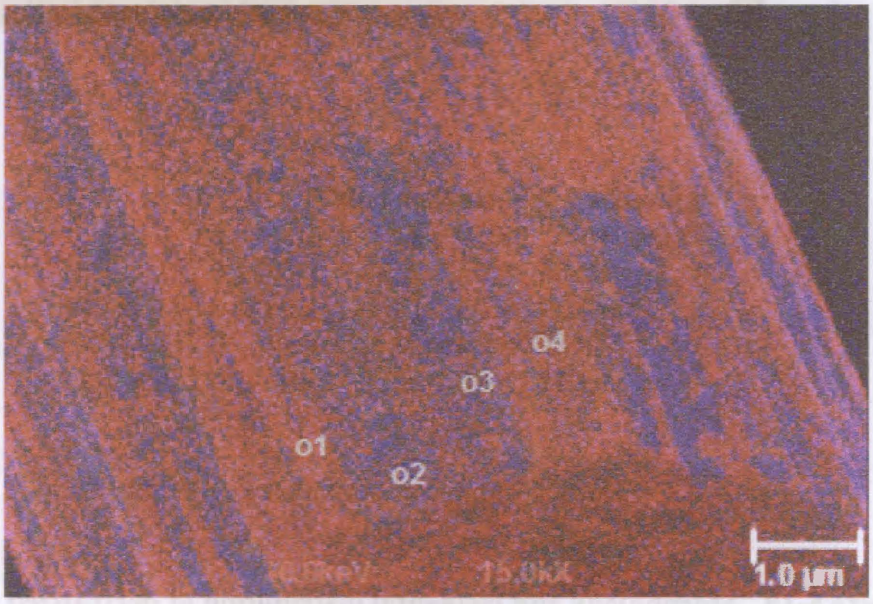

(c) Superimposed image

Figure 5-19. Continued.

5.4 Interphase Chemistry Characterization by FTIR Imaging Technique

This technique enables the imaging of the spatial distribution of functional groups present within a given area. The contrast in the image arises from the inherent infrared absorptions of the functional groups present in the sample. Every chemical compound has its own characteristic absorption pattern or spectrum.

The first sample used was conventional fibers treated by ozone to investigate the feasibility of using this new technique for research on carbon fiber-matrix interphase. The spectra were collected from different areas within the sample and the results provided images of the spatial distribution of chemical bonding. The results are shown in Figure 5-20 and Table 5-14.

The functional chemical groups resulting from surface treatment of the fibers can be carbonyl (C=O), carboxyl (-COOH) and ether (C-O-C). The urethane amide (NH-) group present in the polyurethane has the ability to form hydrogen bonds with the oxygen functionalities deposited (–C=O) on the carbon fiber surface.

The formation of hydrogen bonding with amide (NH) leads to a change in shape and shift in position of the absorption band. The inter-phase chemistry was monitored by following the changes in the spectral position and shape of the infrared absorption bands. Normally shifts from approximately 3400 cm-1 to within the range of 3325-3200 cm^{-1}. In each picture shown in Figures 5-20 an image of the spatial distribution of N-H group along a single fiber is provided on the left. From the image, one can clearly see a single fiber (yellow) is embedded in the polyurethane matrix (blue). And between these

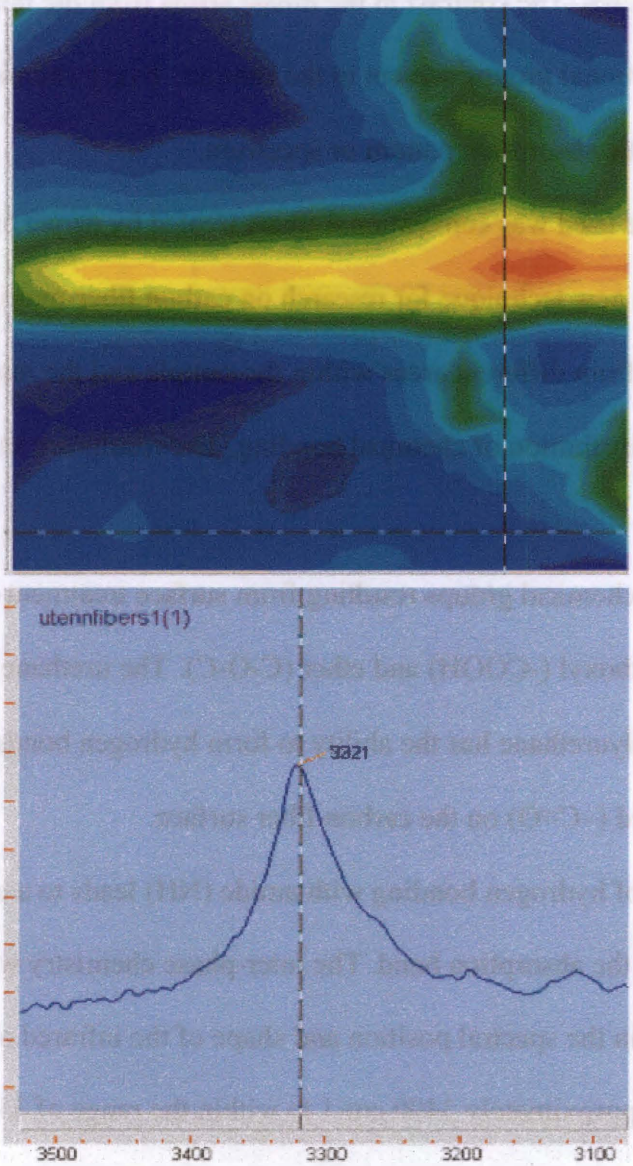

(a) FTIR image and spectrum taken from position 1

Figure 5-20. FTIR image and spectrum for conventional samples treated

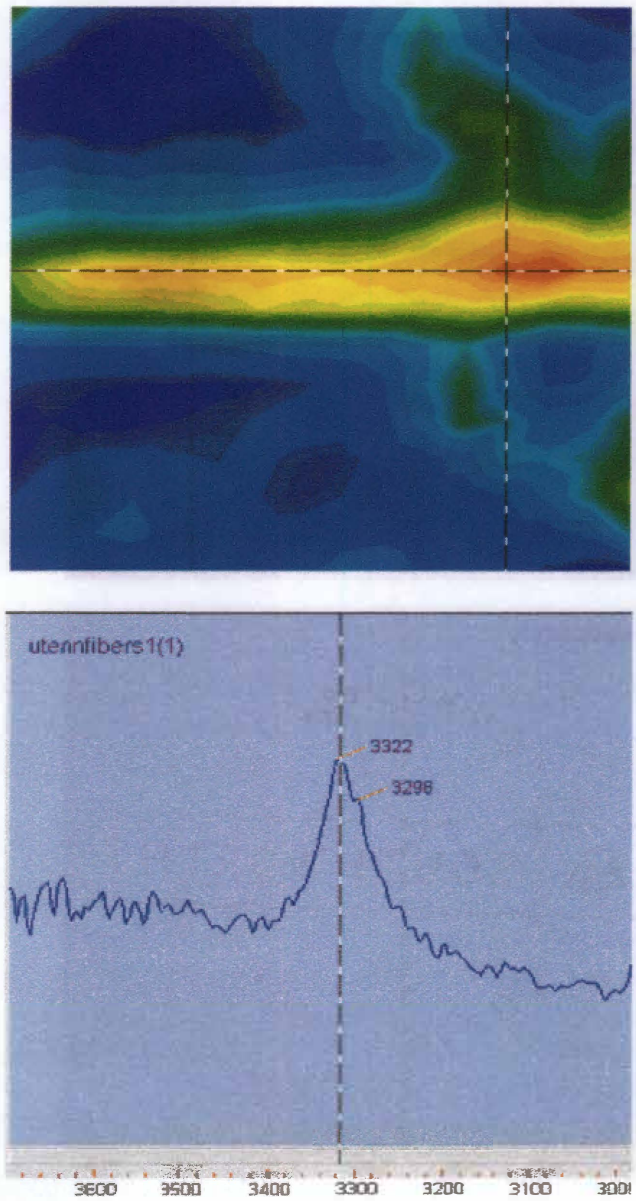

(b) FTIR image and spectrum taken from position 2

Figure 5-20. Continued.

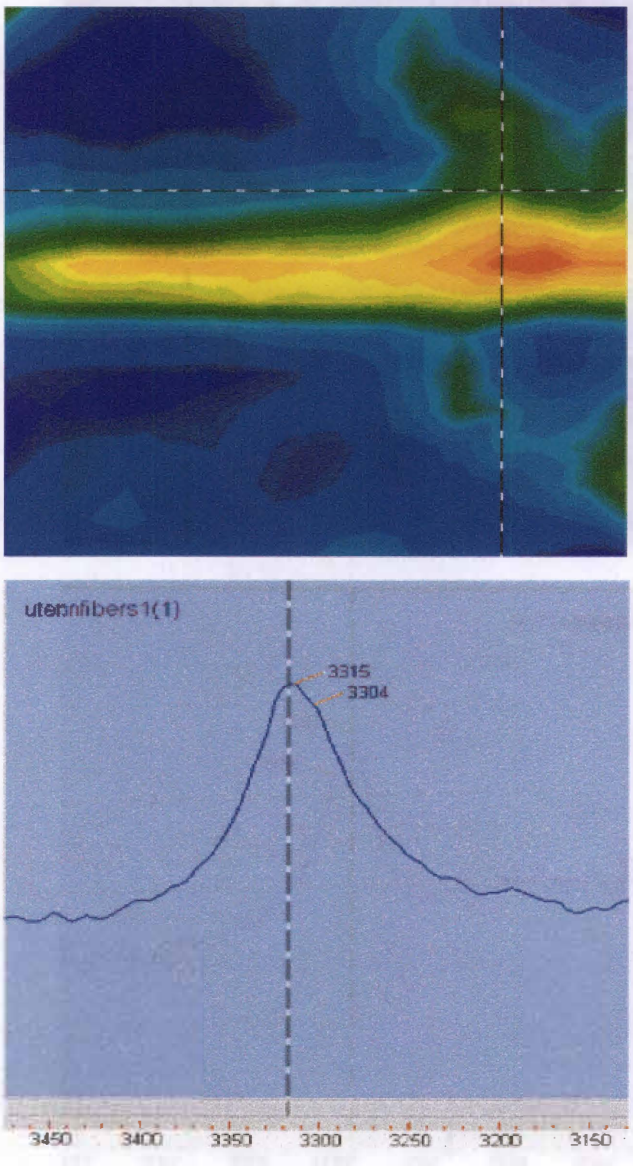

(c) FTIR image and spectrum taken from position 3

Figure 5-20. Continued.

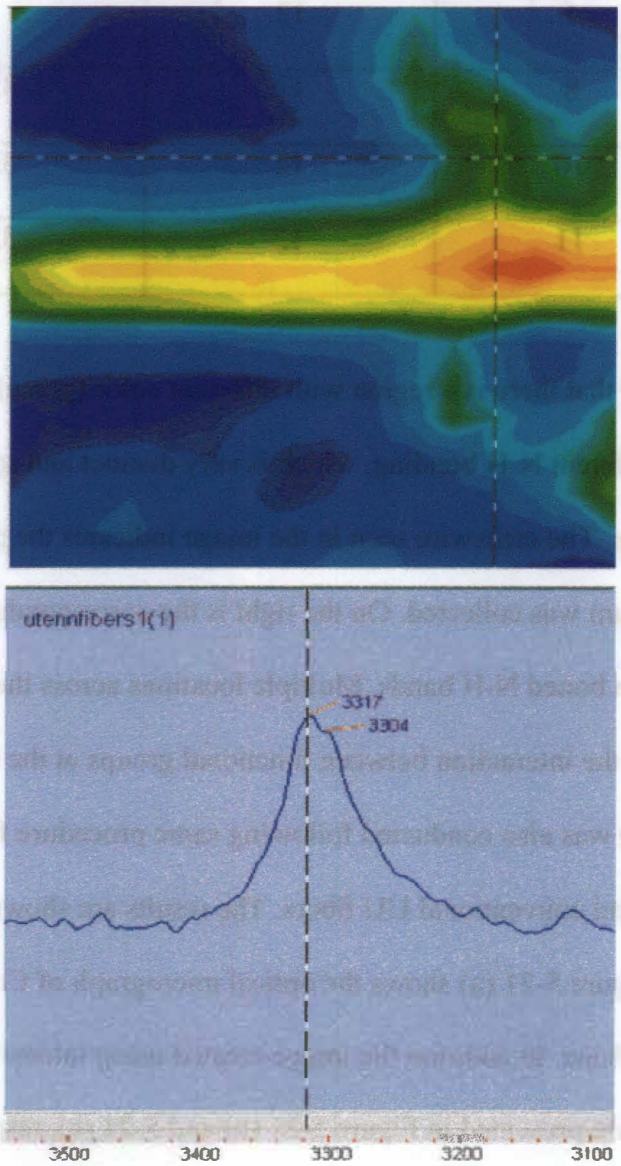

(d) FTIR image and spectrum taken from position 4

Figure 5-20. Continued.

Table 5 –14. N-H band positions in different locations

	Number of Row	Number of Column	Wave number (N-H) (cm^{-1})
Position 1	1	12	3321
Position 2	8	12	3322, 3298
Position 3	10	12	3315, 3304
Position 4	11	12	3317, 3304

two phases it is noted that there is a region with different color (green) indicating there is third phase with a different N-H bonding, which is very distinct and spatially separated from other two phases. The crosswire seen in the image indicates the position where the corresponding spectrum was collected. On the right is the corresponding spectrum showing the hydrogen boned N-H bands. Multiple locations across the interphase region were chosen to study the interaction between functional groups at the inter-phase.

FTIR imaging was also conducted following same procedure for selected fibers treated with plasma and conventional UU fibers. The results are shown in Figure 5-21, 5-22, 5-23 and 5-24. Figure 5-21 (a) shows the optical micrograph of Con UU fibers imbedded in polyurethane. In addition the image created using intensity of N-H band and peak position image are presented in Figure 5-21 (b) and 5-21 (c), respectively. The peak position image was obtained by plotting the position of the maximum of the N-H band in the 3200 – 3400 cm^{-1} spectral range. While Figure 5-21 (c) provides information regarding distribution of wavenumbers of N-H band, the exact position and shape of the

(a) Optical Micrograph

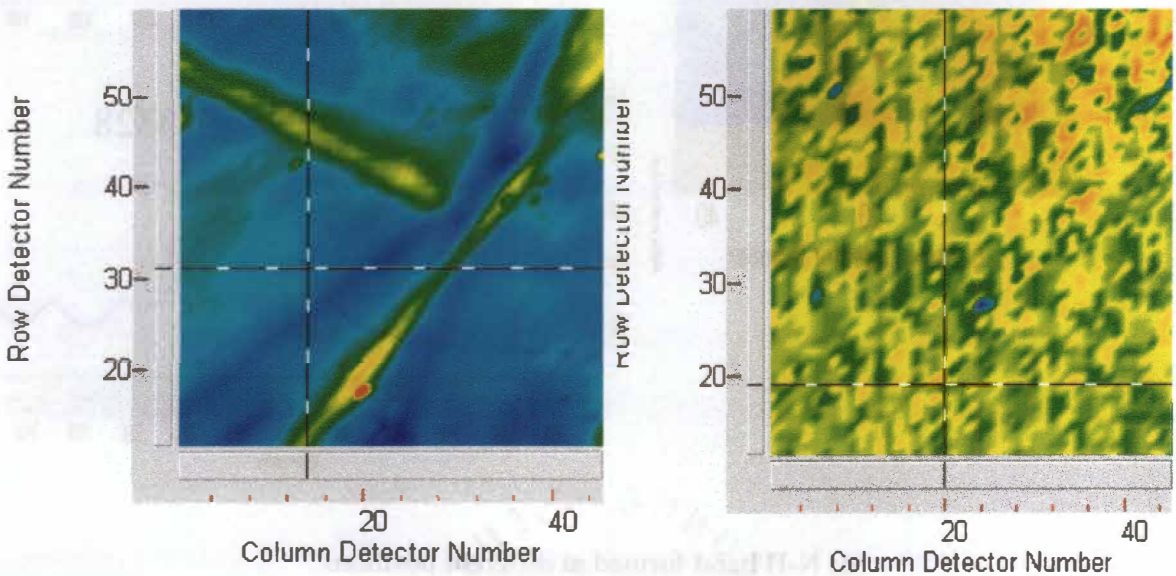

(b) Infrared Image

(c) Peak Position Image

Figure 5-21. Optical micrograph and FTIR image of Con UU/PU

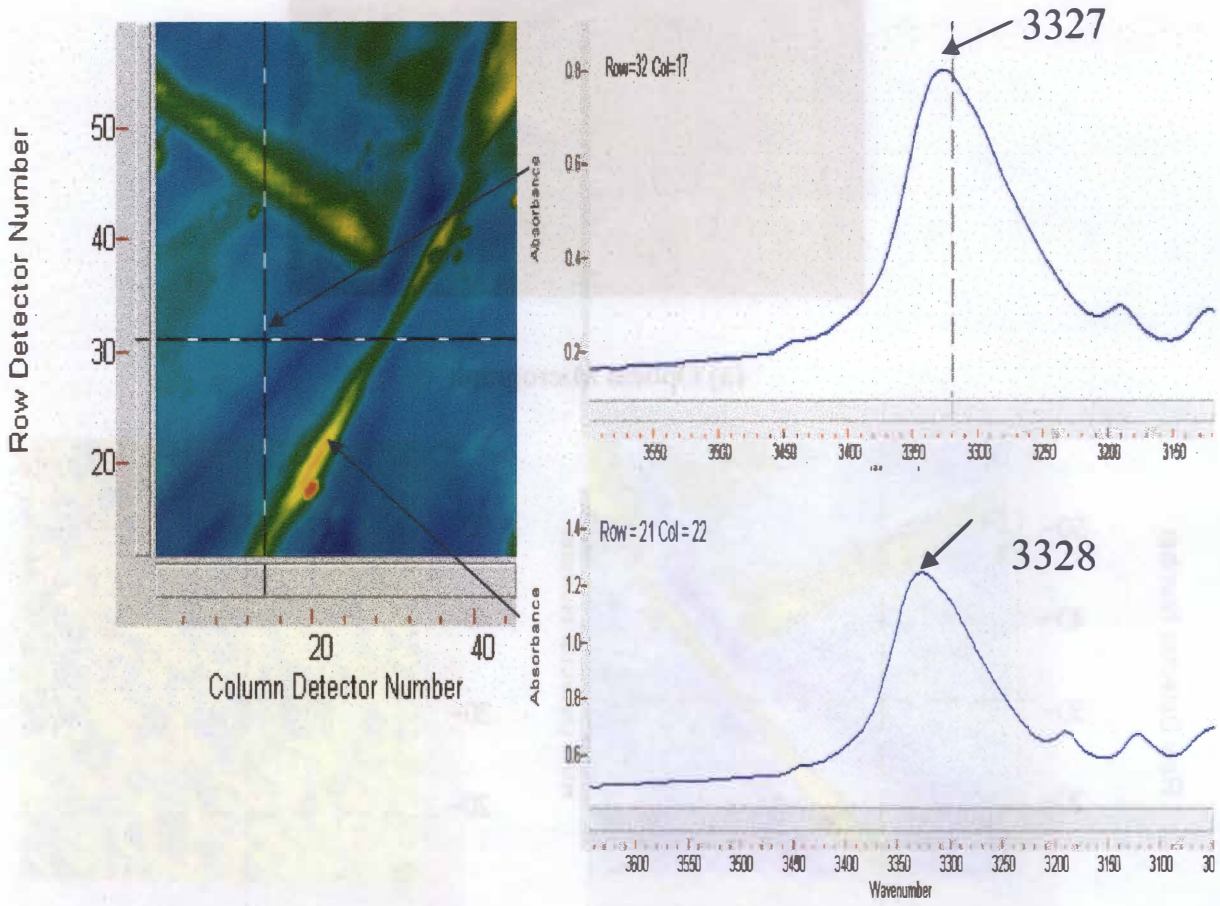

(d) N-H band formed at different positions

Figure 5-21. Continued

(a) Optical Micrograph

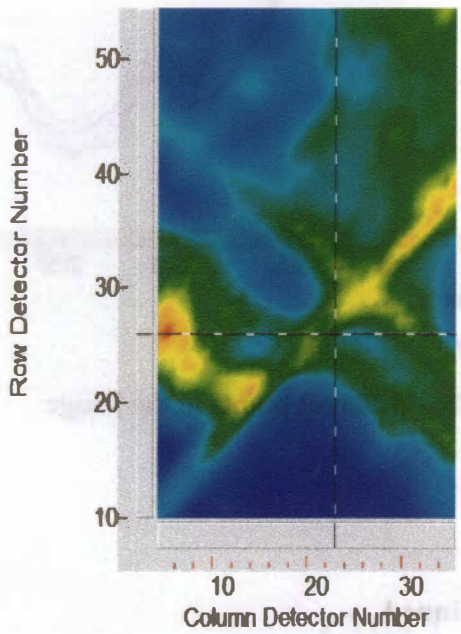

(b) Infrared Image

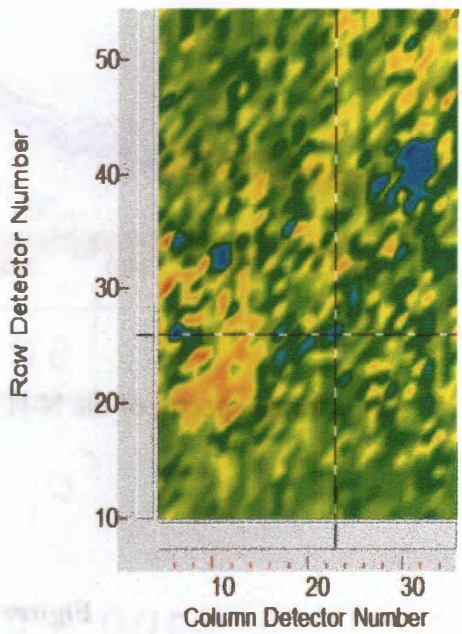

(c) Peak Position Image

Figure 5-22. Optical micrograph and FTIR image of AP-B/PU

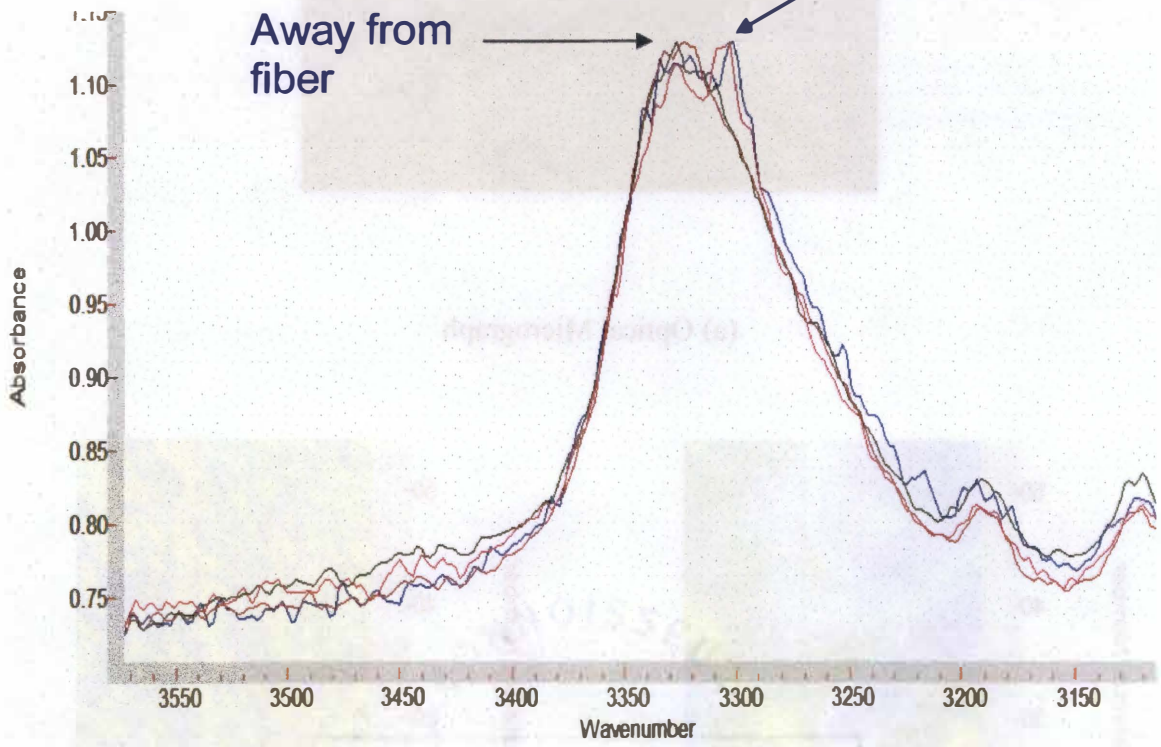

(d) Infrared spectra of the N-H peak from four different points in the image

Figure 5-22. Continued

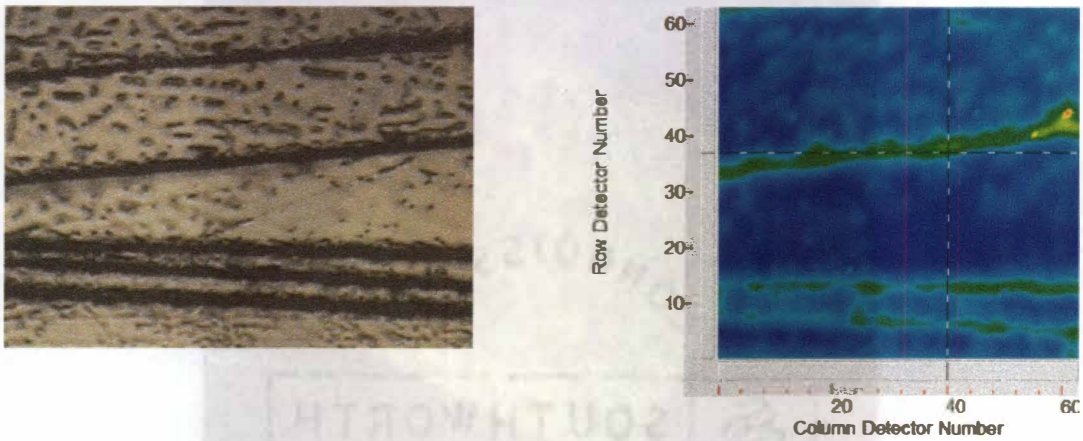

(a) Optical Micrograph (b) Infrared Image

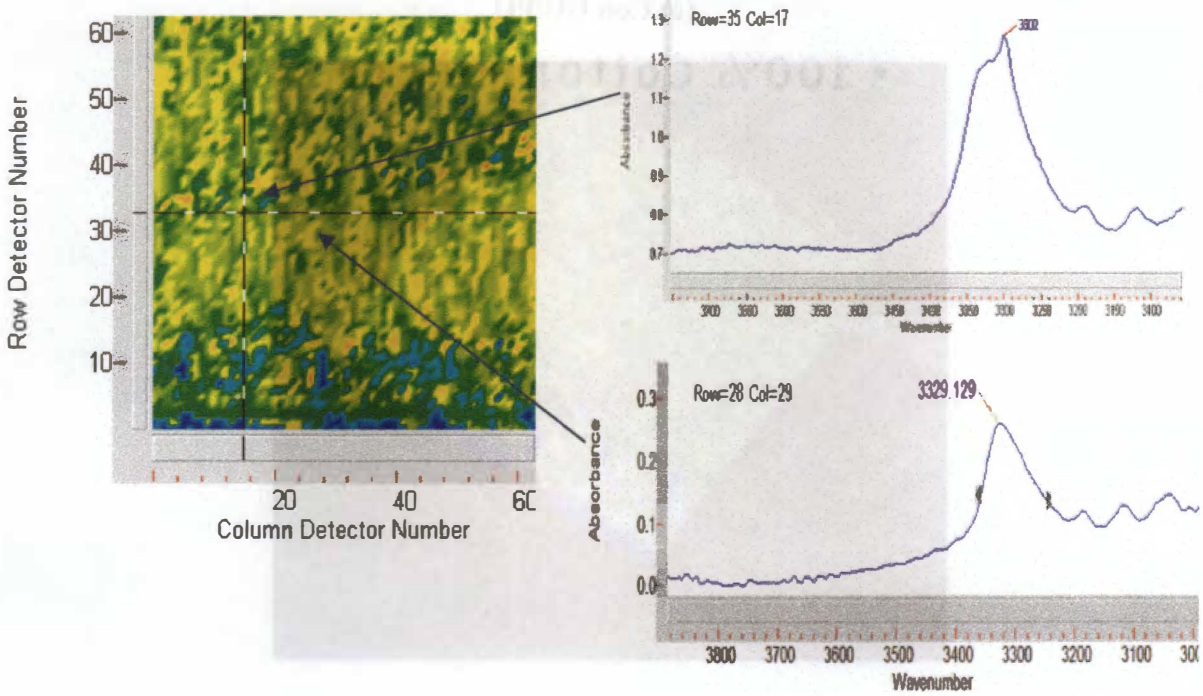

(c) Peak position image and N-H band formed at different positions

Figure 5-23. Optical micrograph and FTIR image of RA-j/PU

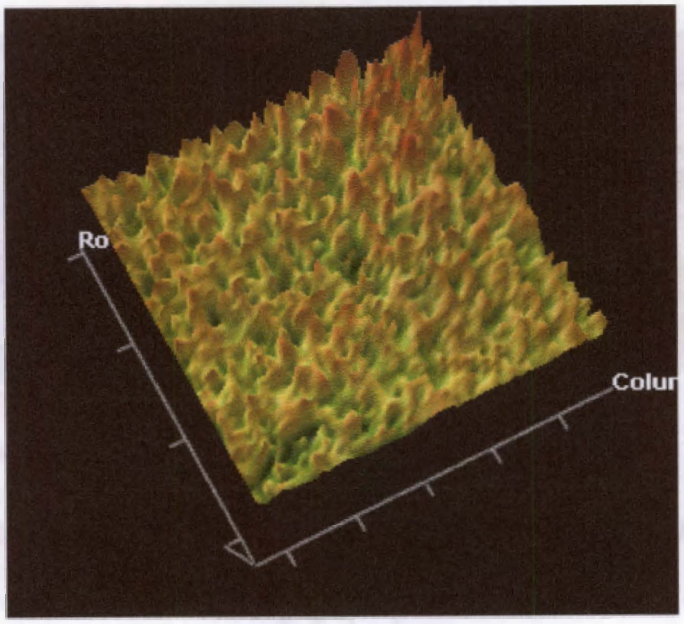

(a) Con UU/PU

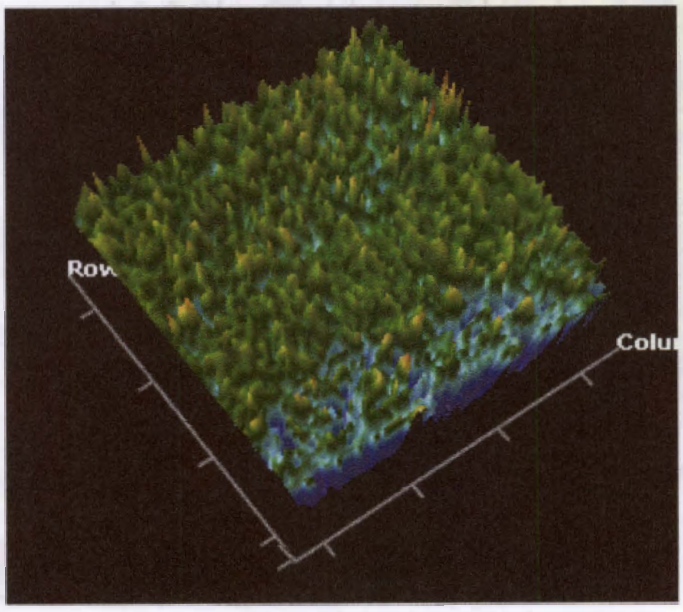

(b) RA-j/PU

Figure 5-24. 3-D images of Con UU/ PU and RA-j/PU

band from selected area can be obtained by performing single position analysis. Figure 5-21 (d) shows the results from the single point analysis of two selected areas. One point is from urethane matrix region (3327 cm^{-1}), the other (3328 cm^{-1}) is from region on the Con UU fiber. Note the position and shape of N-H band are similar. Figure 5-22 (a) shows the optical micrograph of atmospheric plasma treated sample AP-B fibers imbedded in urethane matrix. The infrared image of N-H band and peak position image are shown in Figure 5-22 (b) and 5-22 (c). Four areas were selected from both matrix regions and fiber regions and the composite plot of N-H band is shown in Figure 5-22 (d). As can be seen, for areas away from fiber the position and shape of N-H band are different from the ones close to fiber. Figure 5-23 (a) is the optical micrograph of fibers treated in remote applicator (RA-j) imbedded in urethane. N-H band image and peak position image for RA-j/PU sample are shown in Figure 5-23 (b) and Figure 5-23 (c), respectively. Two areas were selected for single position analysis, one is from urethane matrix and the other one is from fiber and the results are shown in Figure 5-23 (c). The differences in the position and shape of N-H band for these two regions are obvious.

To different extent, two plasma treated samples have shown a tendency of lower wavenumber area (blue) being aligned with the fiber direction, i.e., from peak position image one can see the location of fibers, which is not the case for conventional UU/PU sample. Figure 5-24 shows 3-D peak position images to have a better understanding of the distribution of N-H wavenumber. The difference between ConUU/PU and RA-j/PU is quite clear.

CHAPTER 6

DISCUSSION

6.1. Comparison of Conventional Fiber and MAP Fiber

Compared to conventional carbon fibers, an increase in oxygen concentration is observed on MAP fiber surface. The higher oxygen concentration corresponds to a higher concentration of oxygen-contained functional groups on the fiber surface, which is a key factor for the improvement of interphase strength. In the following sections, a discussion of the differences between conventional and MAP fibers is presented in terms of surface elemental oxygen concentration, functional group distribution, and the effect of surface treatment.

6.1.1. Oxygen concentration along the fiber

Carbon fibers have a heterogeneous microstructure with a turbostratic crystallite characteristic. The basic unit is a planar hexagonal sheet of carbon atoms. The external surface of carbon fiber is different from the internal structure, the former having a more ordered structure with preferred orientation parallel to the fiber surface. But the turbostratic stacking of the graphene planes in the fibers leads to disordered structure that is far from the ideal graphite and results in disruption and curvatures of basal plane, which will leave incompletely bonded edges on the graphite crystal surface. Those chemically active sites are generally thought to accommodate active chemical species to form polar groups on the fiber surface through surface treatment. During the

manufacturing of carbon fibers, heating temperature up to 2500°C will cause partial or full graphitization of fiber, which has less amount of turbostratic disorder. Paulauskas and Spruiell [90] characterized carbon fibers using wide angle X-ray diffraction and found that MAP fibers have a roughly equivalent morphology to the conventional fibers (Fortafil F3(c)). The similarities include stack height of graphene planes, Lc, crystal size, La and orientation of the graphene planes relative to the fiber axis. Their data suggest that MAP processed fiber were treated at a temperature in the range of 1200-1500°C. Therefore, both MAP and conventional fibers we used in the work are carbonized fibers.

The comparison in Figure 6-1 shows that though going through same ozone surface treatment, MAP TU fibers shows almost double amount of oxygen on the surface than conventional TU fibers. The explanation is that during MAP process, the volumetric heating of stabilized precursor throughout the fiber cross section leads to the carbonization of fibers, the structure of the fibers formed are comparable to the conventional one. But it must be recognized that WAXD data gives information from both the sheath and the core of the fiber, while XPS gives information from the very top layers in a depth of a few nanometers. So, it seems the MAP process also has an effect on the fiber surface similar to general plasma surface treatment upon completion of the process. The off-gases released in the carbonization process was consumed leading to formation of plasma particles that bombard the surface of carbon fiber etching out the loose material and producing more active sites on the surface. This highly reactive surface allows the formation of oxygen functionality on the fiber surface, which might be

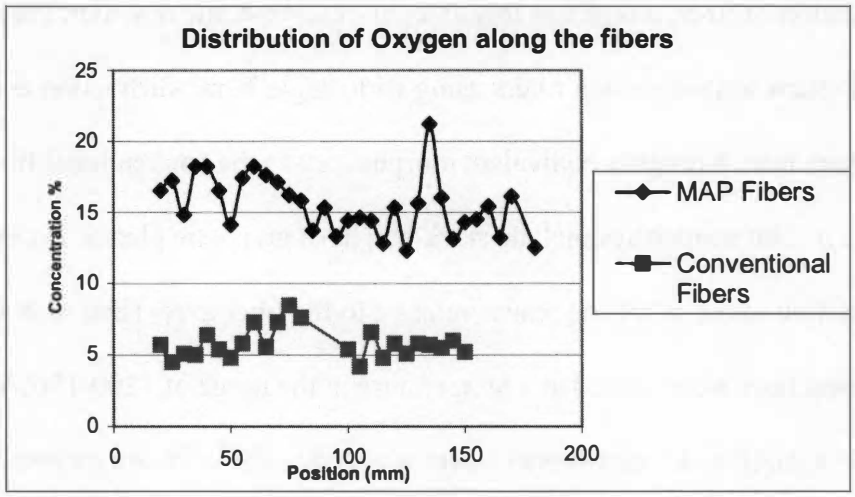

Figure 6-1. Comparison of MAP TU fiber and conventional TU fiber

caused by the presence of small amount of oxygen due to air leaks at the end of carbonization process or due to oxidation, happened when fibers are exposed to air. The formation of oxygen functionalities during MAP processing leads to higher oxygen concentration compared to conventional UU fibers. The larger number of active sites on the surface of MAP UU fibers is the reason for same ozone treatment resulting in much higher oxygen functionality on MAP TU fibers than conventional TU fibers.

6.1.2 Effect of surface treatment

The effect of surface treatment on conventional fiber leads to small differences in the concentration of elemental oxygen (Figure 6.2). But for MAP fiber, after surface treatment, about 100% increase on oxygen concentration was achieved. As discussed

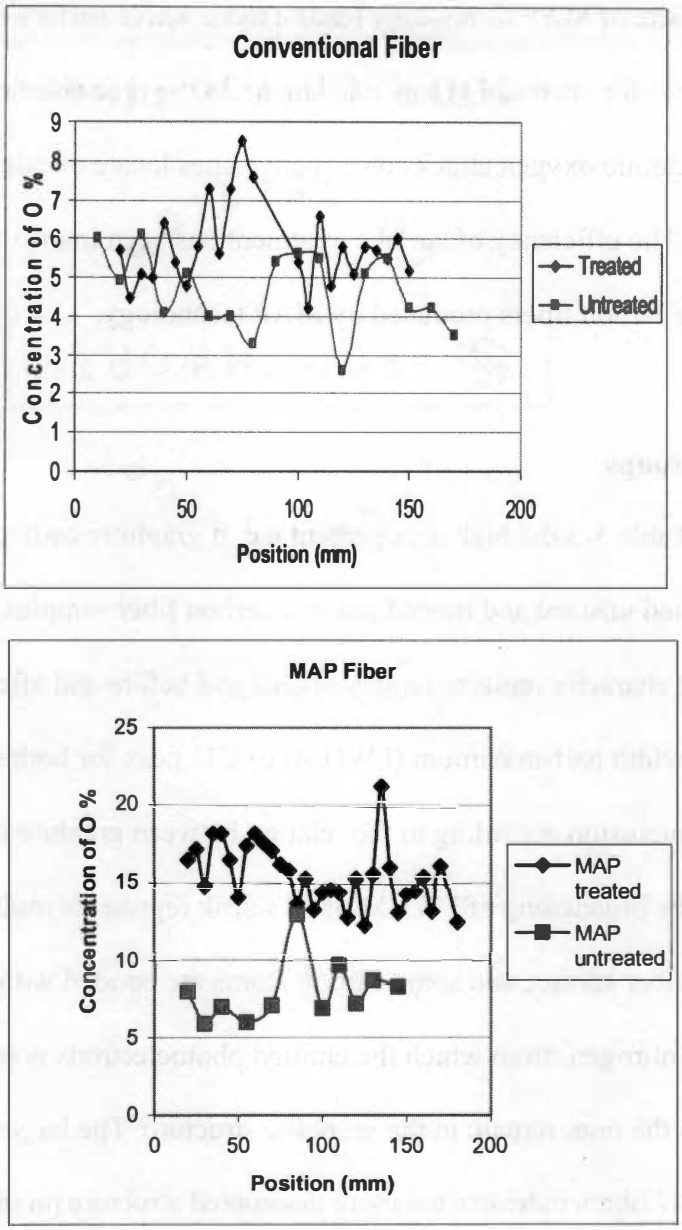

Figure 6-2. Comparison of effect of surface treatment on MAP fiber and Conventional fiber

above the characteristic of MAP technology leads a more active surface due to formation of more activated sites for chemical group attachment. In the process of ozone treatment, the highly reactive atomic oxygen attacks these active sites locate on edge planes and oxidize the surface. The efficiency of surface treatment has been improved immensely when it is applied to carbon fibers produced by MAP technology.

6.1.3 Functional groups

As seen in Table 5-5 the high area percentage of graphitic carbon in both conventional untreated unsized and treated unsized carbon fiber samples indicates that the overall graphitic character remains largely unchanged before and after surface treatment. The full-width half-maximum (FWHM) of C1s peak for both samples also leads to the same conclusion according to the relation between graphite order and XPS main peak width. The broadening of FWHM of C1s peak represents multiple oxidation states occurring on fiber surface and some carbon atoms are bonded with other atoms, such as oxygen and nitrogen, from which the emitted photoelectrons posses different binding energy than the ones remain in the graphitic structure. The larger value of FWHM for MAP UU fibers indicates the more disordered structure on the surface than for conventional UU fibers. It is seen that Con UU sample contains a significant percentage of peak 1 corresponding to C-OH and C-O-C groups, which is due to oxidation in storage. There is a generally a small increase in the level of surface oxidation after ozone treatment on conventional fibers, which is illustrated by the increase in all three oxide peaks. The order of graphitic structure is reduced, which is indicated by the

larger value of FWHM. The results for MAP fibers show a dramatic decrease of graphitic peak even before the surface treatment. The high percentage of peak 1 for untreated unsized MAP fiber indicate that the plasma process has changed the graphitic structure on the fiber surface to a great extent that surface is not completely inert, though the overall morphological structure is comparable to conventional fibers indicated by WAXD data. The active character of the surface allows oxygen functionality formation that might be caused by the presence of some oxygen due to air leaks upon the completion of carbonization process. Another reason could be the oxidation of this reactive surface once exposed to air. After the untreated unsized MAP fiber was subjected to ozone treatment, the principal changes are increases in the amount of C=O (peak 2) and COOH or COOR (peak 3) functionality, which approximately double in intensity. The active surface of untreated unsized MAP fiber is the reason for a better efficiency during ozone treatment compared to conventional fibers.

6.2 Analysis of Plasma Treatment

The nature of plasma treatments are known to be affected by operating parameters such as power input, gas flow rate, reactor pressure, treatment time and the location of the fibers with respect to the glow region. This section will include the discussion of two plasma treatment processes: remote applicator and atmospheric plasma. The relationship between process parameters and characteristic of the modified fiber surface will be presented.

6.2.1 RA samples

1. Effect of input power

Concentrations of oxygen found on the samples treated with remote applicator system are given in Table 5-7. In order to investigate the effect of input power used in the process of surface treatment, samples are divided into two categories: short treatment time (70 sec) and long time treatment time (3 min). The results and comparison are presented in Table 6-1, 6-2, and Figure 6-3 and 6-4.

Four samples were treated under 70 sec, but for these four samples, four different gas systems were used (Table 6-1 and Figure 6-3). And meanwhile the input power and pressure applied were also different. So, it is very difficult to investigate the effect of input power on the surface treatment without having a series samples undergone different input power with other parameters being constant. RA-d and RA-g were treated with air plasma and oxygen plasma under input power of 2kw and 1.1kw, respectively. The oxygen concentrations from these two samples are very close to ozone treated conventional fibers. It is known that electron density in plasma n_e increases linearly (at a first qualitative approximation) with an increase in input power [91]. As we know the success of cold plasma in surface treatment of fibers relies on its very high electronic temperature, T_e, which is the electronic energy given in Kelvin. These electrons possess enough energy to break typical chemical bonds. Generally, the higher the frequency and power input, the more profound is the surface modification. But surface oxygen concentration of RA-d and RA-f are in the same level with RA-h, which was treated with input power of only 129 w, though compared to oxygen plasma, the addition of 50%

Table 6-1. Comparison of oxygen concentration of RA samples treatment time of 70 seconds

Sample		Oxygen % *	Oxygen % **
RA-d	Average	9.2	9.4
Air, 2 kw	STDEV	0.5	0.5
RA-g	Average	8.9	9.7
O_2, 1.1 kw	STDEV	3.1	3.7
RA-h	Average	9.2	9.4
N_2/O_2, 50/50, 129 w	STDEV	1.0	1.1
RA-j	Average	16.4	16.7
N_2/O_2, 5/95, 220 w	STDEV	6.3	6.4

* Sodium concentration included in calculation

** Sodium concentration excluded in calculation

Table 6-2. Comparison of oxygen concentration of RA samples treatment time of 3 minutes

Sample		Oxygen % *	Oxygen % **
RA-a Air, 500 w	Average	12.7	15.1
	STDEV	2.7	3.6
RA-b Air, 1 kw	Average	8.0	8.3
	STDEV	2.0	2.0
RA-c Air 2 kw	Average	6.0	6.3
	STDEV	1.6	1.8
RA-e O_2, 1.1 kw	Average	12.4	13.2
	STDEV	5.3	5.4
RA-e-2	Average	7.6	8.3
	STDEV	3.8	1.9
RA-f O_2, 2.6 kw	Average	9.5	10.7
	STDEV	1.5	1.9
RA-e-2	Average	12.8	16.3
	STDEV	1.5	6.4

* Sodium concentration included in calculation

** Sodium concentration excluded in calculation

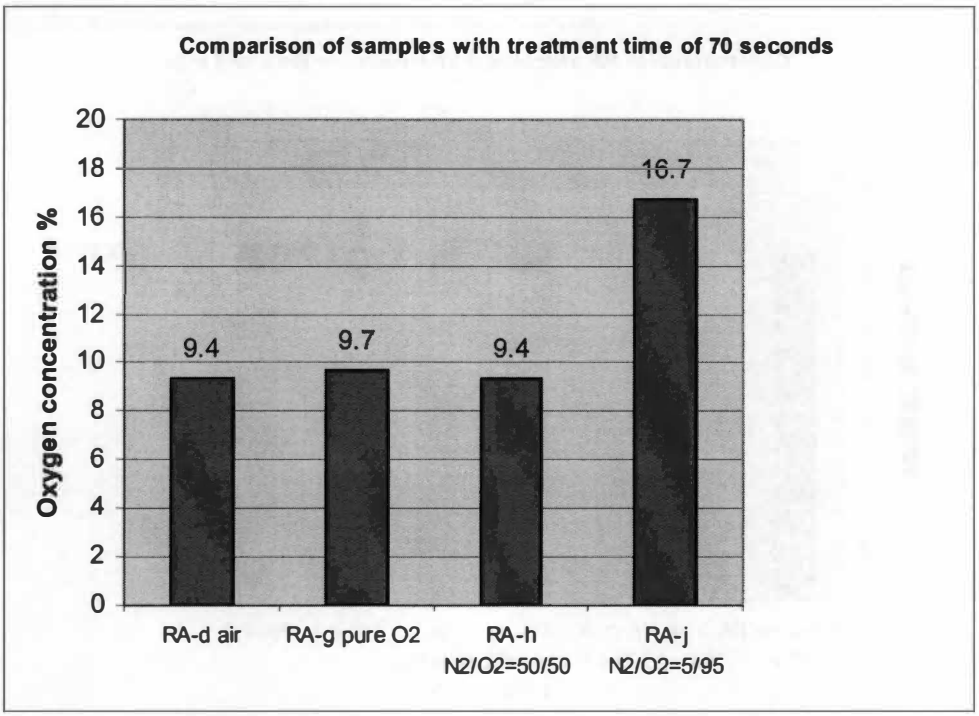

Figure 6-3. Comparison of samples with processing time of 70 seconds

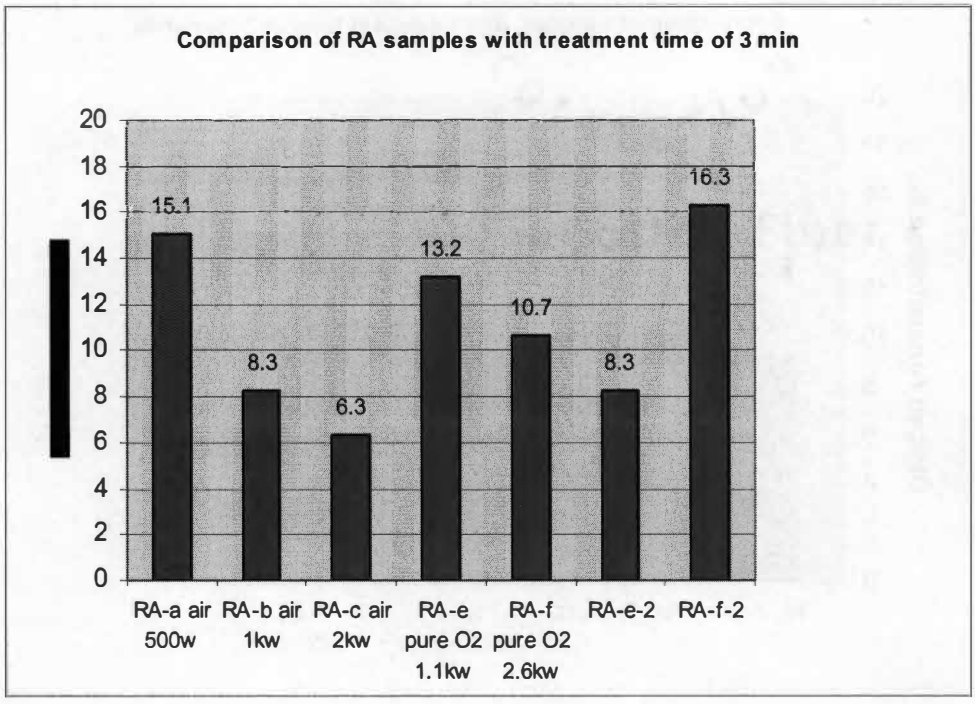

Figure 6-4. Comparison of samples with processing time of 3min seconds

nitrogen should reduce the efficiency of plasma treatment due to the less excited or ionized oxygen particles formed in plasma medium to initiate a chemical reaction on the fiber surface. It is assumed that this loss of surface material caused by local surface heating or ablation resulting loss of surface functionality. As mentioned before, because of lacking enough samples, it is not possible to draw a conclusion on the effect of input power on surface functionality implanted on fiber surface.

Among all the samples prepared by remote applicator process (RA), sample RA-j, which was treated in an environment consisting of 5% nitrogen, 95% oxygen using input power of 220 w for 70 s, gives the highest concentration of surface energy. Nitrogen has lower excitation energy than oxygen though having a higher dissociation and ionization energy. Adding of small amount of nitrogen helps to sustain the discharge without reducing the efficiency of plasma treatment. Series of sample are needed to determine the effect of input power on fibers treated with this gas mixture for 70 seconds to optimize the process.

Results from samples treated for 3 min give a clearer trend on the effect of input power (Table 6-2 and Figure 6-4). The concentrations of oxygen on fiber surface in sample RA-a, RA-b and RA-c, which were produced with same gas mixture (air) and treatment time (3 min), suggests that surface oxygen concentration decreased with the power input. The decrease in surface oxygen concentration is more than 100% when the power was increased to 2 kW. It seems that ablation or local overheating takes place when power increases to a critical level when treatment time was kept 3 minutes. The lost functionality could evolve as gases such as CO_2, CO and water [92]. So for air plasma

produced in remote applicator, when extremely high input power (more than 1kw) was used, the results obtained so far have been poor. When processing time was decreased to 70 seconds (sample RA-d, 2kw), the oxygen concentration was 9.2% only a little higher than the average value from ozone treatment. The samples treated between 70s and 3min are not available, therefore it is not clear at this stage to identify the critical time to avoid damage of carbon fiber surface under high power. Sample RA-e and RA-f were treated with oxygen plasma for 3 minutes as pressure being 2.0 torr and 3.0 torr, respectively. The resulted oxygen concentration for RA-e and RA-f are 12.8 and 10.7%, respectively. The comparison of RA-e and RA-f appear to show the same trend that oxygen concentration decreases with the increase of input power applied. But the repeat samples RA-e-2 and RA-f-2 show oxygen level of 7.9% and 16.3%, respectively, thus indicating increase in oxygen concentration with increase in input power. Due to the complication of plasma process, there are so many factors that may dramatically change the results of plasma reaction. Between these two samples, other than the different input power, the pressures applied were also different. As the pressure increases, the increased frequency of elastic collisions leads to a decrease in electron energy and electron density, the effect would be similar to reducing the input power. In addition, other factors, like gas flow rate and sample location in the reactor will also affect the final results. These could be the reasons for the poor repeatability.

2. Effect of time

Meaningful comparison can only be made between two samples RA-c and RA-d, since inconsistency in processing parameters. The comparison is shown in Figure 6-5.

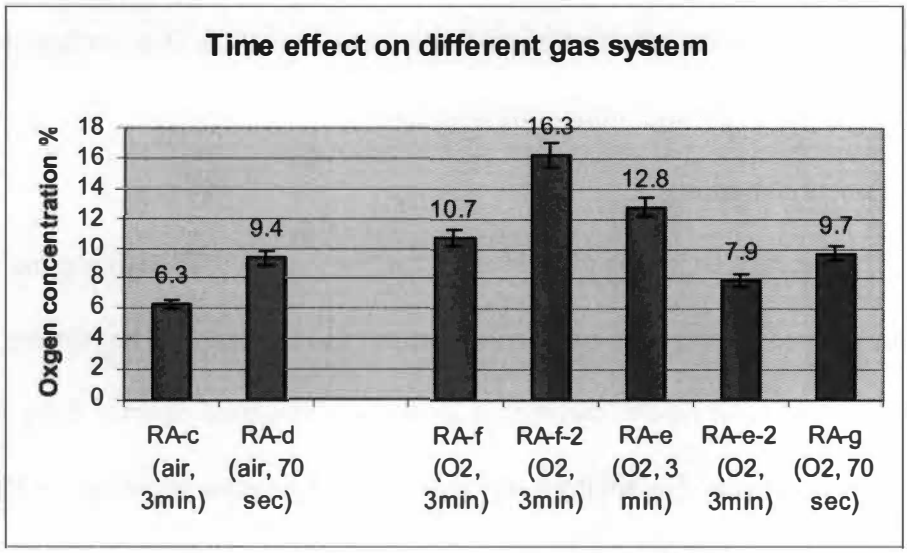

Figure 6-5. Time effect on oxygen concentration

Comparison between RA-f and RA-g was also included in Figure 6-5. It shows that for air environment with treatment time increased from 70 seconds to 3 minutes, the oxygen concentration decreased about 30%. It leads one to conclude that there is a critical treatment time less than 3 minutes with an input power of 2 kw, beyond this level, the loss of attached functional groups can not be avoided. As for oxygen environment, comparison between RA-e and RA-g indicates that increasing treatment time results in a higher oxygen concentration but the comparison between RA-g and the repeat sample RA-e-2 shows the opposite. RA-f was treated with higher power than both RA-e and RA-g; the purpose to include it in the comparison is to show that it seems in oxygen environment the long treatment time up till 3 minutes has not reached the critical point where functionality on the surface starts dropping. The inconsistency in data for sample RA-e and RA-f could be caused by small changes in other parameters that will

significantly change the effect of plasma treatment on carbon fiber surface, such as pressure, gas flow rate and number of filaments.

3. Functional groups

The functional groups generated on the fiber surface through plasma treatment for RA samples were determined by deconvolution of C 1s spectra. The relative concentration of each type of functional groups was obtained directly from the area of the each component peak. The relative concentrations of functional groups on RA samples are shown graphically in Figure 6-6.

It is evident that treatment by remote applicator plasma can change the carbon fiber surface chemistry considerably. The results indicate that sample RA-a, RA-e and RA-j, which have the highest elemental oxygen concentration (Table 5-8, RA-e-2 and RA-f-2 excluded), show a highly reactive surface because in each of them graphitic carbon shows a composition less than 40%, which means approximately two third of the carbon atoms on the top surface are associated with certain oxygen-containing functional groups. Sample RA-a was treated with air plasma, compare to Con UU fibers (Table 5-6), the results suggests plasma treatment causes an increase in -C-OH and –C-OR groups (41%), while oxygen plasma increase both –C=O and –C-OH or –C-OR groups (sample RA-e). When increase input power in oxygen plasma, the result indicated a considerable increase in carboxyl or ester group (RA-f). Sample RA-j shows significant increase in all three types of oxygen-containing functional groups, especially carboxyl and ester groups (20%). It can be concluded that RA plasma can increase various functional groups on carbon fiber surfaces to different extents. The effect of selection of plasma gas and

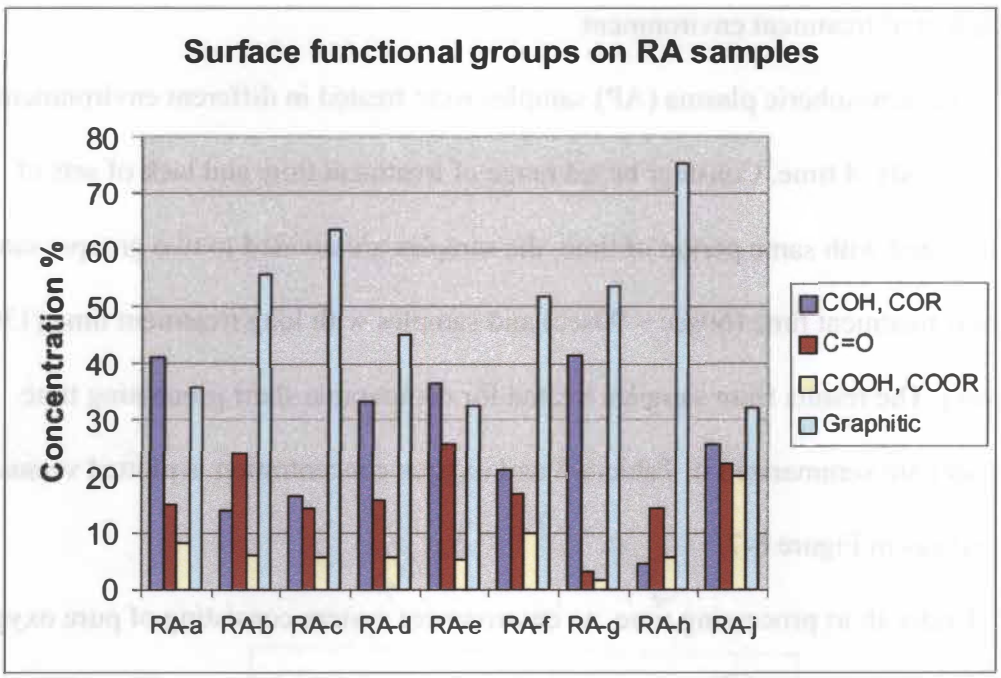

Figure 6-6. Surface functional groups of RA samples

parameters on placement of specific chemical functional groups on carbon fiber surface needs to be further investigated.

6.2.2 Atmospheric Plasma (AP) samples

1. Effect of treatment environment

The atmospheric plasma (AP) samples were treated in different environment for various periods of time. Consider broad range of treatment time and lack of sets of sample treated with same period of time, the samples are divided to two groups: samples with short treatment time (60sec ~ 90sec) and samples with long treatment time (130sec to 310sec). The results from samples treated for comparable short processing time (60~90sec) are summarized in Table 6-3 and oxygen concentration is plotted versus the treatment gas in Figure 6-7.

Under short processing time, an environment system consisting of pure oxygen and water (AP-E) gives the best result (18. 3%), followed by AP-K (20/80 N_2/O_2 + water) of 10%. There is only small difference between samples treated with air and oxygen plasma under short treatment time. Most of the samples give a result very close to conventional fibers treated with ozone (Table 5-2).

The results from samples processed for longer time (130s~210s) are presented in Table 6-4 and Figure 6-8

Table 6-3. Comparison of AP samples with short processing time (60~90sec)

	Oxygen Concentration %	
	Average	STDEV
AP-A air 70s	7.7(6.1)*	0.9(0.9)
AP-C O_2 70s	5.3(9.4)*	0.9(1.4)
AP-E O_2 +water 60/90s	18.3(11.8)*	2.3(2.3)
AP-G O_2 75s	6.8	1.2
AP-H air 75 s	8	0.8
AP-K 20/80 N_2/O_2 + water 60/90s	10	2
AP-L 80/20 N_2/O_2 + water 69/90s	6.4	0.5

*Values for AP-A-2, AP-C-2 and AP-E-2

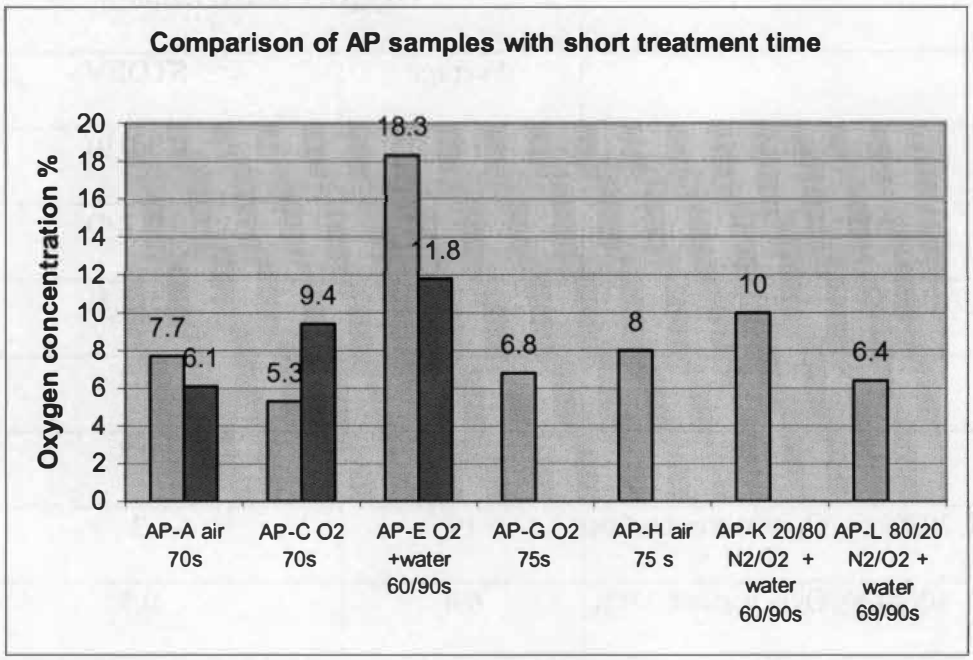

Figure 6-7. Comparison of AP samples with short treatment time

Table 6-4. Comparison of AP samples with long processing time (130s~210s)

	Oxygen Concentration %	
	Average	STDEV
AP-B air 180s	12.7(8.3)*	2.7(1.6)
AP-D O_2 190s	10.8(9.2)*	1.8(0.6)
AP O_2 130s	11.8	2.3
AP-J 20/80 N_2/O_2 3.5min	5.5	1.3

*Values for AP-B-2 and AP-D-2

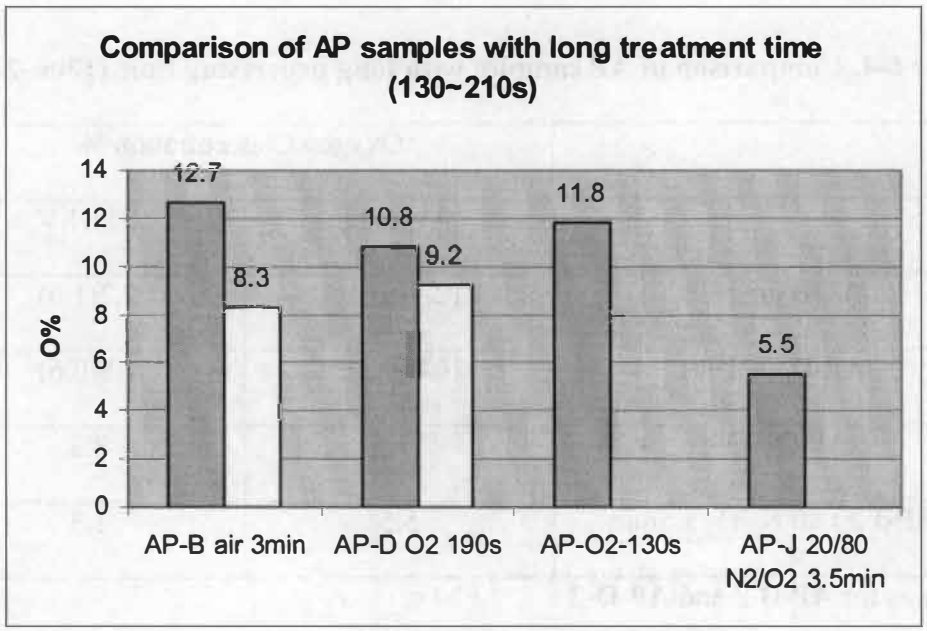

Figure 6-8. Comparison of AP samples with long treatment time (130~210s)

It is observed that under long treatment time, sample AP-J, which is the only sample treated with 20/80 N_2/O_2 environment, shows a very poor level of oxygen. The other samples in general possess higher level of oxygen than samples treated with short time except for the one treated with pure oxygen with water. Fibers treated with air plasma and oxygen plasma do not show significant difference in surface oxygen concentration for both short and long treatment time. Compared to ozone treated conventional fiber, atmospheric plasma produces more oxygen when treatment time is long.

2. Effect of treatment time

The effect of treatment time in different treatment gas systems on surface oxygen concentration on carbon fiber surface is presented in Table 6-5 to Table 6-7 and Figure 6-9 to Figure 6-11.

- Pure oxygen environment

Table 6-5. Time effect in pure oxygen plasma

	Oxygen Concentration %	
	Average	STDEV
AP-C 70s	5.3(9.4)*	0.9(1.4)*
AP-G 75s	6.8	1.2
AP $O_2$130s	11.8	2.3
AP-D 190s	10.8	1.8

*Value for sample AP-C-2

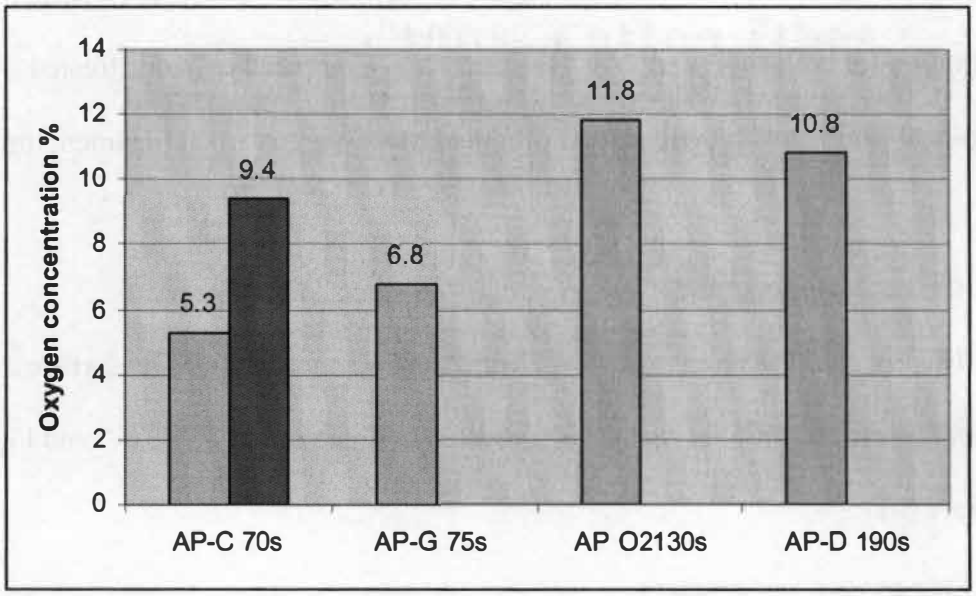

Figure 6-9. Time effect on samples treated in pure oxygen

- Air (80% N_2 /20% O_2) environment

Table 6-6. Time effect in air environment

	Oxygen Concentration %	
	Average	STDEV
AP-A 70s	7.7(6.3)*	0.9(0.9)*
AP-H 75s	8	0.8
AP-B 3min	12.7(8.3)	2.7(1.6)

*Values for AP-A-2 and AP-B-2

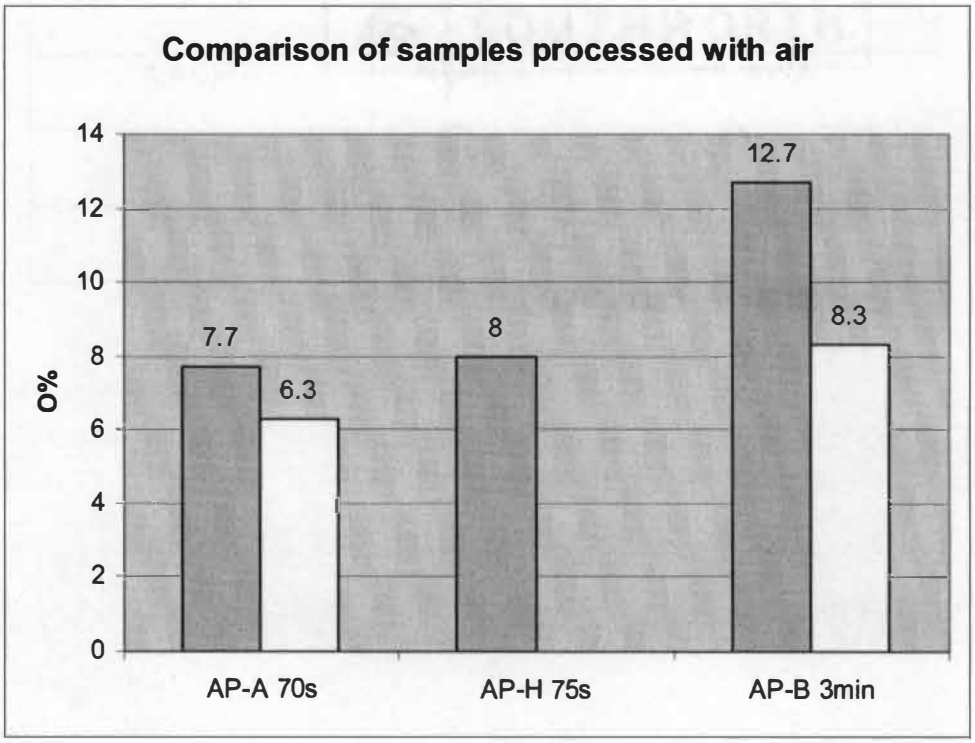

Figure 6-10. Time effect on samples treated in air

- Effect of environment with water

Table 6-7. Samples treated in environment with water

	Oxygen Concentration %	
	Average	STDEV
AP-E pure O_2	18.3(11.8)*	2.3(2.3)*
AP-K 80/20 O_2/N_2	10	2
AP-L air 80/20 N_2/O_2	6.4	0.5

*Values of AP-E-2

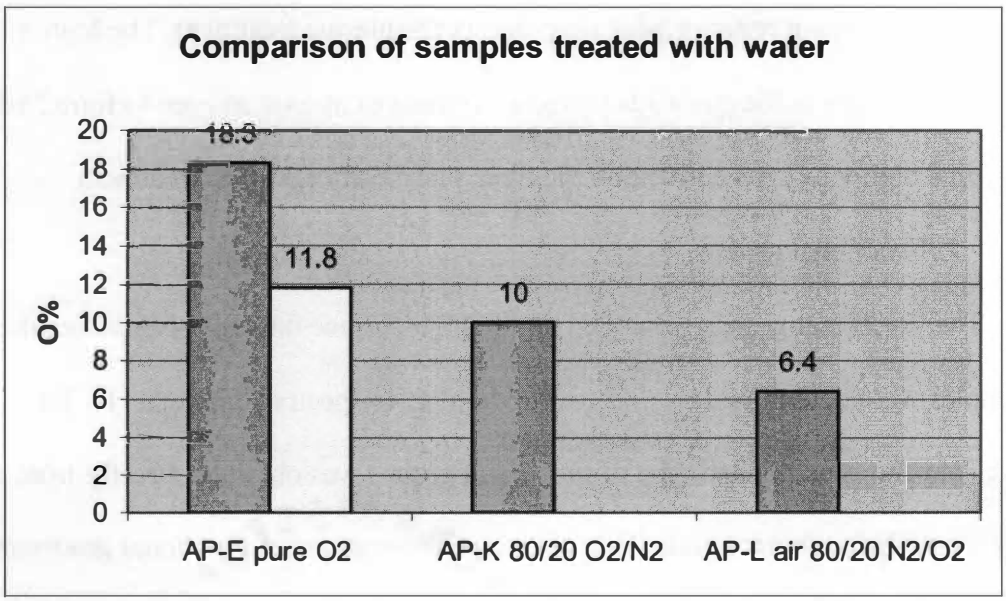

Figure 6-11. Effect of water

Though repeatability is poor in sample AP-A and AP-B, it is reasonable to say that oxygen content increases with increasing treatment time. Similar to oxygen plasma, air plasma only increase oxygen content to higher level than ozone treatment when treatment time is long. Here again, there are not enough samples treated with different periods of time to identify a critical time period that leads to a plateau of oxygen content.

Samples AP-E, AP-K and AP-L were treated using same time, 60sec on one side and 90sec on another side. The only difference is the gas used. It seems the oxygen content on the fiber surface decreases when proportion of oxygen in the gas system decreases. When water is added, the reaction of excited atomic oxygen with water produces hydroxyl radicals (·OH) that are very reactive. The reactive hydroxyl radicals will be incorporated into the fiber surfaces at reactive edge sites during the plasma treatment. The higher proportion of oxygen in the gas leads to higher amount of atomic oxygen to form hydroxyl radicals, thus higher oxygen content on the fiber surface after surface treatment.

3. Functional groups

The functional groups generated on the fiber surface through plasma treatment for AP samples were determined by deconvolution of C 1s spectra (Figure 5-11). The relative concentration of each type of functional groups was obtained directly from the area of the each component peak. The relative concentrations of functional groups on AP samples are shown graphically in Figure 6-12.

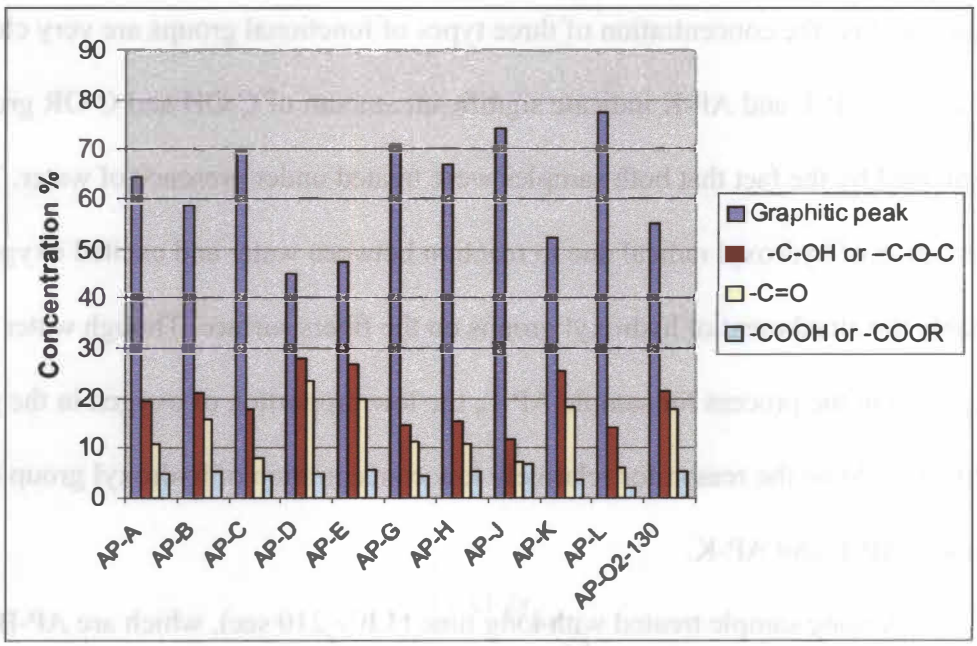

Figure 6-12. Surface functional groups of AP samples

Among samples treated with short time (60 ~90 sec), which are AP-A, AP-C, AP-E, AP-H, AP-K and AP-L, comparison between AP-A and AP-C indicates that when treatment time is short, oxygen plasma and air plasma produce similar kind of oxygen functionality, the concentration of three types of functional groups are very close. Results of sample AP-E and AP-K indicate significant amount of C-OH and C-OR groups. It is explained by the fact that both samples were treated under presence of water. The formation of hydroxyl radical due to reaction between water and excited oxygen atoms enable the attachment of hydroxyl groups on the fibers surface. Though water was involved in the process for sample AP-L, the low proportion of oxygen in the gas mixture (20%) could be the reason for relatively low concentration of hydroxyl group compare to sample AP-E and AP-K.

Among sample treated with long time (130 ~210 sec), which are AP-B, AP-D, AP-J and AP-O_2-130, AP-J shows low concentration of all three types of functional groups. It might due to the loss of functionality caused by local heating or ablation when treatment time was 3.5 minutes. Sample AP-B, AP-D and AP-O_2-130 indicate a tendency of producing carbonyl groups when treatment is long. When fiber treated with oxygen plasma for 190 seconds, the concentration of carbonyl groups reached 23%. It seems that long-time treatment tends to produce more highly oxidized products such as carbonyl type groups, and short-time treatment gives less oxidized products such as hydroxyl and ether groups.

6.3 Effect of Carbon Fiber Surface Morphology on Acid Groups Placement

6.3.1 Chemistry of the cobalt marker

A cobalt compound used as a marker formed a coordinated compound with the carboxylic oxygen atoms present on the surface of the carbon fibers. Consideration of stoichiometric reactions leads to an appropriate equation to enable conversion of the cobalt concentration to a surface carboxyl concentration:

$$[COOH] = 100x[Co] / [C](100-5[Co]) \qquad 6.1$$

Where [COOH] is the concentration in atomic percent of COOH groups on the derivizatized sample, [C] is the concentration in atomic percent of carbon for the same sample before derivatization, [Co] is the concentration in atomic percent of cobalt for the derivatized sample. The calculated concentration of [COOH] is tabulated in Table 6-8.

A noticeable increase is observed in the oxygen concentration after derivatization. The increase is due to presence of oxygen atoms in the coordination compound. The calculated results are different from the XPS data shown in Table 5-9 and Table 5-11. It should be emphasizing that XPS deconvolution cannot differentiate between carboxyl groups and ester groups and is a relatively subjective method, the difference is not surprising. But the existence of cobalt on the fiber surface after thorough rinse process is evident. The calculated results for [COOH] determined by equation 6.1 are relatively

Table 6-8. Calculated concentration of [COOH] (%) coordinated with cobalt compound

	Con UU	RA-a	RA-f	RA-j	AP-B	AP-E
Calculated [COOH]	2.0	9.0	5.9	13.6	7.0	6.6
[COOH] by deconvolution	1.30	8.27	10.03	20.10	6.13	5.29

close to the results obtained from deconvolution of C 1s peaks. The much lower cobalt concentration for Con UU fibers is supported by previous results that show very low oxygen concentration and little carboxyl groups on the surface (Table 5-1, 5-12 and 6-1). The presence of cobalt atoms on the surface after rinsing and the correlation between cobalt concentration and oxygen concentration on Con UU proves that this deritivization technique has been successful in labeling acid groups and cobalt concentration level as an indication of carboxyl group concentration on the fiber surface. And this technique was combined with AES to investigate the distribution of these carboxyl groups with respect to fiber surface morphology.

6.3.2 Effect of surface morphology

The surface morphology of carbon fibers varies depending on the precursor and process. Based on micrometric scale, PAN-based carbon fiber surface has characteristic

features of longitudinal ridges and valleys that extend the whole length of the fiber. These features were attributed to the spinning and stretching processes [2].

AES images and superimposed images (Figure 5-14 ~ Figure 5-19) for both RA and AP samples have shown that cobalt element has preferentially distributed in valley regions while leaving ridge regions covered mainly by carbon. Cobalt element is connected to acid groups by coordination bonds, which means that most carboxyl groups formed during plasma treatment are located preferentially in the valleys instead of ridges. SEM images indicate that, compared to valleys, ridges on fiber surface generally have larger dimension in width and are relatively flatter and smoother.

It is known that the mechanical properties of a particular fiber-matrix composite are determined to a great extent by the degree of bonding between the fiber and the matrix material, i.e., the number of chemical bonds. The number of chemical bonds is related to the accessible active sites where carbon atoms have unbalanced electrons functioning as free radicals. On a clean carbon surface, these active sites would be located on the edges of exposed layer planes as well as at imperfections in the structure including vacancies, dislocations, and steps in the outer basal plane [93]. The preferential tendency of cobalt to be placed in valleys indicates that the accessible active sites (i.e., exposed sheet edges) are located preferentially in the valleys.

The basic structural unit (BSU) in carbon fiber is stacks of aromatic layers of sp2 type carbon in the form like a ribbon with a width of about 60 angstroms and a length several thousand Angstroms [94]. A sketch of stacks of BSU is in Figure 6-13 [4].

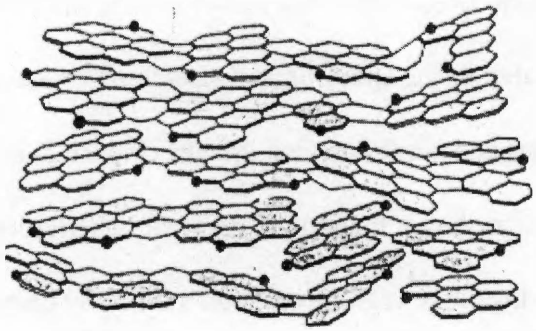

Figure 6-13. Sketch of stacks of BSU [4]

BSU formation starts in stabilization stage with the remaining nitrogen atoms left on the edges. During carbonization BSUs continue to coalesce into distorted stacks due to lack of face-to-face configuration during denitrogenation, which results in the so-called turbostratic stacking. As the heat temperature increases, the formed distorted stacks tend to follow a preferred orientation along the fiber axis under stretching. At the same time increasing carbonization temperature increases the stack height of graphene planes and crystal size that is the regular portion within a BSU. At this stage, when two adjacent sheets contact each other with the remaining nitrogenated edges in contact, lateral bonding are formed by nitrogen elimination. The model of this structure was proposed by Oberlin and shown in Figure 6-14 [2].

The model was built of individual BSU with a random local molecular orientation instead of forming a continuous layer. The stacking graphene planes have a preferential orientation parallel to fiber axis. The individual stacks oriented in random

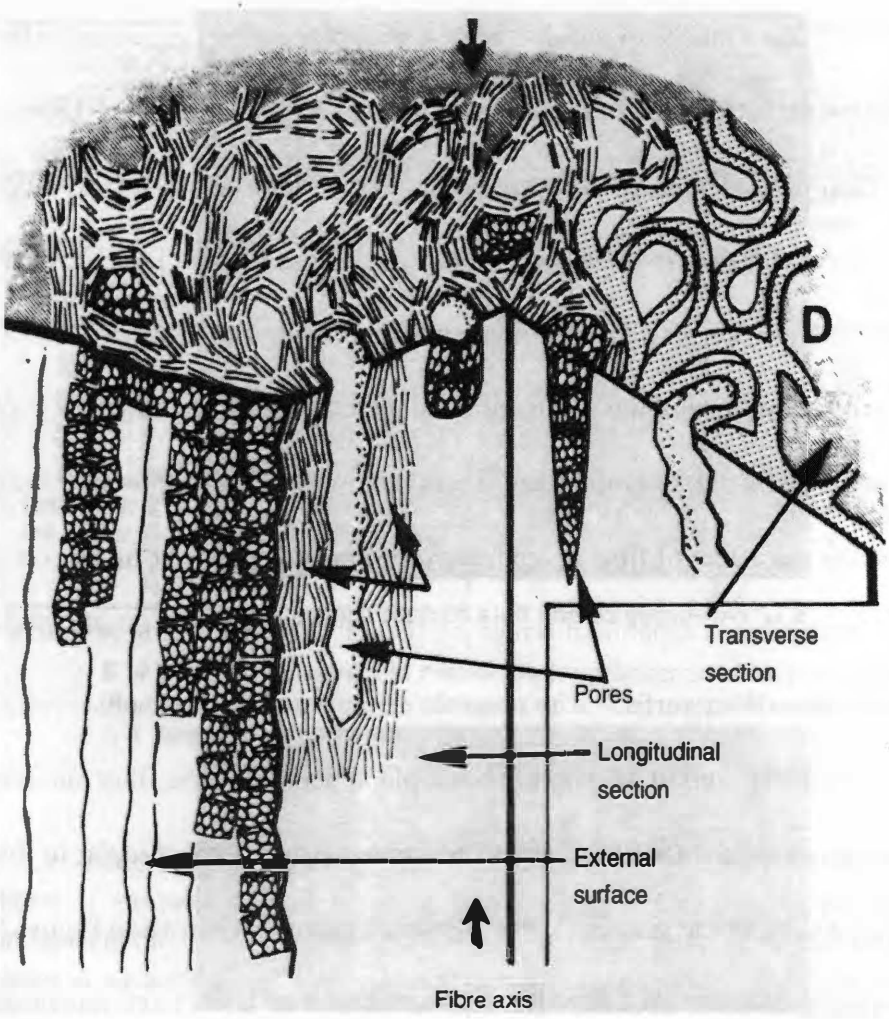

Figure 6-14. Oberlin model for HT carbon fibers

with regard to the fiber surface at the core, the lateral cohesion between BSUs results in strongly distorted sheet including pores elongated along the fiber axis; the external skin has a better organized structure with the BSU stacks tending to arrange parallel to fiber surface but still leave stacks in the skin region with plane edges exposing to the surface.

The model introduced in section of Literature Review (Figure 2-13) is proposed for HM carbon fiber. The main difference is that BSU have coalesced into distorted continuous layer stacks, which has a concentric skin arrangement [2]. The surface in this type of fiber mainly consists of basal plane with low chemical reactivity.

The previous discussion has mentioned the conventional UU fibers supplied for this work are carbonized, ungraphitized fibers. So, model shown in Figure 6-14 will be used to discuss the effect of fiber morphology on the attachment of functional groups. The plasma treatment is capable of removing the outer layer, leaving graphene planes inclined relative to fiber surface. The possible explanation for these observations is that ridge regions mainly consist of graphite basal plane parallel to the fiber surface, while in the valleys and sidewalls the sheet edges present are either perpendicular to the fiber surface or exposing to the sidewalls, the possible structure is shown in Figure 6-15. This model will allow placement of functional groups in the valleys in agreement with the observation from the AES/SEM superposition images.

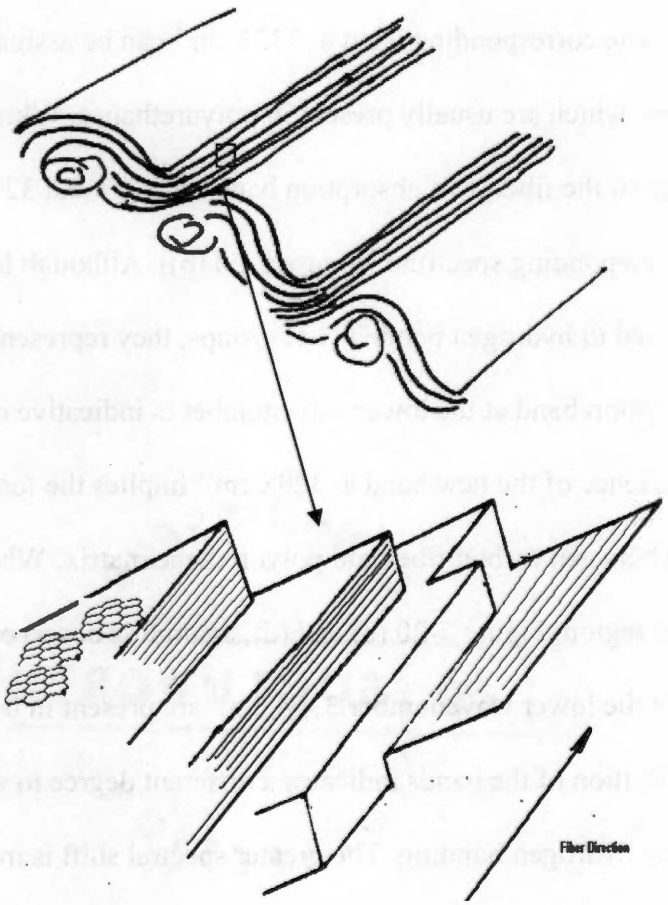

Figure 6-15. Sketch of morphology of carbon fiber surface

6.4 Interphase Chemistry Characterization by FTIR Imaging Technique

The spectrum collected from the location far from the inter-phase region is shown in Figure 5-20 (a). The corresponding band at 3321 cm^{-1} can be assigned to hydrogen bonded N-H groups, which are usually present in polyurethanes. When the crosswire moved to the center of the fiber, two absorption bands at 3322 and 3298 cm^{-1} were observed in the corresponding spectrum (Figure 5-20 (b)). Although both absorption bands can be assigned to hydrogen bonded N-H groups, they represent different bonding strength. The absorption band at the lower wavenumber is indicative of a stronger bonding. The occurrence of the new band at 3298 cm^{-1} implies the formation of new hydrogen bonding between carbon fiber and polyurethane matrix. When the crosswire moved to the green region, Figure 5-20 (c) and (d), again it is observed that the absorption bands at the lower wavenumber 3304 cm^{-1} are present in both spectra. The slight shift in the position of the bands indicates a different degree to which the fiber and matrix are linked by hydrogen bonding. The greater spectral shift is indicative of either stronger or formation of more hydrogen bonding. The spectral information obtained from the N-H absorption bands representing a stronger bonding suggests a three-phase system, which is supported by the observed third phase between fiber and matrix shown in the image.

These results indicate the formation of chemical bonding between carbon fiber and polymer matrix due to incorporation of oxygen containing chemical functional groups.

As shown in Figure 5-21, the general outlines of the fibers can be seen in the infrared image and corresponds well with the optical image. The corresponding peak position image was generated from the same area, which shows the variation in position of the N-H peak maximum in the 3400 – 3200 cm^{-1} region. There are individual blue dots present but there is no pattern to follow. The blue areas indicate lower wavenumber. As can be seen, for Con UU/PU sample there is no general shift from bulk of the urethane and positions close to the fiber. N-H peak were analyzed when positions were selected from both matrix and fiber regions, which shows neither position nor shape of N-H band has changed. This indicates that no significant amount of chemical bonding formed between urethane and untreated conventional fibers due to lack of reactive functional groups present on fiber surface.

In Figure 5-22, the peak position image includes more blue areas appeared and the distribution of these blue regions seems to show a pattern corresponding to fiber positions. Infrared spectra from several different image points were examined with particular attention to the shape and wavenumber of N-H band. Four of these spectra are shown in Figure 5-22. As can be seen, there are differences in the peak shape between the blue image areas (red and blue spectra) and the other areas of the image (green and orange spectra), especially those further away from the fibers. N-H band in the blue areas show a small shoulder at around 3304 cm^{-1} when compared to the band from other image areas.

This small shoulder was seen in all the spectra examined from the blue image areas. The existence of blue areas indicates the formation of new hydrogen bonding and the distribution of these blue areas following fiber direction implies stronger hydrogen bonding formation between plasma treated fiber (AP-B) and urethane.

Figure 5-23 shows the results of RA-j/PU sample. A comparison with the infrared and visible images clearly establishes that in peak position image the blue areas occur where fibers are located. The expanded N-H bands from fiber region and matrix indicate a spectral shift of 27 wavenumbers.

The 3-D peak position images of Con UU/PU and RA-j/PU (Figure 5-24) provide a good comparison of interphase of these two fibers. Due to the existence of functional groups on the fiber surface introduced by plasma treatment, hydrogen bonding formed between fiber and matrix; while for untreated fibers the uniform distribution of N-H position throughout the entire area indicates that no chemical bonding has formed between fiber and matrix. Though FTIR imaging does not possess a spatial resolution to probe interphase directly, it is capable of providing information on interphase chemistry.

CHAPTER 7

CONCLUSIONS AND FUTURE WORK

7.1 Conclusions

MAP technology can produce PAN-based carbon fibers with better surface chemical property than commercial fibers due to unique plasma processing that is assumed to enhance the number of accessible graphene sheet edges, which function as reactive sites during surface treatment. Both conventional and MAP fibers show variations of oxygen concentration on fiber surface due to the heterogeneous characteristic of carbon fiber surface. Compare to conventional fibers, the efficiency of surface treatment has been improved significantly, which is believed to facilitate the matrix-carbon fiber adhesion when forming composites.

Functional groups on the treated carbon fiber surface have a heterogeneous distribution. Morphological features (ridges and valleys) of carbon fibers have an effect on the placement of chemical functional groups. Auger electron spectroscopy in conjunction with chemical derivatization technique offers the possibility to investigate the distribution of functional group implanted during plasma treatment in nano-meter scale. A possible morphology structure of plasma treated conventional fibers has been proposed.

The interphase chemistry was investigated for the first time by using FTIR microspectroscopy coupled with Focal Plane Array detector. The direct chemical

information on interphase region shows the evidence of chemical bonding between fiber and matrix, which was not seen in the case of untreated fibers.

Both remote applicator system and atmospheric plasma can change the carbon fiber surface chemistry considerably. Both air and oxygen plasma treatments lead to higher concentration of oxygen functionality. In the presence of small amount of nitrogen, the efficiency of plasma treatment was improved.

7.2 Future Work

The future work can be directed toward the following areas. First, to gain more information about MAP fibers, plasma treatment needs to be applied for untreated unsized MAP fibers to investigate elemental composition, functional group composition and effect of morphological effect on the attachment of oxygen-containing functional groups.

Secondly, it is evident that both remote applicator and atmospheric plasma treatment increased oxygen concentration on fiber surface. To optimize the process, systematic samples with different processing parameters need to be investigated to establish the correlation between elemental composition and plasma parameters.

Actual testing of mechanical properties of composites made with fibers having different treatment is necessary to investigate the factors that contribute to the fiber-matrix adhesion.

Thirdly, develop derivatization technique to selectively label functional groups such as hydroxyl and carbonyl groups to investigate the effect of morphology features of fiber surface on the attachment of these groups.

Techniques with atomic resolution such as STM, AFM and high resolution SEM could be used to determine orientation of graphite planes with regard to the fiber surface in both ridges and valleys; and the graphitic organization in both areas, i.e. any distortion present to examine the validity of the proposed model.

Finally, further effort needs to be made using FTIR imaging technique to determine the chemical nature of interphase between carbon fiber and matrix. An improved sample preparation and ATR imaging would offer a better image quality with higher spatial resolution. Different polymer resins can be selected to form stronger chemical bonding between fiber and polymer.

LIST OF REFERENCES

References:

1. Marcus Langley, Carbon Fibers in Engineering, McGraw-Hill, New York;

2. Donnet, J. B., Bansal, R. C., Carbon Fibers, Marcel Dekker, Inc., 1990 New York and Basel;

3. Hearle J W S, High Performance Fibers, Woodhead, Cornwall, England;

4. Donnet, J. B., Bansal, R. C., Carbon Fibers, Marcel Dekker, Inc., 1998 New York and Basel;

5. Paulauskas, Felix L., Yarborough, Kenneth D., Meek, Thomas T., United States Patent, 6,372,192, April 16, 2002;

6. Rongzhi Li, Lin Ye and Yiu-Wing Mai, Composites Part A 28A, 1997, pp73-86;

7. Vladimir Cech, Proceedings of the International Conference on Fibre Reinforced Composites, 8th, Newcastle upon Tyne, United Kingdom, Sept. 13-15, 2000, pp 246-252. Woodhead Publishing Ltd., Cambridge, UK

8. David, R. L., CRC Handbook of Chemistry and Physics, 74th Edn. CRC press, Boca Raton, FL, USA, 1993;

9. J.D.H. Hughes, Composites Science and Technology 41, 1991, 13-45;

10. Yatchko Ivanov, Valerii Cheshkov, Polymer Composite Materials – Interface Phenomena & Processes, Kluwer Academic Publishers, Boston, 2001;

11. E.fitzer, Carbon Fibers and Their Composites, UNFSSTD, New York, USA, 1985;

12. Chung, Carbon Fiber Composites, Butterworth-Heinemann, Boston, USA1994;

13. Herrick, J. W., Gruber, P. E., and Mansur, F. T., Surface Treatments for Fibrous carbon Reinforcements, AFML-TR-66-178, Part I, Air Force Materials Laboratory (July 1996);

14. Donnet, J. B. and Ehrburger, P., Carbon 15, 142, 1977;

15. Rand B., and Robinson, R., carbon 15, 257, 1977;

16. McKee, D. W., Carbon, 8, 131, 1970;

17. Walker, P.L., Jr., Shelef, M., and Anderson, R. A. Chemistry and Physics of Carbon, Vol.4, Marcel Dekker, New York (1968), p. 287;

18. Rand, B., and Robinson, R., Carbon, 15, 311, 1977;

19. Wu, Z., Pittman, C. U., and Gardner, S. D., Carbon 33, 597 (1995);

20. J.B.Donnet and G. Guilpain, Composites, vol. 22, no.1, Jan. 1991;

21. N.Dilsiz and J.P.wightman, colloids and Surfaces A, 164, 2000, pp 325-336;

22. M.C.Zhang and E. T. Kang, Polymer, 42 2001, 453-462;

23. Chawla, K. K, Composite Material science and engineering, Springer-Verlag, New York, USA, 1987;

24. W. H. Lee, applied Surface Science, 171, 2000, pp 136-142;

25. Liston, E. M. Journal of Adhesion 1989, 30, pp199-218;

26. C. Jones, Composites Science and Technology, 42, 1991, pp275-298;

27. Yasuda, H.K. 'Plasma Polymerization and Plasma Treatment'. J. Wiley, New York, 1984;

28. Sun, M., Hu, B., Composites Science and Technology, 1989, 34, 353-364;

29 J.P. Boudou, J.I. Paredes, Carbon 41 (2003) pp41-56;

30. Farrow, G.J., Atkinson, K.E., Surf. Interface Anal. 1995, 23, pp313-318;

31. Lefebvre, Advanced Composites 93, The Minerals, Metals & Materials Society;

32. C. L. Heisey and P.A.Wood, Journal of Adhesion, 1995, Vol. 53, pp117-147;

33. Yu-Qing, Wang, Chem. Materr., 12 (4), 2000, pp1100-1107;

34. A. Proctor and P.M.A. Sherwood, Carbon 21, 53, 1983;

35. C. Kozlowski and P.M.A. Sherwood, J. Chem.. soc. Faraday I 80, 2099, 1984;

36. C. Kozlowski and P.M.A. Sherwood, J.Chem.. soc. Faraday I 81, 2745, 1985;

37. J. Harvey, C. Kozlowski and P.M.a. Sherwood, J. Mat. Sci. 22, 1585, 1987;

38. C. Kozlowski and P.M.A. Sherwood, Carbon 24, 357, 1986;

39. C. Kozlowski and P.M.A. Sherwood, Carbon 25, 751, 1987;

40. Y. Xie and P.M.A Sherwood, Chem. Mater. 2, 293, 1990;

41. Y. Xie and P.M.A Sherwood, Chem. Mater. 3, 164, 1991;

42. Y. Xie and P.M.A Sherwood, Appl. Spect. 45, 1158, 1991;

43. Y.Xie, T.Wang, O. Franklin and P.M.A. Sherwood, Appl. Spect. 46, 645, 1992;

44. Dilsiz, N., Ebert, E., weisweiler, w. and Akovali, G, J. colloid Interf.Sci. 1995, 170, pp 241-248;

45. Okhusen, O., Cochran, R. C., Sposili, R. and Donnellan, T.M., Journal of Adhesion, 1994, 45, 3-14;

46. Y.Nakayama, Carbon 28, (1990) pp21-26;

47. Y. Xie and P.M.A. Sherwood, Chem. Mater. 1, 427, 1989;

48. P.M.A. Sherwood, practical Surface Analysis, Second Edition, vol 1: Auger and X-ray Photoeletron Spectroscopy, John Wiley and Sons, Chichester, 1990;

49. P.M.A. Sherwood, J. Vac. Sci. Technol. A9, 1493, 1991;

50. A. Proctor and P.M.A. Sherwood, Anal. Chem. 52, 2315, 1980;

51. Y. Nakayama and F. Soeda, Carbon 28, 43 1990;

52. Sin-Shong Lin, U.S.Aray Materials Technology Laboratory, 1989;

53. T. Ohwaki and H. Ishida, Applied Spectroscopy vol.49, no. 3, 1995 pp341-348;

54. T. Takahagi and A. Ishitani, Carbon Vol. 22, No. 1 pp 43-46;

55. S. Shin, J. Jang, carbon vol. 35, No. 12 pp.1739-1743 1997;

56. D.M. Brewis, Fibre Science Technology 12, 41, 1991;

57. Z.H. Wu and C.U.Pittman, Carbon Vol. 33, No. 5, 1995, pp597-605;

58. Qing Wu, Huifang, Chen, Gaofenzi Cailiao Kexue Yu Gongcheng (2002), 18(2), 147-150;

59. D.S.Everhart and c.N Reilly, Anal. Chem., 53, 665, 1981;

60. T. Takahagi and A. Ishitani, Carbon, vol. 26, No.3, pp. 389-396;

61. P.Denison, F.R.Jones and J. F. Watts, J. Mat. Sci. 20, 4647, 1985;

62. Alexander Bismarck, M. Emin Kumru, Journal of Colloid and Interface Science 210, 60-72, 1999;

63. Tsutsumi, K., Ishida, s., Colloid and polymer Sci. 268,31 (1990);

64. L. G. Tand J. China Text. Uni., 11, 80, 1994;

65. E. Desimoni, G. I. Casella, A. Morone and A. M. Salvi, Surf. Interface Anal., 15, 627, 1990;

66. E. Desimoni, G. I. Casella, T.R. I. Cataldi, A.M.Salvi, Surf. Interface Anal., 18, 623, 1992;

67. W. K. J. Huttinger, S. Hohmann-Wien and M. Seiferling, Carbon 29, 449, 1991;

68. K. J. Huttinger, S. Hohmann-Wien and G. Krekel, Carbon 29, 1281, 1991;

69. K. J. Huttinger, S. Hohmann-Wien and G. Krekel, J. adhes. Sci. technol. 6, 317, 1992;

70. P.E.fanning and M.A.Vannice, Carbon 31, 721, 1993;

71. C. Sellitti, J.L.Koenig and H.Ishida, Carbon 28, 221, 1990;

72. P.M.A.Sherwood, Research into Structural Carbons, Edited by M. A. Wright and K.R.Palmerr, pp. 53-75;

73. A.Proctor and P.M.A.Sherwood, J. Electron. Spectr. Relat. Phenom., 27, 39, 1982;

74. C.Kozlowski and P.M.A.Sherwood, J.Chem. Soc., Faraday trans., 81, 2745, 1985;

75. C.Kozlowski and P.M.A.Sherwood, Carbon 25, 751, 1987;

76. W.P.Hoffman, W.C.Hurley, P.M.Liu and T.W.Owens, J. Mater. Res., 6, 1685, 1991;

77. W.P.Hoffman, V.B.Elings and J.A.Gurley, Carbon, 26, 754, 1988;

78. W.P.Hoffman, carbon, 30, 315, 1990;

79. U.Zielke, Carbon Vol. 34, No. 8, pp. 983-998, 1996;

80. L.T.Drzal, Proceedings of the Annual Meeting of the Adhesion Society (1997), 20th; 477-480;

81. Guigon, M, Journal of Materials Science, 1, 1992, pp 4591-4597;

82. Arvanitopoulos, C. D, Applied Spectroscopy, volume 50, No. 1, 1996;

83. Narkis, M. and Chen, J.H., Polymer Composites, Vol. 9, August 1998, pp245-251;

84. Herrara-Franco, P., 46th Annual Conference, Composites Institute, The Society of the Plastics Industry, February 18-21,1991;

85. Herrara-Franco, P. and Drazl, L.T., Composites, Vol. 23, January 1992, pp2-27;

86. E.Desimoni, G. I. Casella, a. Morone and A. M. Salvi, Surf. Interface Anal, 15, 627,1990;

87. P. Marshall and J. Price, Composites 22, 388, 1991;

88. F. Nakao, Y. Takenaka and H. Asai, Composites 23, 365, 1992;

89. Farrow, G.J., Atkinson, K.E.,Fluck, N. and Jones, C. Surf. Interface Anal. 1995, 23, 313-318;

90. F. Paulauska, J, Spruiell, SAMPE Journal, Vol.40, No.4, July/August, 2004;

91. J Zawadzki, Chemistry and Physics of Carbon, Vol. 21, Marcel Dekker, New York, 1989;

92. Yaoming Xie, Peter M.A. Sherwood, Applied Spectroscopy, Vol 43, no.7, 1153, 1989;

93. W.P.Hoffman, W.C. Hurley and T.W. Owens, Journal of Materials Science, Vol 26, 1 Sept , 1991;

94. R.Perret, W. Ruland, Journal of Applied Crystal; 3, 525, 1970;

VITA

Xiaoyu Luo was born and raised in Beijing, the People's Republic of China. She joined the Department of Materials Science and Engineering at Beijing University of Aeronautics and Astronautics in 1988. Four years later, she received a Bachelor of Engineering degree in Polymer Science. From 1992 to 1998, she worked as an engineer in Research Institute of Chemical Industry, Beijing, China. In August of 1998, she joined the Department of Materials Science and Engineering at the University of Tennessee, Knoxville to pursue a PhD degree in polymer engineering. She completed all the requirements for the Doctor of Philosophy degree in December 2005.